Relativistic quantum systems in the framework of quantum information and quantum foundations

Thesis Submitted for the Degree of
Doctor of Philosophy (Science)
in Physics (Theoretical)

By

Riddhi Chatterjee

Department of Physics
University of Calcutta

2022

মুখবন্ধ ঃ-

এই থিসিসে আপেক্ষিকতাবাদ তত্ত্বের পটভূমিতে কোয়ান্টাম তত্ত্বের কিছু ভিত্তিগত ও তথ্যতাত্ত্বিক বিষয়ের গবেষণামূলক পর্যালোচনা করা হয়েছে। প্রথমে আমরা আপেক্ষিক কোয়ান্টাম পদার্থ বিজ্ঞানের ধারণা সম্পর্কে মৌলিক পর্যালোচনা করেছি। আমরা পোঁয়াকারে গ্রুপের স্পিনর রিপ্রেজেন্টেশন নিয়ে আলোচনা করেছি এবং এর ভিত্তিতে দেখেছি কিভাবে একটি স্পিন ১/২ কণা, যার ভরবেগের গাউসিয়ান বিন্যাস রয়েছে, দুটি অসমরৈখিক লরেন্টস্ বুস্ট এর প্রভাবে রূপান্তরিত হয়। তারপর আমরা কোয়ান্টাম স্কেলার ক্ষেত্র তত্ত্বে কণার ধারণা এবং ফক স্পেসের সংজ্ঞা নিয়ে আলোচনা করেছি। আমরা সমতল স্থান কালে অজড় কোয়ান্টাম ক্ষেত্র তত্ত্বের কণা উৎপাদনের ঘটনা নিয়েও আলোচনা করেছি।

উপরোক্ত তত্ত্বগুলি ব্যবহার করে আমরা বিভিন্ন গুরুত্বপূর্ণ ঘটনাবলী নিয়ে গবেষণামূলক অধ্যয়ন করেছি।

আমরা স্পিন-১/২ গাউসিয়ান ভরবেগ বিন্যাস সমন্বিত তরঙ্গ প্যাকেটের কোহেরেন্স পরিমাপ করেছি যখন তন্ত্রটির উপর পর্যায়ক্রমিক অসমরৈখিক লরেন্ট্স্ বুস্ট প্রয়োগ করা হয়েছে। কোহেরেন্স পরিমাপের জন্য আমরা কোয়ান্টাম রিসোর্স তত্ত্বের বিভিন্ন পরিমাপককে ব্যবহার করেছি। আমাদের কাজ আপেক্ষিকতাবাদের পটভূমিতে এই রিসোর্সতাত্ত্বিক পরিমাপগুলির সঙ্গতি ও দক্ষতার উপর আলোকপাত করেছে। এরপর আমরা দুটি অভিন্ন নিরপেক্ষ পরমাণুর মধ্যে অনুরণন মিত্রস্ক্রিয়া অধ্যয়ন করেছি যখন পরমাণু দুটি দুটি সমান্তরাল আয়নার মধ্যবর্ত্তী স্থানে ত্বরিত হচ্ছে। অনুরণন মিথস্ক্রিয়ার দরুন পরমাণু দুটি শক্তিস্তর পরিবর্তন করে। আমরা এই শক্তিস্তরের পার্থক্য এবং শক্তি পরিবর্তনের শিথিলকরণ হার গণনা করেছি। আমরা পরমাণুদুটির শক্তিস্তর পরিবর্তনের উপর তাদের ত্বরণ, পারস্পরিক দূরত্ব, আয়না দুটির

পারস্পরিক দূরত্ব ও আয়নাদুটি থেকে পরমাণুদুটির দূরত্বের নির্ভরশীলতা অধ্যয়ন করেছি। এর থেকে আমরা দেখি যে উপরোক্ত পরামিতি ব্যবহার করে পরমাণুদুটির অনুরণন মিথস্ক্রিয়ার কৌশলগত পরিচালনা সম্ভব। বাস্তব পরীক্ষামূলক পরামিতি ব্যবহার করে আমরা ত্বরণের প্রভাবে পরমাণুদুটির অনুরণন শক্তির পরিবর্তনের মান সংশোধন গণনা করেছি।

আমরা কোয়ান্টাম ক্ষেত্রতত্ত্বের পটভূমিতে থাকা একটি পরমাণু - আয়না তন্ত্রকে অধ্যয়ন করেছি। আমরা ধরে নিয়েছি কোয়ান্টাম ক্ষেত্র, সাধারণ অনিশ্চয়তা নীতি মেনে চলে। আমরা পটভূমিকায় থাকা একক মোড স্কেলার কোয়ান্টাম ভ্যাকুয়ামের সঙ্গে মিথস্ক্রিয়ার ফলে পরমাণুটির স্বতঃস্ফূর্ত্ত উত্তেজনাকে অধ্যয়ন করেছি। এক্ষেত্রে আমরা দুটি ঘটনা বিবেচনা করেছি।

১) ত্বরিত পরমাণু ও স্থির আয়না।

২) স্থির পরমাণু ও ত্বরিত আয়না।

আমরা দেখি যে সাধারণ অনিশ্চয়তা নীতির প্রভাবে, উপরোক্ত ঘটনা দুটির মধ্যে আইনস্টাইনের উইক ইকুইভ্যালেন্স নীতি লঙ্ঘিত হয়। সাধারণ অনিশ্চয়তা নীতির প্রভাবে উভয়ক্ষেত্রেই পরমাণুদুটির উত্তেজনার সম্ভাবনা ক্রমহ্রাসমান হয় এবং দ্বিতীয় ক্ষেত্রে আনরুহ্ তাপমাত্রার পরিবর্তন হয়। এরপর আমরা একটি সুপার কন্ডাটিং সার্কিটের মধ্যে ডাইনামিকাল ক্যাসিমির বিকিরণের দ্বারা বেল-ইনইকুয়ালিটির লঙ্ঘন কে অধ্যয়ন করি। আমরা বেল ইনইকুয়ালিটি লঙ্ঘনের পরিমাপের জন্য নন্‌গাউসিয়ান সিউডো স্পিন পরিমাপ প্রয়োগ করেছি। উপরোক্ত অধ্যয়নে মাইক্রোওয়েভ ক্ষেত্রের মোডের উপর স্থানীয় নয়েজের প্রভাব, ক্ষেত্রের মোডগুলির মধ্যে অসমতা এবং মাইক্রোওয়েভ সঙ্কেতের ক্ষয় বিবেচনা করেছি। আমরা উপরোক্ত বেল ইনইক্যুয়ালিটি লঙ্ঘন পর্যবেক্ষণ করার উপযুক্ত সার্কিট পরামিতির মানের সীমা চিহ্নিত করেছি।

Dedicated to my parents.

Abstract

This thesis is devoted to study some quantum foundational and information theoretic aspects of quantum systems in the relativistic background. First we have reviewed some basic notions of relativistic quantum physics. We have discussed spinor representation of Poincaré group and how a spin-1/2 particle with Gaussian momentum wave packet transforms under two successive noncollinear Lorentz boosts. Then we discuss the definition of Fock space and notion of particle in the context of scalar quantum field theory. We also discuss particle production phenomena and related concepts in noninertial quantum field theory in the flat space-time.

Using above formalisms we study several interesting phenomena :

We quantify coherence of spin-1/2 Gaussian momentum wave packet under successive noncollinear Lorentz boosts, using various resource theoretic quantifiers. Our work sheds light on the efficiency and consistency of these quantifiers in relativistic background. Next we have studied resonance interaction of two identical neutral atoms accelerating between two parallel mirrors. We have calculated energy level shift and relaxation rate of change of energy due to resonance interaction and study their dependence on acceleration, interatomic separation, separation between mirrors and distance of the atoms from the mirrors. Our work shows that resonance interaction can be manipulated using above parameters. We estimate the correction in the resonance energy shift due to acceleration using realistic experimental parameters.

Next we have studied spontaneous excitation of an atom in an atom-mirror system in relative acceleration in presence of single mode scalar quantum vacuum that obeys (generalized uncertainty principle) GUP. Our work shows that GUP induces violation of equivalence between excitation probability of atom in two cases: accelerating atom-static mirror and accelerating mirror-static atom. GUP introduces damping in both of these cases and modification of Unruh temperature in case of accelerating mirror-static atom. Next we have studied Bell's inequality violation of dynamical Casimir radiation simulated in superconducting microwave circuit. Employing non-Gaussian pseudospin measurement, we have analytically evaluated the amount of Bell violation and studied their variation with various circuit parameters. We have considered the effects of local noise in the microwave field modes, asymmetry between the field modes, and signal loss. We have identified the the appropriate parameter regions, in order to observe Bell violation in this set-up.

Acknowledgement

I would like to express my deepest gratitude towards my Ph.D. supervisor Prof. Archan S. Majumdar for his patient support, guidance and suggestions during the time of carrying out my research work. He has always encouraged me to think independently. He has allowed me to get introduced to all the areas of his research interest : General relativity, Cosmology and Quantum information theory and inspired me to pursue interdisciplinary research. I cannot thank him enough.

I am also grateful to my collaborator Dr. Sunandan Gangopadhyay. He is one of the best teachers I have ever met. I thank him for his valuable assistance and suggestions during my Ph.D. research work.

I would like to thank Dr. Samir Kumar Paul for his sincere help with the differential geometry lessons during IPh.D. coursework.

I also thank the faculties of the Department of Astrophysics and Cosmology (Now the Department of Astrophysics and High energy physics): Prof. Sandip K. Chakrabarti, Prof. Soumen Mondal, Dr. Ramkrishna Das for their encouragement and support.

I am pleased to thank all the non-academic staff members of SNBNCBS for their excellent help and cooperation.

I acknowledge the Science and Engineering Research Board, Department of Science and Technology, Government of India, for awarding me the "International travel support" (File No. : ITS/2018/002925) for attending the workshop "Gravity in the Quantum Lab" in Benasque, Spain in 2018.

I would like to thank my seniors Tanumoy Pramanik, Priyanka Chowdhury, Subhadipa Das, Hrishit Banerjee, Arpan Krishna Mitra, Karan Fernandes, Pratik Tarafdar. All of them were very supportive and always tried to help and encourage me.

I have been fortunate to have some excellent friends in SNBNCBS. I thank Ayan Bhattacharjee, Ruchi Pandey, Anuvab Banerjee, Shreya Das, Arnab Sarkar and Sanchi Maithani. We had lot of fun together and have so many memories that I will cherish forever. I specially thank Ayan for his counsels and staying beside me in most difficult times.

It would be audacious to thank my parents and still not mentioning them will keep this note of acknowledgement incomplete. This thesis wouldn't have been complete without their unconditional love, constant care and support.

Contents

List of Publications

The thesis is based on the following publications in the journals:

1. **Riddhi Chatterjee**, A. S. Majumdar, Preservation of quantum coherence under Lorentz boost for narrow uncertainty wave packets, Phys. Rev. A **96**, 052301 (2017).

2. **Riddhi Chatterjee**, Sunandan Gangopadhyay, A. S. Majumdar, Resonance interaction of two entangled atoms accelerating between two mirrors, Eur. Phys. J. D **75**, 179 (2021).

3. **Riddhi Chatterjee**, Sunandan Gangopadhyay, A. S. Majumdar, Violation of equivalence in an accelerating atom-mirror system in the generalized uncertainty principle framework, Phys. Rev. D **104**, 124001 (2021).

4. **Riddhi Chatterjee**, A. S. Majumdar, Bell-inequality violation by dynamical Casimir photons in a superconducting microwave circuit, Phys. Rev. A **106**, 042224 (2022).

List of Acronyms and Initialisms

CHSH: J. F. Clauser, M. A. Horne, A. Shimony, and R. A. Holt.

CM: Covariance matrix.

CPW: Coplanar waveguide.

cQED: circuit quantum electrodynamics.

DCE: Dynamical Casimir effect.

DDC: Dalibard, Dupont-Roc and Cohen-Tannoudji.

EPR: Albert Einstein, Boris Podolski and Nathan Rosen.

GUP: Generalized uncertainty principle.

ICPTP: Incoherent completely positive and trace preserving.

QFT: Quantum field theory.

QFTCS: Quantum field theory in curved space-time.

RQI: Relativistic quantum information.

SQUID: Superconducting quantum interference device.

SRDM: Spin reduced density matrix.

UCN: Ultracold neutron.

Chapter 1

Introduction and outline of the thesis

Relativity and quantum theory are two pillars of physics, which describe laws of nature at two different length scales. However, in order to get a fundamental theory that describes our universe as generically both quantum and relativistic, these two theories need to be consistently unified to a more general formulation. Despite of endless efforts for many decades, there have been no successful theory of quantum gravity. This has led the scientific community to study the effect of relativity in smaller length scale leading to the fields of relativistic quantum physics [1,2] and quantum field theory in curved space-time (QFTCS) [3]. Quantum information theory on the other hand explores the ways of encoding information in quantum systems, protecting them from noise and use them to build up very advanced communication protocols and computers that cannot be achieved by classical theory [4]. The quest for unification of relativity and quantum theory has also been propagated in the field of quantum information, giving rise to the field of "Relativistic Quantum Information" (RQI). In a nutshell the aim of RQI is to formulate a quantum information theory which is consistent with background relativistic space-time and exploit it, with the aid of current and future technology, to perform quantum task and verify fundamental phenomena.

Consistency of a theory in the relativistic framework demands Lorentz covariance (at least locally). Quantum mechanics, where the state of a particle is governed by Schrödinger equation, is Galilean covariant. The attempts to formulate a Poincaré covariant quantum mechanics hit the dead end as it leads to unphysical negative probability distribution corresponding to the state of a particle [1]. Subsequently quantum field theory (QFT) replaces relativistic quantum mechanics as a successful Lorentz covariant quantum theory. Here quantum field is considered as the fundamental physical entity and the particles are defined as the excitations of field quanta [5]. In the year *1969* and onwards the novel work

of Leonard Parker explained the cosmological particle production as the radiation from quantized vacuum in expanding universe [6]. Parker's work influenced the scientific community to study particle production phenomena in noninertial and curved space-time. Inspired by Parker's work, Stephen Hawking published his famous works on black hole evaporation in the *1970*s [7,8]. Hawking's work shows that, the vacuum of quantum fields residing on the space-time of black holes emits all species of particles known as Hawking radiation, due to the strong gravitational field of black holes. The work of Moore, DeWitt, Fulling and Davies showed that, vacuum state of quantized free field residing in free space or cavity and subjected to rapid time dependent boundary condition or relativistically moving mirrors also produces particles *1974-1976* [9–11]. The vacuum state of quantum field in the Minkowski space-time appears to be excited with respect to an accelerated (Rindler) observer. This phenomenon is known as Fulling-Davies-Unruh effect or precisely the Unruh effect after the name of the discoverer W. Unruh *1976* [12].

The discovery of Hawking radiation creates controversy as it violates the conservation of information. Quantum fields are generic, omnipresent entities attached to the fabric of the universe. The theory of relativity says that notion of reality in two different reference frames are same only when the frames are inertial to each other. In the space-time of a black hole two observers sufficiently apart from each other are nonintertial due to strong curvature gradient and have different notions of vacuum. So, the vacuum state of quantum field near event horizon will appear to be excited to an observer far away from the event horizon. Hawking's calculations show that the distant observer sees this phenomena as thermal radiation from black hole known as Hawking radiation [7,8]. The temperature of Hawking radiation depends only on the mass, charge and angular momentum of the collapsed objects. As black hole evaporates through Hawking radiation its event horizon shrinks with time and the space-time curvature reduces. When the black hole evaporates entirely the space-time becomes flat. So, the information contained inside the event horizon is completely lost. This is in contradiction with quantum theory which states that time evolution of the state of an isolated object is always unitary and information content of the state is preserved under unitary evolution. This is known as black hole information paradox. This was the first motivation for scientific community to study quantum information in the vicinity of the black holes.

Starting from the dawn of 20^{th} century, quantum theory has revolutionised the field of technology for example the discovery of photo-electric effect, laser, maser, diodes, transistors and superconductors etc. Application of quantum theory in

the field of informatics has given rise to the quantum information theory that has enabled us to realise quantum communications and opened up the possibility to build up fault tolerant quantum computers. The formulation of quantum information theory is based on quantum mechanics where the state of a particle is represented as an element of a Hilbert space and hence can be expressed as linear superposition of the bases that spans the Hilbert space [13]. The elements of a complete set of orthonormal bases are called the eigenstates and each of them are associated to a specific eigenvalues of certain observables. So, the quantum state is delocalised over the eigenbases and hence exhibits wavelike behaviour. When an observer performs measurement, the state will collapse to one of the eigenbasis with probability determined by square of the coefficient corresponding to that basis vector in the linear superposition. Such uncertain behaviours of the quantum systems were counter intuitive from the perspective of the classical physics. However, most revolutionary notion in quantum physics was the quantum entanglement. *A quantum system is entangled if the quantum states of its local constituents cannot be factored in product form* [14]. Entanglement can exist among the modes of quantum field and as well as among the quantum states of particles (eg. atomic energy levels) even when the particles are physically large distance apart.

When measurement is performed on any of the local constituents of an entangled system, the states of all the constituents collapse instantly regardless of the space-time coordinate of the local constituents. This resulted in a paradox as, according to special relativity, information cannot travel faster than light. In *1935* Einstein, Podolski and Rosen (EPR) published a paper that claimed quantum mechanics is incomplete as a physical theory [15]. According to them, in case of a complete theory, outcomes of measurements of observables on any system should be predicted with absolute certainty which is known as the notion of realism. Also measurement on a local constituent should not instantly affect the state of other constituents i.e., notion of locality should hold. Together, these two notions are known as local-realism. EPR suggested that, lack of completeness of quantum theory is the reason of violation of local-realism in case of entanglement [4, 15].

Several attempts were made by scientists to formulate quantum mechanics, consistent with local-realism, in terms of hypothetical parameters known as "local hidden variables" [16]. In a *1964* paper, J. S. Bell presented a quantitative formulation of EPR problem [17, 18] known as Bell's theorem. The violation of Bell-inequality ruled out the possibility to explain entanglement by means of local hidden variable and characterised it as a nonlocal correlation that violates local-realism. Subsequently in *1969*, J. F. Clauser, M. A. Horne, A. Shimony

and R. A. Holt (CHSH) proposed an experiment to verify Bell's theorem and giving rise to the operational perspective of nonlocality [19]. Subsequently quantum theory found its applications in the field of communications [20]. Quantum cryptography (BB84 protocol) was proposed in *1984* [21]. In subsequent years formulations such as quantum state reductions [22] and quantum estimations were started to develop [23]. Around same time, Feynman and Manin propsed the idea of quantum computer, that has capability beyond classical computer [24,25]. In *1970*s, development in atomic, molecular and optical technology enabled us to controlled manipulation of trapped single particle and use them to engineer advanced material architectures needed to realise quantum computers and quantum communications [4]. Since *1990*s progress in quantum information theory and quantum computing started to gain momentum. Significant discoveries were made in the field of quantum algorithm and protocols for quantum information in noisy environments, quantum error corrections etc. [4]. The year *2000* onwards, new quantum correlations such as quantum discord, quantum steering, coherence were introduced in an operational framework in order to exploit them as a resource for quantum tasks [26–28].

As non-relativistic quantum information theory kept developing, in *2000*s attempts were made to extend it in the relativistic regime. One of the earliest attempts was to define quantum information theory of single particle states in Minkowski space-time [29–32]. Subsequently the formulation has also been extended in curved space-time [33,34]. However, solution of single particle relativistic wave equation have negative energy solutions [1]. Also, in relativistic quantum regime notion of particle is not same in all reference frames [3]. So, the single particle picture is not always sufficient for formulation of RQI. The alternative formulations were proposed that consider a bigger Hilbert space such as Fock space [35, 36]. These formulations are consistent with particle production phenomena in noninertial frames and curved space-time. Numerous studies have been performed on quantum correlations in relativistic framework using both the single and multi particle Hilbert spaces. It has been showed that notion of quantum correlations such as entanglement, discord are observer dependent [29,31–39]. These studies have paved the ways to explore quantum foundations and information theory in gravitational and dynamical space-time background [37,40–43]. Studies have also been done on various aspects of quantum communication in above mentioned frameworks [44–48]. Quantum information is an operational theory and hence, unlike quantum theory in curved space-time, RQI did not remain confined within the mathematical formulations. As mentioned in the beginning, that the goal of RQI is to explore relativistic quantum theory in the modern day

experimental regime such as cold atoms, trapped particles, nanomaterials, superconducting circuits and satellites [49–55]. These developments enables us to verify and probe fundamental phenomena and even use them to build up technology.

In this thesis our motivation is to study the dynamics of certain quantum systems where the system is either in relativistic motion or subjected to relativistically modulated boundary conditions. Our aim is to look into some previously unexplored quantum physical phenomena, that are significant in context of quantum foundation or quantum information theory or both, in the above mentioned framework.

Our study explores the behaviour of quantum coherence, quantified by various resource theoretic measures, under relativistic boosts. Such study helps us to understand the consistency of various notions of coherence as a resource and their quantifiers in a fundamentally relativistic space-time background. Then we study resonance interaction between two atoms accelerating between two parallel mirrors. We analyse the possibility of manipulating radiative processes under combined effect of motion and boundary conditions in structured environments. Next we will study violation of weak equivalent principle introduced by Planck scale effect in practically realisable quantum electrodynamical systems. This study is not only fundamentally significant but also opens the possibility to constraining Planck scale physics in the simulated platforms. Next we study Bell nonlocality of particles produced out of vacuum by relativistically moving mirror (dynamical Casimir effect (DCE)) in a circuit quantum electrodynamical set-up. Our work shows the future possibilities to utilise nonlocality of DCE radiation as a resource. We have analysed and estimated our results using parameters from current and future technology. The thesis is organized as follows :

In the Chapter 2 we have reviewed the preliminary mathematical formulations of quantum systems in relativistic background, that is essential for our work. First we will discuss the transformation of a spin-1/2, momentum wave packet under successive noncollinear Lorentz boosts. Then we will review basic formulation of scalar QFT and discuss the phenomena of particle production, such as Unruh effect, Dynamical Casimir effect, by scalar quantum vacuum. We will also discuss the excitation of two level atom due to above particle production phenomena.

In Chapter 3, we will study the quantification of coherence of a spin-1/2 particle under successive noncollinear Lorentz boosts, using various resource theoretic quantifiers. This chapter is based on our publication in ref. [56].

In Chapter 4 we will study energy level shift and rate of change of energy due to resonance interaction of two atoms accelerating between two parallel mirrors. This chapter is based on our publication in ref. [57].

In Chapter 5 we will study violation of equivalence in an atom-mirror system in relative acceleration in presence of background quantum scalar vacuum that satisfy generalized uncertainty principle. This chapter is based on our publication in ref. [58].

In Chapter 6 we will study Bell's inequality violation by DCE radiation in superconducting microwave circuit. This chapter is based on our publication in ref. [59].

In Chapter 7 we will make concluding remarks and discuss future possibilities of work.

Chapter 2

Quantum state and observer in the relativistic background

In this chapter we will discuss how quantum state appears to an observer when the quantum system or the observer or both are undergoing relativistic motion. First we will consider the case when a particle with spin and an observer are in relatively inertial frames connected by Lorentz transformations. Our focus will be on the case when the rest frame of quantum system (state) is connected to the observer by two noncollinear Lorentz boosts resulting Wigner rotation. The spinor representation of Poincaré group is used to transform the quantum state in above mentioned scenario. We also discuss the representation and the properties of Wigner rotation and how it affects the spin of a relativistically moving particle. We then apply this formulation in case of a spinor with momentum wave packet to calculate the transformed density matrices of the particle in the spin bases.

Next we consider the observer in background quantum scalar field. This leads us to move from single particle to multi particle domain. In general quantum field is a fundamental entity attached to the fabric of the space-time. Quantum field has its own information content which is not always measurable or observable. In order to have the notion of measurement or observation of physical phenomena, the quantum theory requires the definition of particle. So, we discuss about the condition when an observer moving along certain space-time trajectory has the well defined notion of particles. This allow us to define multi-particle state (Fock state) in a covariant framework. Using this formulation we discuss how Fock state transforms under noninertial coordinate transformation induced by relative acceleration between the quantum state and the observer or by relativistic boundary condition imposed on the field. Such phenomena also result in par-

ticle production and generation of quantum correlation within the field modes. Our discussion will remain confined within particle production phenomena in flat space-time : the Unruh effect and the dynamical Casimir effect. We will also discuss the definition of Unruh-DeWitt detector and its spontaneous excitation as a result of above particle production phenomena. In this chapter we will use the convention of natural units. The convention of units in the subsequent works will be mentioned in the respective chapters.

The chapter is organized as follows : In Section 2.1 we will discuss the transformation of a spin-1/2, momentum wave packet under successive noncollinear Lorentz boosts. In Section 2.2 we will discuss scalar quantum field theory in noninertial frame.

2.1 Quantum state under relativistic boosts

Let us consider the vector space of positive energy, massive, single particle states in background Minkowski space-time with metric signature $\eta_{\mu\nu} = (+,-,-,-)$. This vector space furnishes the spinor representation space of inhomogeneous Lorentz group or Poincaré group [2, 5, 36, 60]. Poincaré group consists of ten generators associated to the complete set of symmetry transformations in special relativity. Among the generators, four are the linear momentum or the generators of translations $\{p^\mu\}$, three are the angular momentum or the generators of rotations $\{J^i\}$, and three are the generators of pure boosts $\{K^i\}$. In relativistic quantum mechanics, the spin of a particle is not Poincaré or Lorentz covariant and is well defined only in the rest frame of the particle. The spin-momentum of the particles are defined through the Casimir operators : momentum squared $P^2 = p^\mu p_\mu$ and square of Pauli-Lubanski vector $W^2 = W^\mu W_\mu$, where

$$W_\mu = \frac{1}{2}\epsilon_{\mu\nu\eta\kappa}J^{\nu\eta}p^\kappa, \tag{2.1}$$

$\epsilon_{\mu\nu\eta\kappa}$ is 4-dimensional Levi-Civita, $J^{\nu\eta}$ are the generators of the proper orthochronous Lorentz group with $J_{ij} = -J_{ji} = \epsilon_{ijk}J^k$, $J_{i0} = -J_{0i} = K_i$.

The bases of the spinor representation space are designated by $\{|\mathbf{p}, j\rangle\}$, where $\mathbf{p}$ is the spatial component of $\{p^\mu\}$ and j is the component of angular momentum along some quantisation axis and is equal to the intrinsic spin in the rest frame of the particle. The 4^{th} component of the momentum p^0 has not been used to label the state, as it is trivial through the dispersion relation $p^0 = \sqrt{\mathbf{p}^2 + m^2}$, m is the

rest mass of the particle. The normalization rule for the bases is defined as [5]

$$\langle \mathbf{p}', j' \mid \mathbf{p}, j \rangle = \boldsymbol{\delta}(\mathbf{p}' - \mathbf{p})\ \delta_{j'j}\ . \tag{2.2}$$

Let, the particle has momentum $(m, 0, 0, 0)$ in its rest frame and momentum p^μ with respect to the lab frame $\mathcal{O}$. Let, the observer $\mathcal{O}^\Lambda$ connected to $\mathcal{O}$ by Lorentz transformation Λ. The law of transformation of the state $|\mathbf{p}, j\rangle$ under the action of Lorentz transformation Λ is given by [5]

$$U(\Lambda)\,|\mathbf{p}, j\rangle = \sqrt{\frac{(\Lambda p)^0}{p^0}} \sum_{j'} D_{jj'}(W(\Lambda, \mathbf{p}))\,|\Lambda\mathbf{p}, j'\rangle \tag{2.3}$$

where $U(\Lambda)$ is the unitary representation of Λ, and j is considered to be discrete. The term $\Lambda\mathbf{p}$ represents the spatial component of the Lorentz transformed 4-momentum i.e., $(\Lambda\mathbf{p})^i = \Lambda^i_\nu\ p^\nu$. For massive spinor, the matrix $D_{jj'}(W(\Lambda, \mathbf{p})) \in SU(2)$ and has dimension $(2j+1) \times (2j+1)$. The linear momentum dependent rotation $W(\Lambda, \mathbf{p}) \in SO(3)$ is the element of Wigner's little group which is a subgroup of $SO(3)$ [5]. Eq. (2.3) is a group homomorphism which shows that under the action of Lorentz transformation the single basis state (with respect to $\mathcal{O}$), transforms into a superposition of angular momentum states with linear momentum dependent coefficients (with respect to $\mathcal{O}^\Lambda$).

2.1.1 Wigner's little group

Let the basis state, at the rest frame of the particle is labelled as $|\mathbf{0}, s\rangle$ where s is the spin of the particle in the rest frame. Let, $L(p)$ is the pure Lorentz boost that transforms the rest frame energy-momentum to the frame $\mathcal{O}$. Thus,

$$|\mathbf{p}, s\rangle = U(L(p))\,|\mathbf{0}, s\rangle \tag{2.4}$$

where $U(L(p))$ is the unitary representation of $L(p)$. Now, L.H.S of Eq. (2.3) in this case, can be written as [61]

$$\begin{aligned} U(\Lambda)\,|\mathbf{p}, s\rangle &= U(\Lambda)U(L(p))\,|\mathbf{0}, s\rangle \\ &= U(L(\Lambda p))U(L^{-1}(\Lambda p))U(\Lambda)U(L(p))\,|\mathbf{0}, s\rangle \\ &= U(L(\Lambda p))U(W(\Lambda, \mathbf{p}))\,|\mathbf{0}, s\rangle \\ &= U(W(\Lambda, \mathbf{p}))\,|\Lambda\mathbf{p}, s\rangle \end{aligned} \tag{2.5}$$

where we have used the properties of group homomorphism and

$$W(\Lambda, \mathbf{p}) = L^{-1}(\Lambda p)\Lambda L(p). \tag{2.6}$$

From Eq. (2.6) we see that $W(\Lambda, \mathbf{p})$ transforms the rest frame energy-momentum to an arbitrary momentum p (via pure boost $L(p)$), then from p to Λp (via the transformation Λ) and again brings back to the rest frame (via pure boost $L^{-1}(\Lambda p)$). So, the operator $W(\Lambda, \mathbf{p})$ can at most produce a spatial rotation, known as the Wigner rotation, between initial and final rest frame energy-momentum [36, 61]. Hence in Eq. (2.5) the operator $U(L(\Lambda p))$ acts on the momentum basis whereas the operator $U(W(\Lambda, \mathbf{p}))$ causes momentum dependent rotation in the spin basis resulting expression like in Eq. (2.3).

For a massive particle, the standard boost in the direction $\hat{\mathbf{p}} = \mathbf{p}/|\mathbf{p}|$, is parametrized as [36]

$$\begin{aligned}
L(p)^0{}_0 &= \cosh\beta = \frac{p^0}{m} \\
L(p)^0{}_i &= \sinh\beta\ \hat{p}^i = \frac{p^i}{m}\ \hat{p}^i \\
L(p)^i{}_0 &= -\sinh\beta\ \hat{p}_i \\
L(p)^i{}_j &= \delta^i{}_j - (\cosh\beta - 1)\ \hat{p}^i\hat{p}_j
\end{aligned} \tag{2.7}$$

where $\hat{p}^i$ is the i^{th} component of the unit momentum vector $\hat{\mathbf{p}}$. The parameter β is the rapidity parameter. Now let us consider the case of the particle in its rest frame. A standard boost $L(p)$ is applied in an arbitrary direction say $\hat{\mathbf{f}}$. The 4-momentum of the particle can be expressed as

$$p^\mu = (m\cosh\beta, m\sinh\beta\ \hat{\mathbf{f}}) \tag{2.8}$$

Then the particle is subjected to another boost Λ with rapidity α in the direction $\hat{\mathbf{e}}$. Then the particle is brought back to its rest frame via the Lorentz boost $L^{-1}(\Lambda\mathbf{p})$. The $SU(2)$ representation of Wigner rotation matrix in this case can be expressed in terms of the rapidity parameters as [62, 63]

$$D(W(\Lambda, \mathbf{p})) = \cos\frac{\phi}{2}\mathbb{1} + i\sin\frac{\phi}{2}(\boldsymbol{\Sigma}\cdot\hat{\mathbf{n}}) \tag{2.9}$$

where

$$\cos\frac{\phi}{2} = \frac{\cosh\frac{\alpha}{2}\cosh\frac{\beta}{2} + \sinh\frac{\alpha}{2}\sinh\frac{\beta}{2}(\hat{\mathbf{e}}\cdot\hat{\mathbf{f}})}{\sqrt{\frac{1}{2} + \frac{1}{2}\cosh\alpha\cosh\beta + \frac{1}{2}\sinh\alpha\sinh\beta(\hat{\mathbf{e}}\cdot\hat{\mathbf{f}})}}$$
$$\sin\frac{\phi}{2}\hat{\mathbf{n}} = \frac{\sinh\frac{\alpha}{2}\sinh\frac{\beta}{2}(\hat{\mathbf{e}}\times\hat{\mathbf{f}})}{\sqrt{\frac{1}{2} + \frac{1}{2}\cosh\alpha\cosh\beta + \frac{1}{2}\sinh\alpha\sinh\beta(\hat{\mathbf{e}}\cdot\hat{\mathbf{f}})}} \tag{2.10}$$

with vector $\mathbf{\Sigma} = (\Sigma^1, \Sigma^2, \Sigma^3)$, $\{\Sigma^i\}$ are the Pauli matrices, ϕ and $\hat{\mathbf{n}}$ being respectively, the angle and axis of Wigner rotation. Eq. (2.10) shows that Wigner rotation depends upon the magnitude of the rapidity parameters and the angle between the two boosts. The rotation is zero when $\hat{\mathbf{e}}$ and $\hat{\mathbf{f}}$ are parallel (or anti-parallel) i.e., the boosts $L(p)$ and Λ are collinear. Wigner rotation arises when a particle is subjected to two or more non-collinear Lorentz boosts. This is due to the fact that the subset of Lorentz boosts is not a subgroup of the Lorentz group [61, 63]. In general the product of two arbitrary Lorentz boosts $\{\Lambda(\alpha_i)\}$ can be expressed as the product of a pure boost and a spatial rotation $R(\Omega)$

$$\Lambda(\alpha_1)\cdot\Lambda(\alpha_2) = R(\Omega)\cdot\Lambda(\alpha_3) \tag{2.11}$$

2.1.2 Momentum wave packet of spinor under relativistic boosts

A pure single particle state with momentum-space wave function $\psi(\mathbf{p})$ and spin $|s\rangle$ may be written as

$$|\psi\rangle = \sum_s \int d\mathbf{p}\ \psi(\mathbf{p})\,|\mathbf{p}\rangle \otimes a_s\,|s\rangle \tag{2.12}$$

with respect to the reference frame $\mathcal{O}$. An observer in the frame $\mathcal{O}^\Lambda$ will see the state in Eq. (2.12) as

$$|\psi^\Lambda\rangle = \sum_s \int d\mathbf{p}\ \sqrt{\frac{(\Lambda p)^0}{p^0}}\psi(\mathbf{p})\ a_s \sum_{s'} D_{ss'}(W(\Lambda,\mathbf{p}))\,|\Lambda\mathbf{p}, s'\rangle \tag{2.13}$$

where we have used the definition in Eq. (2.3). The state $|\psi\rangle$ in Eq. (2.12) is separable in spin and momentum. However in the state $|\psi^\Lambda\rangle$ in Eq. (2.13), the spin basis states have momentum dependent coefficients resulting entanglement in spin and momentum bases. This is known as the spin-momentum entanglement [30, 32].

The density matrix corresponding to the state $|\psi\rangle$ is given by

$$\rho = \sum_{s_1,s_2} \int\int d\mathbf{p}_1 d\mathbf{p}_2 \; \psi(\mathbf{p}_1)\psi^*(\mathbf{p}_2) \; a_{s_1} a^*_{s_2} \, |\mathbf{p}_1, s_1\rangle \, \langle \mathbf{p}_2, s_2| \, . \tag{2.14}$$

Tracing out the momentum degrees of freedom we get the spin reduced density matrix (SRDM) [30,62], given by

$$\rho_s = \sum_{s_1,s_2} \int\int d\mathbf{p} \; \psi(\mathbf{p})\psi^*(\mathbf{p}) \; a_{s_1} a^*_{s_2} \, |s_1\rangle \, \langle s_2| \, . \tag{2.15}$$

The density matrix corresponding to the state $|\psi^\Lambda\rangle$ is given by

$$\begin{aligned} \rho^\Lambda = \sum_{s_1,s_2} \int\int d\mathbf{p}_1 d\mathbf{p}_2 \; \sqrt{\frac{(\Lambda p_1)^0 \; (\Lambda p_2)^0}{p_1^0 \; p_2^0}} \; \psi(\mathbf{p}_1)\psi^*(\mathbf{p}_2) a_{s_1} a^*_{s_2} \\ \sum_{s_1',s_2'} D_{s_1 s_1'}(W(\Lambda, \mathbf{p}_1)) \, |\Lambda\mathbf{p}_1, s_1'\rangle \, \langle \Lambda\mathbf{p}_2, s_2'| \, D^\dagger_{s_2 s_2'}(W(\Lambda, \mathbf{p}_2)) \; . \end{aligned} \tag{2.16}$$

The SRDM corresponding to ρ^Λ is

$$\rho^\Lambda_s = \sum_{\substack{s_1,s_2,\\ s_1',s_2'}} \int d\mathbf{p} \; |\psi(\mathbf{p})|^2 D_{s_1 s_1'}(W(\Lambda, \mathbf{p})) \, |s_1'\rangle \, \langle s_2'| \, D^\dagger_{s_2 s_2'}(W(\Lambda, \mathbf{p})) \tag{2.17}$$

where we have used the relation $\delta(\Lambda\mathbf{p}_1 - \Lambda\mathbf{p}_2) = \frac{(p_1)^0}{(\Lambda p_1)^0}\delta(\mathbf{p}_1 - \mathbf{p}_2)$. Since ρ^Λ is spin-momentum entangled, tracing out the momentum variable will introduce mixedness in the state ρ^Λ_s. Hence observer in $\mathcal{O}^\Lambda$ will observe decoherence if the measurement is performed in its spin bases [30]. The state ρ^Λ_s is not Lorentz covariant, as the transformation law of the spin variables depends not only upon the Lorentz transformation Λ, but also upon the momentum variables $\mathbf{p}$.

2.2 Observer in background quantized vacuum

In this section we will move from single particle picture to multi particle Hilbert space of quantum field modes [35,36]. Let us consider quantized, real, massless scalar field $\phi(t, z)$ in $(1 + 1)$ dimensional Minkowski space-time with metric signature $\eta_{\mu\nu} = (+, -)$. The field obeys massless Klein-Gordon equation given by

$$\partial_\mu \left(\eta^{\mu\nu}\partial_\nu \phi\right) = (\partial_t^2 - \partial_z^2) \; \phi(t, z) = 0 \tag{2.18}$$

which can be derived from the Lagrangian density of the field

$$\mathscr{L} = \frac{1}{2}\partial^{\mu}\phi\ \partial_{\mu}\phi. \tag{2.19}$$

For being the quatized field, $\phi(t,z)$ and its conjugate momentum $\Pi(t,z) = \frac{\partial\mathscr{L}}{\partial(\partial_t\phi)} = \partial_t\phi$ are treated as operators which satisfy the commutation relations

$$\begin{aligned}\left[\hat{\phi}(t,z_1),\hat{\phi}(t,z_2)\right] &= \left[\hat{\Pi}(t,z_1),\hat{\Pi}(t,z_2)\right] = 0\\ \left[\hat{\phi}(t,z_1),\hat{\Pi}(t,z_2)\right] &= i\delta(z_1-z_2).\end{aligned} \tag{2.20}$$

The notion of particles as excited field quanta requires the existence of time-like Killing vector field. Let, the metric $g_{\mu\nu}$ of some space-time undergoes the space-time transformation such that the functional form of the metric remains invariant. In that case the space-time transformation is a symmetry transformation known as isometry [64]. Let us consider an infinitesimal space-time transformation $\tilde{z}^{\mu} = z^{\mu} + \delta u Z^{\mu}$, δu is a small parameter. If isometry holds i.e.,

$$g_{\mu\nu}(\mathrm{z}) \to g'_{\mu\nu}(\tilde{\mathrm{z}}) = g_{\mu\nu}(\tilde{\mathrm{z}}) \tag{2.21}$$

where $z^{\mu} \equiv \mathrm{z}$, then the vector field Z^{μ} is known as the **Killing vector** field. It can be shown mathematically that Eq. (2.21) is satisfied iff [64]

$$\mathcal{L}\ g_{\mu\nu}(\mathrm{z}) = Z^{\kappa}\partial_{\kappa}\ g_{\mu\nu} + g_{\mu\kappa}\ \partial_{\nu}Z^{\kappa} + g_{\nu\kappa}\ \partial_{\mu}Z^{\kappa} = 0\ , \tag{2.22}$$

the operator $\mathcal{L}$ is the Lie derivative. So, Z^{μ} is a Killing vector field iff $\mathcal{L}\ g_{\mu\nu}(\mathrm{z}) = 0$. If $g_{\mu\nu} = \eta_{\mu\nu}$ and Z^{μ} is time-like i.e., $Z^{\mu}Z_{\mu} > 0$, then the Lie derivative corresponds to the operator ∂_t.

If a space-time admits time-like Killing vector field, then we can find a basis for solution u_k of Klein-Gordon equation [35,36], such that

$$\mathcal{L}\ u_k = Z^{\mu}\partial_{\mu}u_k = \partial_t u_k = -i\omega_k u_k\ , \quad (\omega_k > 0), \tag{2.23}$$

ω_k is a constant. So, we can rewrite above equation as

$$\begin{aligned}\partial_t u_k &= -i\omega_k u_k\ ,\\ \partial_t u_k^* &= i\omega_k u_k^*\ .\end{aligned} \tag{2.24}$$

From equation above we see that one possible solution of Eq. (2.18) will be the

plane wave solution

$$u_k(z,t) = \frac{1}{\sqrt{2\pi\omega_k}}\, e^{i(kz-\omega_k t)} \tag{2.25}$$

where $\omega_k = |k|$. So, we identify ω_k as the frequency associated to the k^{th} mode function u_k. We can identify u_k and u_k^* as positive and negative frequency solutions respectively. The mode functions $\{u_k(z,t)\}$ form a complete set of orthonormal basis with respect to the Lorentz invariant inner product –

$$(g_1, g_2) = i \int dz\ (g_1^*(\partial_t g_2) - g_2^*(\partial_t g_1)). \tag{2.26}$$

Hence the mode functions satisfy following relations

$$\begin{aligned} (u_k, u_{k'}) &= \delta(k-k') \\ (u_k^*, u_{k'}^*) &= -\delta(k-k') \\ (u_k, u_{k'}^*) &= 0\ . \end{aligned} \tag{2.27}$$

The positive and negative frequency solutions are associated to particle and anti-particle sector respectively. Time-like vectors remain time-like under Lorentz transformation and hence the separation of modes into positive and negative frequency part also remains unchanged. So, the notion of particle is well-defined for an observer moving along time like killing vector field [35,36]. If a space-time does not admit Killing field, the separation of modes into positive and negative frequency will be different in different space-time point and the notion of particles will be ambiguous.

Using the positive frequency solutions mentioned above, we can construct Fock space of particles. Mode expansion of $\phi(z,t)$ is given by

$$\hat{\phi}(z,t) = \int dk \left(u_k \hat{a}_k + u_k^* \hat{a}_k^\dagger\right), \tag{2.28}$$

where $\hat{a}_k^\dagger, \hat{a}_k$ are creation and annihilation operators associated with k^{th}-mode and satisfy commutation relations

$$\begin{aligned} \left[\hat{a}_k, \hat{a}_{k'}^\dagger\right] &= \delta(k-k'), \\ \left[\hat{a}_k, \hat{a}_{k'}\right] &= \left[\hat{a}_k^\dagger, \hat{a}_{k'}^\dagger\right] = 0. \end{aligned} \tag{2.29}$$

The Fock bases can be constructed by the action of creation and annihilation

operators on field vacuum state $|0\rangle$ defined by

$$\hat{a}_k |0\rangle = 0. \tag{2.30}$$

A multi particle state with occupation number n_i in the k^{th}-mode is given by

$$|n_1^1, ..., n_i^k\rangle = \prod_i \frac{(\hat{a}_k^\dagger)^{n_i}}{\sqrt{n_i!}} |0\rangle . \tag{2.31}$$

The Hamiltonian of the system is

$$\hat{H} = \sum_k \omega_k \left(\hat{\mathcal{N}}_k + \frac{1}{2}\right), \tag{2.32}$$

where $\hat{\mathcal{N}}_k = \hat{a}_k^\dagger \hat{a}_k$ is the number operator.

Since the timelike killing vector field ∂_t is not unique, there can be another $\partial_{t'}$ and hence corresponding set of orthonormal modes $\{v_k(z,t)\}$ that can also span solutions of the Klein-Gordon equation

$$\hat{\phi}(z,t) = \int dk \left(v_k \hat{b}_k + v_k^* \hat{b}_k^\dagger\right) \tag{2.33}$$

where $\hat{b}_k^\dagger, \hat{b}_k$ are creation and annihilation operators associated with k^{th}-mode. We can construct a new Fock basis by the action this new set of creation and annihilation operators on corresponding vacuum $|\tilde{0}\rangle$ defined as

$$\hat{b}_k |\tilde{0}\rangle = 0. \tag{2.34}$$

Transformation law between the two sets of creation and annihilation operators is given by [3, 35, 36]

$$\hat{a}_k = \int dk' \left(\alpha_{kk'}^* \, \hat{b}_{k'} - \beta_{kk'}^* \, \hat{b}_{k'}^\dagger\right). \tag{2.35}$$

This transformation is linear and known as Bogolyubov transformation. $\alpha_{kk'} = (u_k, v_{k'})$ and $\beta_{kk'} = -(u_k, v_{k'}^*)$ are known as Bogolyubov coefficients. The transformation law between $\{u_k(z,t)\}$ and $\{v_k(z,t)\}$ can be obtained using Eq. (2.30), Eq. (2.34). Now we apply number operator of the un-tilded basis on the vacuum state in the tilded basis

$$\langle\tilde{0} \mid \hat{\mathcal{N}}_k \mid \tilde{0}\rangle = \langle\tilde{0} \mid \hat{a}_k^\dagger \hat{a}_k \mid \tilde{0}\rangle = \int dk |\beta_{kk'}|^2, \tag{2.36}$$

So, as long as $\beta_{kk'} \neq 0$, vacuum state in tilded basis will be populated with respect to un-tilded basis and vice-versa.

2.2.1 Observer in uniform acceleration : Unruh effect

In flat space-time the trajectory of the inertial observer and uniformly accelerated (Rindler) observer admits time-like Killing vector field and have well defined notion of particles [3, 35, 36]. The trajectory of uniformly accelerated observer is a hyperbola and parametrized by Rindler coordinates (η, χ) as

$$t = \frac{e^{a\chi}}{a} \sinh a\eta \qquad\qquad z = \frac{e^{a\chi}}{a} \cosh a\eta \tag{2.37}$$

where $ae^{-a\chi}$ is observers proper acceleration and a is an arbitrary reference acceleration. Associated metric

$$ds^2 = e^{2a\chi} \left(d\eta^2 - d\chi^2\right) \tag{2.38}$$

is known as Rindler metric. A Rindler observer with $\chi = 0$ has proper time η and proper acceleration a. This is the maximum attainable value of acceleration by an observer whose motion is described by Eq. (2.37). Figure (2.1) shows trajectory of an observer Alice who is at rest in Minkowski space-time and the Rindler observer Rob. $\chi = constant$ gives the hyperbolic trajectories and $\eta = constant$ are the straight lines passing through the origin. The trajectories in Eq. (2.37) describes only the region within $z > |t|$ known as right Rindler wedge (region R in the Figure (2.1)). The region within $z < |t|$ (region L in the Figure (2.1)) is known as the left Rindler wedge, which can be obtained by reflecting right rindler wedge in t axis (by transformation $t \to -t$) and then in z axis (by transformation $z \to -z$) respectively [3]. The region R and L are causally disconnected by the past and future horizon ($z = \pm t$) of Minkowski lightcone. Proper time of a Rindler observer Rob in the right Rindler wedge flows forward with the Minkowski time and the proper time of a Rindler observer AntiRob in the left Rindler wedge flows backward relative to the Minkowski time. As $\eta \to \pm\infty$ the trajectory of Rindler observer becomes asymptotic with the Minkowski horizon i.e., the velocity of observer approaches the speed of light.

The massless Klein-Gordon equation in Rindler space-time is

$$\left(\partial_\eta^2 - \partial_\chi^2\right) \phi(\eta, \chi) = 0 \tag{2.39}$$

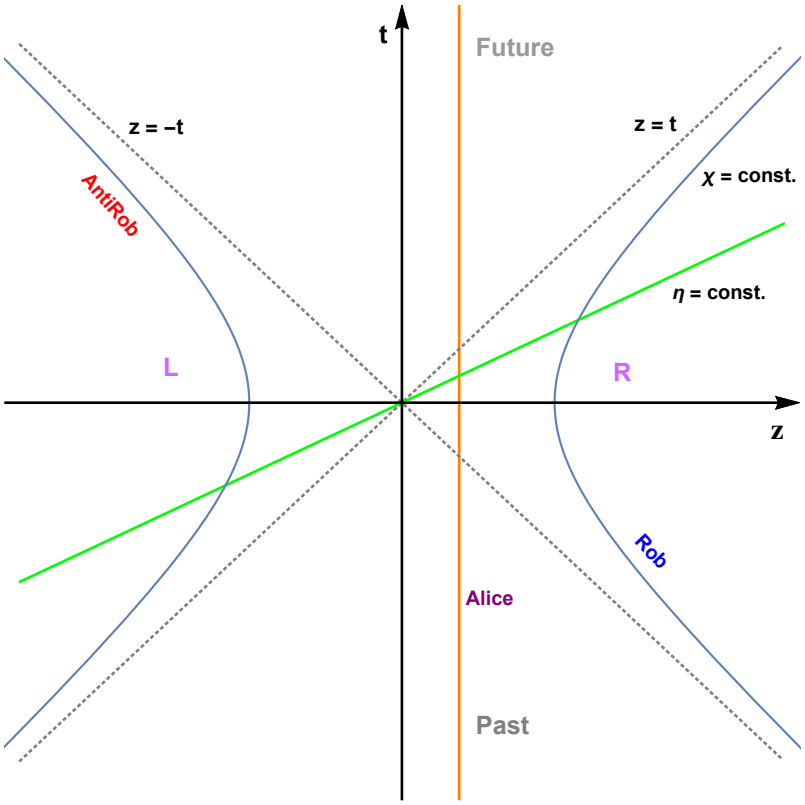

Figure 2.1: Observer trajectories in Rindler space-time: $\chi = constant$ are hyperbolae and $\eta = constant$ are straight lines passing through origin. The trajectory of uniformly accelerated observer Rob is a hyperbola constrained to either the right Rindler wedge (region - R) or the left Rindler wedge (region - L).

The solution of Eq. (2.39) is

$$\begin{aligned} v_k^R &= \frac{1}{\sqrt{2\pi\omega_k}}\, e^{i(k\chi-\omega_k\eta)} \\ v_k^L &= \frac{1}{\sqrt{2\pi\omega_k}}\, e^{i(k\chi+\omega_k\eta)} \end{aligned} \tag{2.40}$$

where $\omega_k = |k|$, v_k^R and v_k^L are positive frequency orthonormal modes in right and left Rindler wedges,which along with their complex conjugates furnish a complete set of orthonormal basis. The mode expansion of scalar field $\phi(\chi, \eta)$ is given by

$$\phi(\chi,\eta) = \int dk \left(v_k^R\ \hat{b}_k^R + v_k^L\ \hat{b}_k^L + hc. \right). \tag{2.41}$$

The Rindler vacuum is defined as

$$|0^{\mathcal{R}}\rangle = |0\rangle_R \otimes |0\rangle_L \tag{2.42}$$

where

$$\hat{b}_k^R |0\rangle_R = \hat{b}_k^L |0\rangle_L = 0 \ . \tag{2.43}$$

Following Eq. (2.35) we can define Bogolyubov transformation between the states of the Minkowski and the Rindler space-time respectively. The Bogolyubov coefficients are given by

$$\begin{aligned} \alpha^R_{kk'} &= (u_k^{\mathcal{M}}, v^R_{k'}) \qquad \beta^R_{kk'} = -(u_k^{\mathcal{M}}, (v^R_{k'})^*) \\ \alpha^L_{kk'} &= (u_k^{\mathcal{M}}, v^L_{k'}) \qquad \beta^L_{kk'} = -(u_k^{\mathcal{M}}, (v^L_{k'})^*) \end{aligned} \tag{2.44}$$

where $\{u_k^{\mathcal{M}}\}$ are the mode functions in the Minkowski space-time. However, calculation of Bogolyubov coefficients using above formulae are mathematically tedious. Hence a new basis, known as Unruh basis is introduced [3, 35, 36]

$$v_k^U = \cosh r \ v_k^R + \sinh r \ (v_k^L)^* \tag{2.45}$$

where $\tanh r = e^{-(\pi\omega_k/a)}$. The expression above shows that Unruh basis is a linear combination of solutions in the region R and L. Hence Unruh modes are analytic in both right and left Rindler wedges. It can be shown mathematically that Unruh vacuum coincides with Minkowski vacuum $|0^{\mathcal{M}}\rangle$ which can be expressed as [35, 36]

$$|0^{\mathcal{M}}\rangle = \frac{1}{\cosh r} \sum_{n=0}^{\infty} (\tanh r)^n \ |n^k\rangle^R |n^k\rangle^L \tag{2.46}$$

where $|n^k\rangle^{R\ (L)}$ are the number state corresponding to k^{th}-mode in the Rindler space. Eq. (2.46) represents a two mode squeezed state with squeezing parameter $r = \tanh^{-1}(e^{-(\pi\omega_k/a)})$. So, the modes of region L and R are entangled with respect to the Rindler observer. Since region L and R are causally disconnected no Rindler observer can access the full state described by RHS of Eq. (2.46). The density matrix corresponding to this state is $\rho^{\mathcal{M}}_{vac} = |0^{\mathcal{M}}\rangle \langle 0^{\mathcal{M}}|$. Tracing out the states in region L we get [35, 36]

$$\rho_U^R = \frac{1}{\cosh^2 r} \sum_{n=0}^{\infty} (\tanh r)^{2n} \ |n^k\rangle \langle n^k| \ . \tag{2.47}$$

The state ρ_U^R is a thermal state with mean photon number

$$\bar{n} = \sinh^2 r = \left(e^{2\pi\omega_k/a} - 1\right)^{-1} = \left(e^{\omega_k/k_B T_U} - 1\right)^{-1} \tag{2.48}$$

with k_B is the Boltzmann constant and $T_U = \frac{a}{2\pi k_B}$ is the Unruh temperature. Hence the Minkowski vacuum will appear as a thermal state to an uniformly accelerated observer. This phenomenon is known as the **Unruh effect**.

2.2.2 Unruh-DeWitt detectors

In the previous two sections we have defined quantum field state that can contain information by means of excited field quanta or correlations among the modes. However we cannot perform projective measurement on the global field modes which extend infinitely throughout the space-time. So, the observer needs some physical probe to measure information content in the field modes. In general a particle detector is used as such a probe. The particle detector is a nonrelativistic system that can access the information content of the quantum field by locally interacting with the field modes. The basic and most commonly used particle detector is the Unruh-DeWitt detector [3, 36, 49, 65].

The Unruh-DeWitt detector is a point-like system with internal degree of freedom that covariantly couples with the second quantized field modes. The detector-field coupling is local.

Physically an Unruh-DeWitt detector could be a two level system or a harmonic oscillator [36]. In our studies we will focus on two level system such as an atom with energy levels – ground state $|g\rangle$ and excited state $|e\rangle$. The difference in energy between the two levels is

$$\Delta E = E_e - E_g = \omega_0 \ . \tag{2.49}$$

The interaction Hamiltonian in the frame of the atom is given by [66]

$$\begin{aligned}\hat{H}_I(\tau) &= \lambda\ \hat{\mu}(\tau)\ \hat{\phi}(t(\tau), z(\tau)) \\ &= \frac{i}{2}\lambda \int dk\ \left(\hat{\sigma}^- e^{-i\omega_0\tau} - \hat{\sigma}^+ e^{i\omega_0\tau}\right)\ \left(\hat{a}\ e^{i(kz(\tau)-\omega_k t(\tau))} + \hat{a}^\dagger\ e^{-i(kz(\tau)-\omega_k t(\tau))}\right)\end{aligned} \tag{2.50}$$

where $\hat{\mu}(\tau) = \frac{i}{2}\left(\hat{\sigma}^- e^{-i\omega_0\tau} - \hat{\sigma}^+ e^{i\omega_0\tau}\right)$ is the monopole moment of the detector. $\hat{\sigma}^+ = |e\rangle\langle g|$ and $\hat{\sigma}^- = |g\rangle\langle e|$ are the atomic ladder operators corresponding to its internal degree of freedom. τ is the proper time of the detector moving along space-time trajectory $(t(\tau), z(\tau))$. The constant λ is the coupling strength of the

detector with the field modes.

Let us assume that $\hat{\phi}$ is in Minkowski vacuum state $|0^{\mathcal{M}}\rangle$. If the detector is in a noninertial frame, $|0^{\mathcal{M}}\rangle$ will appear excited to it. Now the detector, in its ground state $|g\rangle$, can absorb excited field quanta and go to the excited state $|e\rangle$ when $|0^{\mathcal{M}}\rangle$ will go to the excited output state $|E\rangle$. Hence an observer in Minkowski space-time will observe the emission of Minkowski particle which is known as **acceleration radiation** [67]. For small λ, the transition amplitude of the detector is given by [3]

$$\mathcal{A} = i \int d\tau \, \langle E, e|\hat{H}_I(\tau)|g, 0^{\mathcal{M}}\rangle \, . \tag{2.51}$$

The transition probability of the detector is

$$\begin{aligned} \mathcal{P} &= \sum_E |\mathcal{A}|^2 \\ &= \lambda^2 \int d\tau \int d\tau' e^{-i\omega_0(\tau-\tau')} \, W(\tau, \tau') \end{aligned} \tag{2.52}$$

where $W(\tau, \tau')$ is the positive frequency Wightman function given by

$$W(\tau, \tau') = \langle 0^{\mathcal{M}}|\hat{\phi}(t(\tau), z(\tau))\hat{\phi}(t(\tau'), z(\tau'))|0^{\mathcal{M}}\rangle \, . \tag{2.53}$$

The Unruh-DeWitt detector model considered above assumes a basic picture of light-matter interaction. However we have considered scalar field instead of electromagnetic field in order to keep our calculation simple in the context of QFTCS. In case of scalar field, the detector-field coupling strength λ is a scalar quantity. In case of electromagnetic field the λ will be replaced by a vector quantity (dipole moment in case of a two level atom) and such dipolar coupling is responsible for exchange of angular momentum between detector and field [68–70]. Such physics will be missing in the scalar field model we have considered in this thesis.

Also in case of the detector, several additional effects could have been considered that would make the model more realistic. The detector-field interaction Hamiltonian in Eq. (2.50) is oblivious to the transient effect that arises while turning the detector on or off. Such effect is useful when the detector is interacting for finite interval of time. However the studies performed in this thesis assumes that the detector- field interaction is occurring for infinitely long interval. We have assumed the Unruh-DeWitt detector to be point-like. In reality the particle detector will have a finite size which will cause spatial smearing of the

detector. Such effect has to be considered in the interaction Hamiltonian if we go beyond the idea of point-like detector. The centre of mass of the detector is classical in the model considered above. In principle the centre of mass degree of freedom of an Unruh-DeWitt detector should be quantized. In such cases the detector-field dynamics will induce entanglement between centre of mass degree of freedom and internal degree of freedom of the detector. Nevertheless the basic model we have considered here successfully describes the fundamental aspects of detector-field interaction in curved space-time.

2.2.3 Quantum vacuum subjected to moving boundary: Dynamical Casimir effect

The quantum field considered so far is unbounded. Let us now consider the quantized scalar field $\phi(t, z)$ in presence of an infinite, plane, moving mirror (perfectly reflecting boundary) in the $(1 + 1)$-Minkowski space-time. The mirror imposes time dependent Dirichlet boundary condition to the quantum field residing in the same space-time :

$$\phi(t, z_m(t)) = 0 \tag{2.54}$$

where $z_m(t)$ is the trajectory of the mirror in Minkowski space-time. For appropriate choice of mirror trajectory (for example an accelerated mirror), such boundary conditions cause particle production from quantum vacuum.

In $(1+1)$-dimensions all space-time are conformally Minkowski [71] i.e. , their metric $g_{\mu\nu}$ can be expressed as

$$g_{\mu\nu}(\mathrm{z}) = \varsigma^2(\mathrm{z})\ \eta_{\mu\nu}\ . \tag{2.55}$$

For massless scalar field in $(1 + 1)$-dimensions, the Klein-Gordon equation is conformally invariant and its solutions can be mapped to the solutions of Klein-Gordon equation in the flat space-time. This fact can be exploited in case of quantum field subjected to time dependent boundary condition in $(1 + 1)$ dimensions mentioned in the previous paragraph.

Let us consider the conformal transformation [9, 11]

$$\begin{aligned} t - z &= f(\bar{t} - \bar{z}) \\ t + z &= g(\bar{t} + \bar{z})\ . \end{aligned} \tag{2.56}$$

Above transformation preserves the light cone and the metric remains conformally

flat

$$dt^2 - dz^2 = f'(\bar{t} - \bar{z})\ g'(\bar{t} + \bar{z})\ (d\bar{t}^2 - d\bar{z}^2). \tag{2.57}$$

The massless Klein-Gordon equation is given by Eq. (2.18) with t and z replaced by $\bar{t}$ and $\bar{z}$ respectively. Let us now demand that the mirror trajectory $z = z_m(t)$ in the Minkowski frame corresponds to $\bar{z} = 0$ in the conformal frame. So, the boundary condition on the quantum field in the conformal frame is given by

$$\phi(\bar{t}, 0) = 0. \tag{2.58}$$

This condition cannot hold for any f, g and results in the constraint [9,11]

$$\frac{1}{2}\left[g(\bar{t}) - f(\bar{t})\right] = z_m\left(\frac{1}{2}\left[g(\bar{t}) + f(\bar{t})\right]\right). \tag{2.59}$$

So, in the conformal frame the problem reduces to quantized scalar field in presence of static Dirichlet boundary condition. The normalised solution of the Klein-Gordon equation is given by [9,11]

$$u_k^{out}(\bar{z}, \bar{t}) = \frac{1}{\sqrt{4\pi\omega_k}}\left[e^{-i\omega_k g^{-1}(t+z)} - e^{-i\omega_k f^{-1}(t-z)}\right] \tag{2.60}$$

which forms complete set of orthonormal basis $\{u_k^{out}\}$ (outgoing mode functions). The mode expansion of the field operator can be written as

$$\begin{aligned}\hat{\phi}(t, z) &= \int dk\left(u_k^{out}\ \hat{a}_k^{out} + (u_k^{out})^*\ (\hat{a}_k^{out})^\dagger\right) \\ &= \int dk'\left(u_{k'}^{in}\ \hat{a}_{k'}^{in} + (u_{k'}^{in})^*\ (\hat{a}_{k'}^{in})^\dagger\right)\ ,\end{aligned} \tag{2.61}$$

$\{u_k^{in}\}$ is the set of incoming mode functions in the Minkowski frame and also forms a complete basis. The incoming and outgoing modes are connected by Bogolyubov transformation given by the definitions in Eq. (2.35). Using the Bogolyubov coefficients and Eq. (2.36), it can be shown that the vacuum state of the outgoing field modes will appear excited in the basis of incoming modes. This phenomenon is known as the **dynamical Casimir effect** (DCE). The phenomenon were discovered by G. T. Moore in 1970 and hence DCE is also known as Moore effect. Moore's work shows the production of photons in an empty cavity by an oscillating mirror. For nonrelativistic motion of mirror the rate of particle production is very very small. Afterwards, DeWitt [10], Fulling and Davies [11] have generalized moving mirror problem in the framework of quantum field theory in the curved space-time.

Similar to the case of Unruh effect, DCE also generates entanglement within the field modes resulting two mode squeezed state. We will discuss about the explicit form of the state in a specific set-up later in Chapter 6 of this thesis.

Chapter 3

Quantification of coherence of a single particle spinor state under relativistic boosts

Quantum physics is based on the fact that state of a quantum system can be described as a superposition of basis states of certain Hilbert space. Such feature has made the physics of quantum systems different from classical physics. Such ability of a single quantum system to remain in superposed state gives rise to the quantum correlation known as quantum coherence.

The notion of coherence comes from the study of interference phenomena in classical electromagnetic fields. The interference phenomena is a consequence of wave nature of a physical system. The interference pattern depends upon the correlation between the phase of the interfering wave(s). This correlation is known as coherence. With the development of quantum theory of electromagnetic fields, the notion of coherence has also found its way in the quantum regime. The coherence of quantized light is characterized by correlations within electromagnetic fields at two different space-time points. Such study has brought tremendous development in the field of optical technology as well as in the foundation of quantum physics. Quantum coherence in electromagnetic field gives rise to the phenomena such as photoelectric effect, laser, maser etc. [72].

The quantum theory of light assumes wave particle duality of photons. The extension of this notion in case of material particles such as electrons, neutral atoms etc., gave birth to the matter wave that obeys the laws of quantum mechanics. The wave picture of a quantum particle have similar notions as optics such as: a single particle can undergo interference and diffraction. There exists quantum

correlation (coherence) among the superposed basis states that describes the state of the particle. The quantum coherence is responsible for existence of other type of quantum correlation such as entanglement, steering etc. The significance of the quantum coherence is not limited within the theory of quantum foundations. With the development of quantum information theory quantum coherence has become an important resource for future quantum technology [73].

In order to exploit the quantum correlation as a resource to perform quantum tasks, quantum information theory brings the correlations into an operational framework. Such operational theories of quantum correlations are known as resource theory [73–80]. In general the aim of the resource theories is to study the conditions under which quantum operations can be performed on the quantum systems containing the correlation such that the loss of correlation is avoided [73]. The resource theory of quantum coherence analyses the cost of resource required to achieve certain quantum task when we have no means available to generate quantum coherence [73]. A rigorous mathemetical formulation of resource theory of coherence is based on the characterization of quantum state, quantifying the resource contained within the state and manipulating the state under the generic constraints imposed by the physical system under consideration [73,81].

Several resource theories of quantum coherence have been proposed so far where the term coherence has been used in various meanings. The resource theory of quantum coherence is first proposed by Baumgratz *et al.* [81]. In this work the authors have introduced l_1-norm and relative entropic measures of coherence which are basis dependent. Here the coherence of a quantum physical system is manifested by the cross correlation terms or the off-diagonal terms of its density matrix. Subsequently, the works of Girolami [82] and Napoli *et al.* [83] provided the resource theories of quantum coherence with quantifiers such as Wigner-Yanase-Dyson skew informations and robustness of coherence, which are operationally more accessible. Resource theory of coherence has also been studied from the basis independent perspective. In this case the term quantum coherence is used to describe the intrinsic randomness that exists within quantum systems and is related to the purity of the quantum state. The work of Yao *et al.* [84] has proposed the resource theory of basis independent coherence where Frobenius norm based measure has been used as coherence quantifier. The resource theory of coherence has wide range of applications such as detection of quantum correlation, quantum thermodynamics, quantum metrology, quantum computing, quantum material technology and quantum biology [73].

In the previous chapters we have discussed the necessity and significance of studying quantum information theory in relativistic background. One of the basic

physical situation is the observer and quantum system are connected by arbitrary Lorentz transformation as described in Section 2.1. The effect of such relativistic inertial motion on quantum foundation and information was first studied by Peres *et al.* [30]. Here the authors have studied the change in spin entropy of a particle under two successive noncollinear Lorentz transformations which entangles the spin and momentum degree of freedom of the particle. Hence the reduced spin density matrix of the particle is not Lorentz covariant and the spin entropy of the particle is not a Lorentz scalar [30]. As discussed in Section 2.1, successive noncollinear boosts generates momentum dependent Wigner rotation which rotates the spin basis elements. Hence spin basis acquires momentum dependent coefficient resulting spin-momentum entanglement [30]. So, the entropy in the spin basis increases when the observer is oblivious to the relative motion of the its frame and the frame of the particle [30]. Depending upon the magnitudes and relative direction of boosts, the state can be completely decohered with respect to the observer which forbids the communication with single qubit without sharing reference frames [85]. The entanglement and the EPR experiment have also been studied in this framework [29, 31] indicating the observer dependent nature of entanglement [36]. Such studies have also been extended in the curved space-time [33, 34]. Though the study of Peres *et. al.* [30] shows the increase in spin entropy of a single particle state under successive noncollinear boosts, the quantification of quantum coherence in this framework was missing.

In this chapter we will discuss about our work on quantification of quantum coherence of a spin half particle in relativistic background [56]. We consider a single pure spin-1/2 particle that has Gaussian momentum distribution with respect to the laboratory frame. We investigate the change in coherence of the spin state of the particle with respect to a relativistically moving inertial observer. We use various coherence quantifiers to calculate the change in coherence in the above mentioned scenario. Our calculations show the behaviour of quantumness of a particle, defined from various perspective, under relativistic inertial transformations. The results indicate a generic degradation of quantum coherence in the spin basis under arbitrary Lorentz transformations. Such degradation is worse in case of basis dependent quantifiers. In case of purity based basis independent quantifier, the rate of decoherence is slow for lower values of uncertainty. All calculations in this chapter are done in natural units.

The organization of the chapter is as follows. In the Section 3.1 we define the resource theoretic quantifiers which we will use in our calculations. In Section 3.2 we calculate the coherence of a single particle, spin-1/2, massive spinor state with Gaussian momentum distribution with respect to a boosted observer using

various coherence quantifiers. In Section 3.3 we have considered realistic narrow uncertainty wave packet of neutron and calculated coherence of this system. In the Section 3.4 we have discussed the significance of our study and made concluding remarks.

3.1 Some resource theoretic quantifiers of quantum coherence

Coherence quantifiers are functional mappings $C(\rho)$ from the space of quantum states ρ (density matrix) to non negative real numbers. In order to qualify as coherence quantifier, the functional $C(\rho)$ must satisfy certain conditions [81]. Such conditions are based on the constraints imposed on incoherent quantum operation applied on the quantum state. The conditions are as follows [81] :

(I) Coherence $C(\rho)$ of any incoherent state will be zero.

(II) $C(\rho)$ is monotonic under incoherent completely positive trace preserving (ICPTP) operations.

(III) $C(\rho)$ is convex (i.e. the functional C is non-increasing under mixing of quantum states).

Wide variety of coherence quantifiers has been defined in this framework. In this work we will consider both basis dependent and basis independent interpretations coherence which have been explained in the previous section. Let us now focus on the mathematical definitions of some coherence quantifiers that will be used in our calculations.

3.1.1 Quantifiers for basis dependent notion of coherence:

In our calculations in this chapter we will use l_1-norm, relative entropy and Wigner-Yanase-Dyson skew information as basis dependent quantifier of coherence. The first two measures are distance based measures proposed by Baumgratz *et. al.* [81]. The third one is the asymmetry based measure of quantum coherence [82,83].

l_1-norm: It is the sum of absolute value of off-diagonal terms of the density matrix. The mathematical definition is given by [81]

$$C_{l_1} = \sum_{\substack{i,j \\ i \neq j}} |\rho_{ij}| \tag{3.1}$$

where ρ_{ij} is the ij^{th} element of the density matrix ρ.

Relative Entropy of Coherence: Here the quantifier is defined in terms of relative von-Neumann entropy. The mathematical definition is [81]

$$C_{rel.ent.}(\rho) = S(\rho_{diag}) - S(\rho) \tag{3.2}$$

where $S(\rho)$ is the von-Neumann entropy of state ρ. The term ρ_{diag} is the matrix containing the diagonal elements of ρ.

Skew Information: Wigner-Yanase-Dyson skew information has been proposed as a quantifier of coherence [82]. Basically the skew information measures the quantum uncertainty of a state with respect to an observable (additive conserved quantity) [82, 86]. Let, the measurement of an observable $\hat{X}$ is performed on the state ρ. The skew information of the state ρ, associated to the observable $\hat{X}$, is given by [82]

$$\mathcal{I}(\rho, \hat{X}) = -\frac{1}{2} Tr\{[\sqrt{\rho}, \hat{X}]^2\} \ . \tag{3.3}$$

Above expression contains square root of density matrix and hence $\mathcal{I}(\rho, \hat{X})$ cannot be expressed in terms of observables. However the work of Girolami [82] proposes a nontrivial lower bound of $\mathcal{I}$, that can be measured experimentally. A generic quantum state can be represented as

$$\rho = \frac{1}{2} \left(\mathbb{1} + \vec{r} \cdot \mathbf{\Sigma} \right) \tag{3.4}$$

where $\mathbf{\Sigma} \equiv \{\Sigma^1, \Sigma^2, \Sigma^3\}$ are the Pauli matrices and $\vec{r} \equiv \{r_1, r_2, r_3\}$ is the Bloch vector. If we perform measurement of Σ^3 on the state ρ, the associated skew information can be expressed as [87]

$$\mathcal{I}(\rho, \Sigma^3) = \left(1 - \sqrt{1 - |\vec{r}|^2} \right) \left(r_1^2 + r_2^2 \right) \ . \tag{3.5}$$

3.1.2 Quantifiers for basis independent notion of coherence:

The coherence quantifiers discussed above are associated to basis dependent notion of coherence where the amount of coherence in a quantum state depend upon choice of basis. In this subsection we will discuss about the notion of coherence that is independent of choice of basis in which coherence is observed.

Frobenius norm based measure: Such notion of coherence has been implemented by Yao *et. al.* in resource theoretic framework [84]. In this work the coherence implies the intrinsic randomness present in a quantum system. Here the coherence measure is based on the Frobenius norm defined as

$$\|M\|_F = \sqrt{Tr\left(M^\dagger M\right)} \tag{3.6}$$

where M is some operator. The mathematical definition of the Frobenius norm based coherence quantifier is given by [84]

$$C_F(\rho) = \sqrt{\frac{d}{d-1}}\ \left\|\rho - \rho_\star\right\|_F \tag{3.7}$$

where the quantum state ρ is an element of a d-dimensional vector space. The maximally mixed state $\rho_\star$ can be written as

$$\rho_\star = \frac{\mathbb{I}_d}{d} \tag{3.8}$$

where $\mathbb{I}_d$ is the identity element in the Hilbert space of the quantum state. Alternatively the Eq. (3.7) can be written as [84]

$$C_F(\rho) = \sqrt{\frac{d}{d-1}\sum_{j=1}^{d}\left(\lambda_j - \frac{1}{d}\right)^2}\ , \tag{3.9}$$

$\{\lambda_j\}$ are eigenvalues of the density matrix ρ.

Some significant properties of C_F are : [84]

(I) C_F is a normalized quantity i.e. , $C_F(\rho) \in [0, 1]$.

(II) Since C_F measures basis independent notion of coherence it is invariant under unitary transformation (U) –

$$C_F(\rho) = C_F(U\rho U^\dagger)\ . \tag{3.10}$$

(III) C_F is a measure of purity of the quantum state.

(IV) C_F is proportional to the Brukner-Zeilinger information content of the quantum state. Brukner-Zeilinger information is an operational measure of information contained in a quantum system. It is defined as the *the sum of individual measures of information over a complete set of mutually complementary observables* [Ref: Č. Brukner, A. Zeilinger, Phys. Rev. Lett. **83**, 3354 (1999)]. Brukner-Zeilinger information is invariant under unitary transformation of the quantum state or, equivalently, of the choice of the measured set of mutually complementary observables.

3.2 Coherence of a spin-1/2, Gaussian momentum wave packet under relativistic boosts

In this section we consider a single particle state with spin and momentum degree of freedom. We assume that the spin and momentum are separable in the lab frame $\mathcal{O}$. Our aim is to quantify the coherence of the particle, using the quantifiers defined in the previous section, with respect to an relativistic inertial observer $\mathcal{O}^\Lambda$. Using the formulation of Section 2.1, we will calculate the state of the particle with respect to $\mathcal{O}^\Lambda$. Then we will calculate the coherence of this state using various quantifiers.

Let the state of the particle in the frame $\mathcal{O}$ is

$$|\psi\rangle = \frac{1}{\sqrt{2}} \int d\mathbf{p}\ \psi(\mathbf{p})\, |\mathbf{p}\rangle \otimes (|0\rangle + |1\rangle)\ . \tag{3.11}$$

$\{|0\rangle, |1\rangle\}$ are the eigenvector of the 3$^{\text{rd}}$ Pauli matrix Σ^3. $\psi(\mathbf{p})$ is the normalized momentum wave function. For simplicity, let us first consider 1-dimensional momentum of the particle

$$p^\mu \equiv (p^0, p_x\hat{x}) = (m\cosh\beta, m\sinh\beta\hat{x}) \tag{3.12}$$

where β is the rapidity of the pure Lorentz boost that connects the lab frame $\mathcal{O}$ to the rest frame of the particle. Let the observer $\mathcal{O}^\Lambda$ is moving with velocity

$$v = \tanh\alpha\ \hat{z}\ , \tag{3.13}$$

α is the rapidity of the pure Lorentz boost that connects $\mathcal{O}$ to $\mathcal{O}^\Lambda$.

The density matrix of the particle in the frame $\mathcal{O}$ is

$$\rho = \frac{1}{2}\int\int d\mathbf{p}_1 d\mathbf{p}_2\ \psi(\mathbf{p}_1)\psi^*(\mathbf{p}_2)\,|\mathbf{p}_1\rangle\langle\mathbf{p}_2|\otimes(\mathbb{1}+\Sigma^1)\ . \tag{3.14}$$

Corresponding SRDM is given by

$$\rho_s = \frac{1}{2}(\mathbb{1}+\Sigma^1)\ . \tag{3.15}$$

In the set-up described above, the observer $\mathcal{O}^\Lambda$ is connected to the rest frame of the particle by two noncollinear Lorentz boosts along $\hat{x}$ and $\hat{z}$ directions, described by the rapidity parameters β and α respectively. So, applying the formulations in Section 2.1 we write the state of the particle with respect to observer $\mathcal{O}^\Lambda$ as

$$|\psi^\Lambda\rangle = \frac{1}{\sqrt{2}}\int d\mathbf{p}\ \sqrt{\frac{(\Lambda p)^0}{p^0}}\ \psi(\mathbf{p})\ D(W(\Lambda,\mathbf{p}))\ (|\Lambda\mathbf{p},0\rangle+|\Lambda\mathbf{p},1\rangle) \tag{3.16}$$

where the unitary representation of Wigner's little group in this case is

$$D(W(\Lambda,\mathbf{p})) = \cos\frac{\phi_{p_x}}{2}\mathbb{1} + i\sin\frac{\phi_{p_x}}{2}\ \Sigma_2 \tag{3.17}$$

with

$$\begin{aligned}\cos\frac{\phi_{p_x}}{2} &= \frac{\cosh\frac{\alpha}{2}\cosh\frac{\beta}{2}}{\sqrt{\frac{1}{2}+\frac{1}{2}\cosh\alpha\cosh\beta}}\\ \sin\frac{\phi_{p_x}}{2} &= \frac{\sinh\frac{\alpha}{2}\sinh\frac{\beta}{2}}{\sqrt{\frac{1}{2}+\frac{1}{2}\cosh\alpha\cosh\beta}}\ .\end{aligned} \tag{3.18}$$

The axis of Wigner rotation is along $\hat{z}\times\hat{x}=\hat{y}$.

Plugging the Eq. (3.17), Eq. (3.18) in the Eq. (3.16) and simplifying we get

$$|\psi^\Lambda\rangle = \frac{1}{\sqrt{2}}\int d\mathbf{p}\ \sqrt{\frac{(\Lambda p)^0}{p^0}}\psi(\mathbf{p})\Big[(\cos\frac{\phi_{p_x}}{2}+\sin\frac{\phi_{p_x}}{2})\,|\Lambda\mathbf{p},0\rangle+(\cos\frac{\phi_{p_x}}{2}-\sin\frac{\phi_{p_x}}{2})\,|\Lambda\mathbf{p},1\rangle\Big]\ . \tag{3.19}$$

The corresponding density matrix is given by

$$\rho^{\Lambda} = \frac{1}{2}\int\int d\mathbf{p}_1 d\mathbf{p}_2 \sqrt{\frac{(\Lambda p_1)^0\ (\Lambda p_2)^0}{p_1^0\ p_2^0}}\ \psi(\mathbf{p}_1)\ \psi^*(\mathbf{p}_2)\ \Big[A_{p_{x1}}A_{p_{x2}}\left|\Lambda\mathbf{p}_1,0\right\rangle\left\langle\Lambda\mathbf{p}_2,0\right| + A_{p_{x1}}B_{p_{x2}}\left|\Lambda\mathbf{p}_1,0\right\rangle\left\langle\Lambda\mathbf{p}_2,1\right| + A_{p_{x2}}B_{p_{x1}}\left|\Lambda\mathbf{p}_1,1\right\rangle\left\langle\Lambda\mathbf{p}_2,0\right| + B_{p_{x1}}B_{p_{x2}}\left|\Lambda\mathbf{p}_1,1\right\rangle\left\langle\Lambda\mathbf{p}_2,1\right|\Big]\ , \tag{3.20}$$

where the coefficients $A_{p_{xi}}, B_{p_{xi}}$ are given by

$$\begin{aligned} A_{p_{xi}} &= \left(\cos\frac{\phi_{p_{xi}}}{2} + \sin\frac{\phi_{p_{xi}}}{2}\right) \\ B_{p_{xi}} &= \left(\cos\frac{\phi_{p_{xi}}}{2} - \sin\frac{\phi_{p_{xi}}}{2}\right)\ . \end{aligned} \tag{3.21}$$

Using Eq. (2.17) we write the SRDM of the particle with respect to the observer $\mathcal{O}^{\Lambda}$ as

$$\rho_s^{\Lambda} = \frac{1}{2}\int d\mathbf{p}\ \ |\psi(\mathbf{p})|^2\ \Big[A_{p_x}^2\left|0\right\rangle\left\langle 0\right| + A_{p_x}B_{p_x}\big(\left|0\right\rangle\left\langle 1\right| + \left|1\right\rangle\left\langle 0\right|\big) + B_{p_x}^2\left|1\right\rangle\left\langle 1\right|\Big]\ . \tag{3.22}$$

As we intent to study Gaussian momentum wave packet in this context, let us now define the momentum wave function. Initially we will study the 1-dimensional scenario and we choose the wave function as

$$\psi(\mathbf{p}) = f(p_x)\delta(p_y)\delta(p_z) \tag{3.23}$$

where $f(p_x)$ is a Gaussian function. In our calculation we will consider two type of Gaussian wave function:

Case (i) The Gaussian wave packet centred at zero i.e. ,

$$f(p_x) = \frac{1}{(\sqrt{\pi}\sigma)^{1/2}}\ e^{-\frac{1}{2}(p_x/\sigma)^2}\ . \tag{3.24}$$

Case (ii) The Gaussian wave packet centred at $\mathfrak{p}$, ($\mathfrak{p}$ is some constant value of relativistic momentum) i.e. ,

$$f(p_x) = \frac{1}{(\sqrt{\pi}\sigma)^{1/2}}\ e^{-\frac{1}{2}((p_x-\mathfrak{p})/\sigma)^2}\ . \tag{3.25}$$

Substituting Eq. (3.23) in Eq. (3.22) we get

$$\rho_s^{\Lambda} = \frac{1}{2}\int dp_x \ |f(p_x)|^2 \left[A_{p_x}^2 \left|0\right\rangle\left\langle 0\right| + A_{p_x}B_{p_x}\left(\left|0\right\rangle\left\langle 1\right| + \left|1\right\rangle\left\langle 0\right|\right) + B_{p_x}^2 \left|1\right\rangle\left\langle 1\right|\right] \tag{3.26}$$

From now on we will use the notation p instead of p_x for convenience (in case of 1-dimensional wave function).

We write the rapidity parameters as

$$\begin{aligned} \cosh\beta &= \sqrt{1+\frac{p^2}{m^2}} \\ \sinh\beta &= \frac{p}{m} \\ \cosh\alpha &= b \\ \sinh\alpha &= a \ . \end{aligned} \tag{3.27}$$

Substituting above relations of rapidity parameters in Eq. (3.26) we evaluate the coefficients

$$\begin{aligned} A_p^2 &= 1 + \frac{a\ \frac{p}{m}}{1+b\sqrt{1+\frac{p^2}{m^2}}} \ , \\ B_p^2 &= 1 - \frac{a\ \frac{p}{m}}{1+b\sqrt{1+\frac{p^2}{m^2}}} \ , \\ A_pB_p &= \frac{b+\sqrt{1+\frac{p^2}{m^2}}}{1+b\sqrt{1+\frac{p^2}{m^2}}} \ . \end{aligned} \tag{3.28}$$

The components of the SRDM ρ_s^Λ in Eq. (3.26) are

$$\left(\rho_s^\Lambda\right)_{11} = \frac{1}{2}\int dp\ |f(p)|^2 \left(1 + \frac{a\ \frac{p}{m}}{1 + b\sqrt{1+\frac{p^2}{m^2}}}\right) ,$$

$$\left(\rho_s^\Lambda\right)_{22} = \frac{1}{2}\int dp\ |f(p)|^2 \left(1 - \frac{a\ \frac{p}{m}}{1 + b\sqrt{1+\frac{p^2}{m^2}}}\right) , \tag{3.29}$$

$$\left(\rho_s^\Lambda\right)_{12} = \left(\rho_s^\Lambda\right)_{21} = \frac{1}{2}\int dp\ |f(p)|^2 \left(\frac{b + \sqrt{1+\frac{p^2}{m^2}}}{1 + b\sqrt{1+\frac{p^2}{m^2}}}\right) .$$

We use Eq. (3.29) to calculate the coherence of the system under consideration using various quantifiers defined in the Section 3.1.

Our aim here is to study the variation of quantum coherence, quantified using different quantifiers, with the variation in the velocity of observer $\mathcal{O}^\Lambda$ and the uncertainty σ of the wave packet. In order to calculate coherence we need to evaluate the components of density matrix in Eq. (3.29). The diagonal elements $\left(\rho_s^\Lambda\right)_{11}$ and $\left(\rho_s^\Lambda\right)_{22}$ can be evaluated as

$$\left(\rho_s^\Lambda\right)_{11} = \left(\rho_s^\Lambda\right)_{22} = \frac{1}{2} . \tag{3.30}$$

The off-diagonal components can only be evaluated analytically for very small value of uncertainty in nonrelativistic limit [56]. However our goal is to study the variation of coherence with larger uncertainty in the relativistic regime. Hence we numerically evaluate the components $\left(\rho_s^\Lambda\right)_{12} = \left(\rho_s^\Lambda\right)_{21}$. In our calculation we assume the following value of parameters : $m \approx 0.5$ MeV (mass of an electron) and $\mathfrak{p} = 1/2\sqrt{3}$ MeV (the momentum of an electron moving with half of the velocity of light).

The plot in the Figure (3.1) shows the variation of $\left(\rho_s^\Lambda\right)_{12}$ with respect to the rapidity parameter α of the observer $\mathcal{O}^\Lambda$ and the uncertainty σ, for the Gaussian momentum wave packet centred at zero. The Figure (3.2) shows the same for wave packet centred at $\mathfrak{p}$. These two plots are very significant, as the basis dependent measures are manifested by off-diagonal terms of the density matrix. So, the decrease in the value of off-diagonal elements of density matrix will imply decoherence. Such loss of coherence is resulted due to the spin-momentum

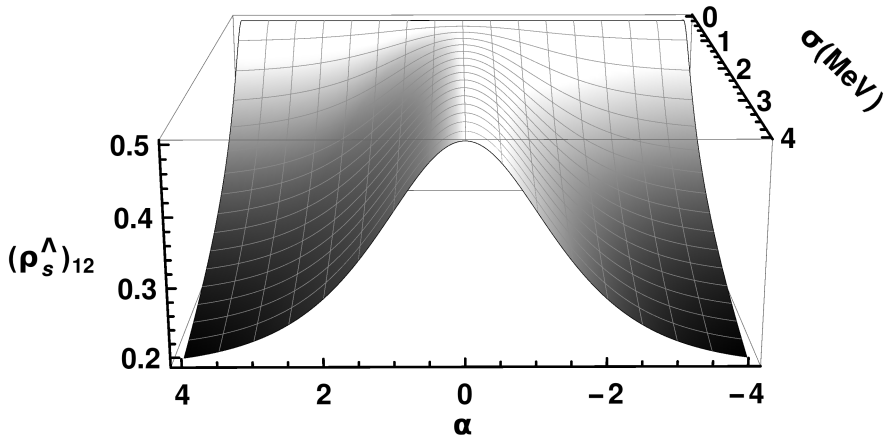

Figure 3.1: Variation of $\left(\rho_s^{\Lambda}\right)_{12}$ with respect to the rapidity α and uncertainty σ (MeV) for wave packet centred at zero. $m = 0.5$ MeV.

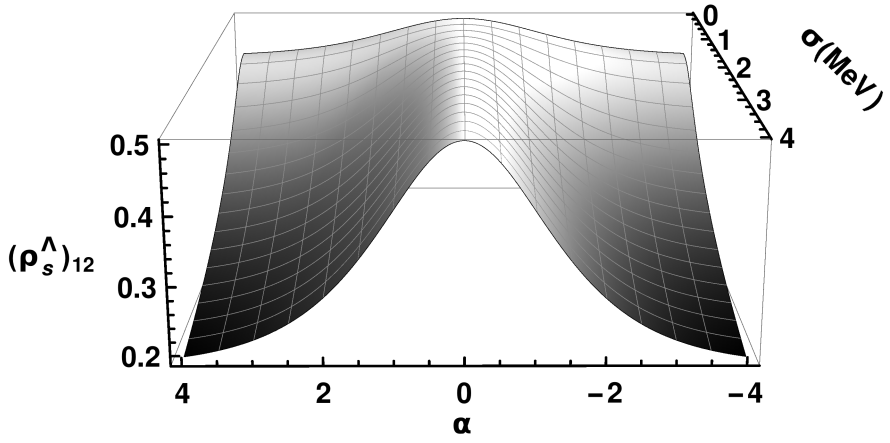

Figure 3.2: Variation of $\left(\rho_s^{\Lambda}\right)_{12}$ with respect to the rapidity α and uncertainty σ (MeV) for wave packet centred at $\mathfrak{p}$. $m = 0.5$ MeV, $\mathfrak{p} = 1/2\sqrt{3}$ MeV.

entanglement through Wigner rotation [30]. From the Eq. (3.1), we see that the l_1-norm based measure of coherence is basically the sum of off-diagonal terms of

the density matrix i.e. , in the present case

$$C_{l_1} = \left(\rho_s^{\Lambda}\right)_{12} + \left(\rho_s^{\Lambda}\right)_{21} = 2\left(\rho_s^{\Lambda}\right)_{12} \ . \tag{3.31}$$

Hence the coherence C_{l_1} can be studied by multiplying the readings of the plots in Figure (3.1) and Figure (3.2). From the plots we see that the maximum value of $\left(\rho_s^{\Lambda}\right)_{12}$ is 0.5 that corresponds to maximum value of $C_{l_1} = 1$. The coherence decreases with increase in the magnitude of rapidity α. It is important to note here that the +ve and and −ve values of α implies the velocity of $\mathcal{O}^{\Lambda}$ in two opposite directions. The plots are symmetric with respect to the sign of α.

In case of wave packet centred at zero, the plot in Figure (3.1) shows that the coherence remains constant with the variation of α when the uncertainty $\sigma \to 0$. This is due to the fact that $\sigma = 0$ limit implies the momentum of the particle is localised at zero. In that case, the rest frame of the particle and the frame of the observer $\mathcal{O}^{\Lambda}$ are connected by a pure boost. We have seen in the Section 2.1, Wigner rotation is generated by two or more noncollinear boosts. A single pure boost cannot generate Wigner rotation. So, when momentum of the particle tents to zero, only the motion of the observer $\mathcal{O}^{\Lambda}$ does not induce momentum dependent coefficients in the spin basis of the particle. Hence the spin and momentum state of the particle remains separable with respect to $\mathcal{O}^{\Lambda}$. As $\mathcal{O}^{\Lambda}$ performs measurement in the spin basis of the particle, no decoherence is observed. For larger values of uncertainty spin-momentum entanglement occurs and the spin basis acquires momentum dependent coefficients. As the observer performs measurement only on the spin basis, being oblivious to the information associated to the momentum degree of freedom, decoherence is observed. The decoherence increases with increase in the uncertainty σ. It is important to note here that the small value of uncertainty in case of wave packet centred at zero gives the nonrelativistic limit.

In case of wave packet centred at $\mathfrak{p}$, the plot in Figure (3.2) shows decoherence with increase in the magnitute in α even when $\sigma \to 0$. The $\sigma = 0$ limit implies the momentum of the particle is localised around a single sharp value $\mathfrak{p}$. So the quantum state will undergo a single pure rotation represented by $(\cos\frac{\phi_p}{2}\mathbb{1} + i\sin\frac{\phi_p}{2}\Sigma_2)$. No spin-momentum entanglement will occur and the SRDM ρ_s and ρ_s^{Λ} are connected by a unitary transformation. The basis dependent elements of density matrix will change under unitary transformation. The basis dependent notion of coherence is not invariant under unitary transformation. So the decoherence is observed in case of $\sigma = 0$. For nonzero values of uncertainty, the decoherence is observed due to spin-momentum entanglement. The decoherence increases with

increase in uncertainty.

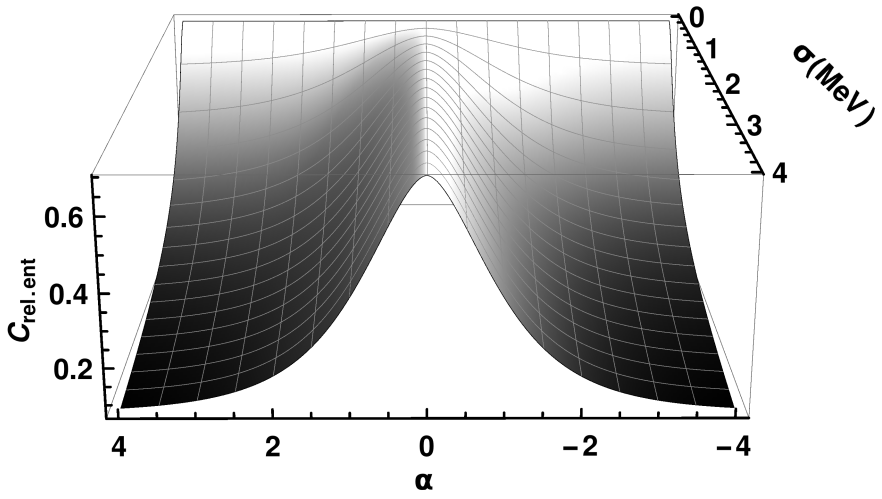

Figure 3.3: Variation of $C_{rel.ent}$ with respect to the rapidity α and uncertainty σ (MeV) for wave packet centred at zero. $m = 0.5$ MeV.

Now we present the plots of relative entropy of coherence and skew information defined in Eq. (3.2) and Eq. (3.5). In the Figure (3.3)and Figure (3.4), the plots show the variation of relative entropy of coherence with respect to the rapidity parameter α of the observer $\mathcal{O}^{\Lambda}$ and the uncertainty σ, for the Gaussian momentum wave packet centred at zero and $\mathfrak{p}$ respectively. In a similar way the the plots in Figure (3.5) and Figure (3.6), show the variation of skew information with respect to the rapidity parameter α of the observer $\mathcal{O}^{\Lambda}$ and the uncertainty σ, for the Gaussian momentum wave packet centred at zero and $\mathfrak{p}$ respectively. The maximum value of coherence in case of $C_{rel.ent}$ and $\mathcal{I}$ are given by $\ln 2$ and 1 respectively. In case of wave packet centred at zero, both $C_{rel.ent}$ and $\mathcal{I}$ attain maximum value when either of the α or σ goes to zero. In case of the wave packet centred at $\mathfrak{p}$, both $C_{rel.ent}$ and $\mathcal{I}$ attain maximum value only at $\alpha = 0$. At $\sigma = 0$, their values decrease with increase in α as a consequence of basis dependent notion of coherence. The plots are symmetric with respect to the sign of α. The plots in Figure (3.5) and Figure (3.6), show the sharp degradation of skew information with increasing α and σ. For larger values of uncertainty the skew information is almost fully lost.

So far we have studied the basis dependent notion of quantum coherence in

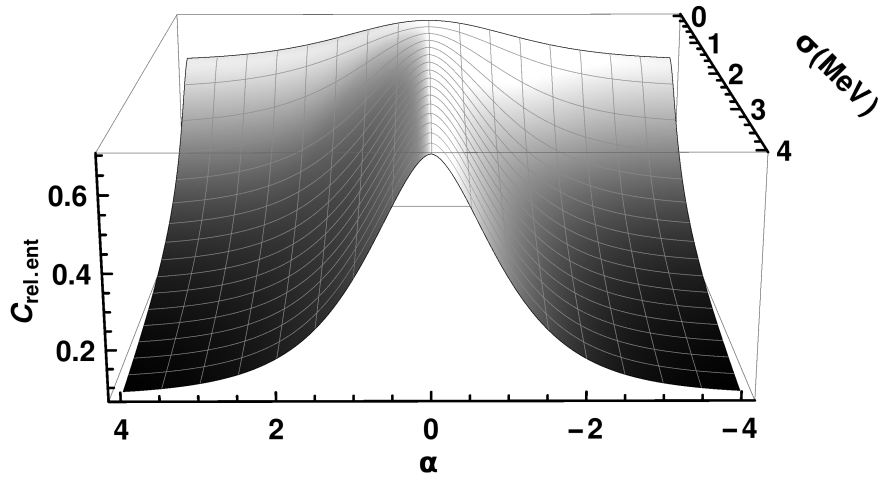

Figure 3.4: Variation of $C_{rel.ent}$ with respect to the rapidity α and uncertainty σ (MeV) for wave packet centred at $\mathfrak{p}$. $m = 0.5$ MeV, $\mathfrak{p} = 1/2\sqrt{3}$ MeV.

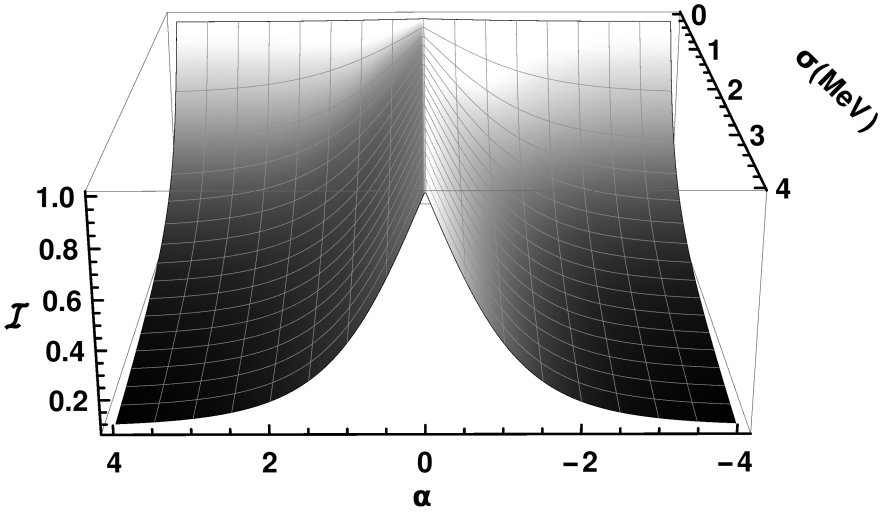

Figure 3.5: Variation of "Skew Information" $\mathcal{I}$ with respect to the rapidity α and uncertainty σ (MeV) for wave packet centred at zero. $m = 0.5$ MeV.

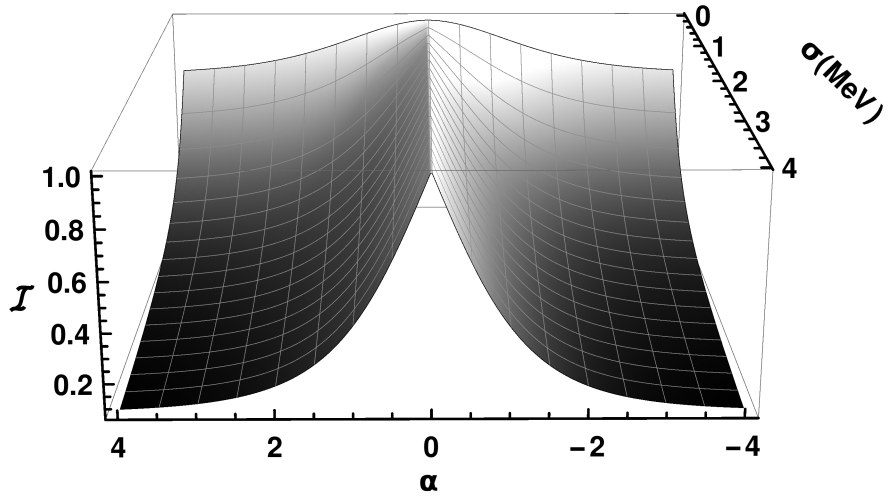

Figure 3.6: Variation of "Skew Information" $\mathcal{I}$ with respect to the rapidity α and uncertainty σ (MeV) for wave packet centred at $\mathfrak{p}$. $m = 0.5$ MeV, $\mathfrak{p} = 1/2\sqrt{3}$ MeV.

inertial relativistic background. Our study indicates that, in general the basis independent measures do not perform well under arbitrary Lorentz transformations. Here we identify two sources of decoherence. First, the observer measures in the spin basis however in relativity spin is not an independent degree of freedom but couples with spatial momentum degree of freedom under Lorentz transformations. So, the observer's lack of knowledge about the motion of the particle causes the decoherence. Second, composition of noncollinear Lorentz boost generates spatial rotation (Wigner rotation). As basis dependent measures are not unitary invariant, such spatial rotation will affect the measurement and degrade the quantum coherence. In order to avoid loss of information the observer needs to have knowledge of the Lorentz transformation that connects its frame to that of the particle. Also the plots show that the decoherence is smaller for smaller value of uncertainty. So, minimizing uncertainty is another good option.

Next we will focus on the basis independent notion of quantum coherence. To be more consistent with the relativistic background we can demand that coherence should manifest an intrinsic physical property of a quantum system that is independent of choice of basis. This motivates us to quantify coherence in the same set-up with basis independent quantifiers. So, we use Frobenius norm based

quantifier defined by Eq. (3.7), Eq. (3.9) for our study.

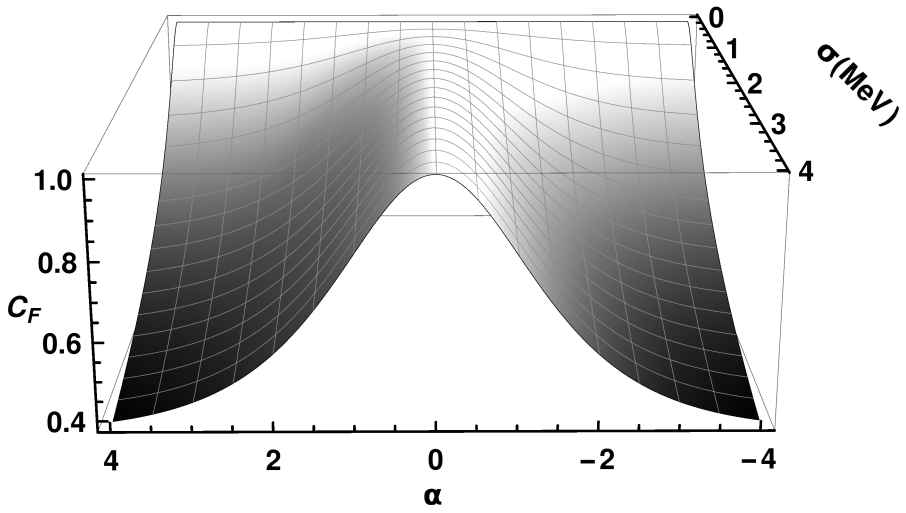

Figure 3.7: Variation of "Frobenius norm based measure of coherence" C_F with respect to the rapidity α and uncertainty σ (MeV) for wave packet centred at zero. $m = 0.5$ MeV.

Figure (3.7) and Figure (3.8) show the variation of Frobenius norm based coherence C_F with respect to the rapidity parameter α of the observer $\mathcal{O}^\Lambda$ and the uncertainty σ, for the Gaussian momentum wave packet centred at zero and $\mathfrak{p}$ respectively. The maximum value attained by C_F is 1. At $\alpha = 0$, for both the wave packets, C_F is maximum for any value of σ. But the most significant result is at $\sigma = 0$, for both wave packets, C_F is maximum for any value of α. This is due to the unitary invariance of C_F (independence to the choice of basis) defined by Eq. (3.10). For nonzero values of both α and σ coherence degrades with the increase in values of these two variables. The plots are symmetric with respect to the sign of α.

Our study indicates that unitary invariant or basis independent notion of coherence is preserved if the uncertainty of an wave packet is small. This is because of the fact that, pure rotation does not affect C_F and only source of decoherence here is the observer $\mathcal{O}^\Lambda$'s lack of knowledge about the momentum of the particle. Hence we trace out the density matrix over all possible values of the momentum variable, introducing mixedness in the SRDM. When uncertainty is small, the range of possible value of the momentum of the particle becomes

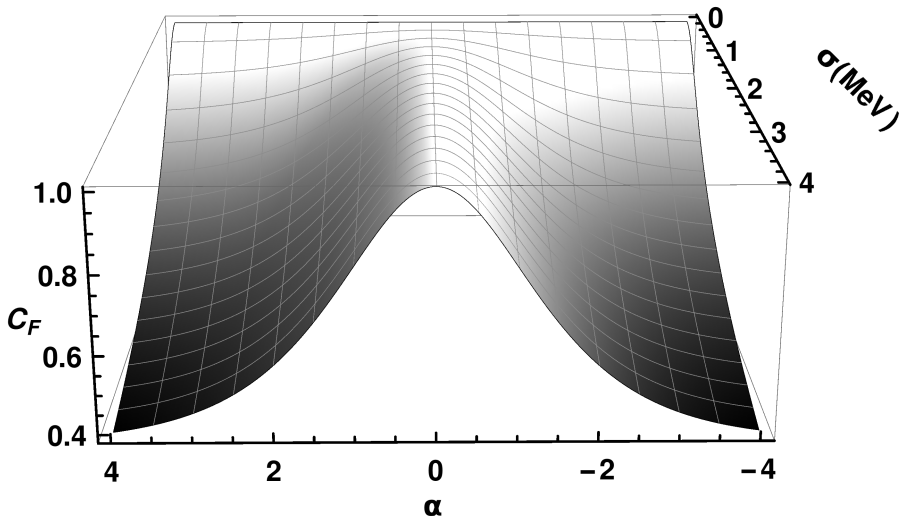

Figure 3.8: Variation of "Frobenius norm based measure of coherence" C_F with respect to the rapidity α and uncertainty σ (MeV) for wave packet centred at $\mathfrak{p}$. $m = 0.5$ MeV, $\mathfrak{p} = 1/2\sqrt{3}$ MeV.

narrow which minimizes the loss of information when the momentum is traced out.

Thus the basis independent notion of coherence is relatively more consistent in the relativistic background. If the frame of two observers are connected by arbitrary Lorentz transformations and the observers do not have the knowledge about the transformation between the two frame. Still the observer in one frame can access such notion of information of a quantum state minimizing the decoherence due to the lack of knowledge. Though the decoherence will increase with increase in uncertainty of the quantum state.

3.3 Examples

In this section we will study the basis independent notion of coherence of 3-dimensional narrow uncertainty wave packet using relalistic parameters. We consider a narrow uncertainty Gaussian wave packet centred at zero in the lab frame $\mathcal{O}$. There are many ways in which such system can be produced, for example hydrogen atom cooled in the temperature range of milli-Kelvin [85], ultracold

neutrons (UCN) [88] or thermal neutrons [89]. In our calculation we will use parameters of UCN whose kinetic energy is less than 300 neV [88]. UCN is very sensitive to gravitational, magnetic or material potential, due to their low energy. Hence they are often used as a probe in the experiments related to quantum theory and gravity [90, 91]. A significant feature of gravitational background is that it causes decoherence of quantum system. This motivates us to study coherence of low energy neutrons in a more basic relativistic framework i.e., under Lorentz transformations.

Let us now define a 3-dimensional wave packet centred at zero in the frame $\mathcal{O}$,

$$|\psi\rangle = \frac{1}{(\sqrt{\pi}\sigma)^{3/2}} \int d\mathbf{p}\; e^{-\frac{\mathbf{p}^2}{2\sigma^2}} |\mathbf{p}\rangle \otimes |0\rangle \tag{3.32}$$

where $\mathbf{p} = (p_x, p_y, p_z)$ is the spatial 3-momentum of the particle that satisfies the dispersion relation $p^0 = \sqrt{\mathbf{p}^2 + m^2}$. We assume that the observer $\mathcal{O}^\Lambda$ is moving along $\hat{z}$ direction with rapidity α, velocity described by equation

$$v = \tanh\alpha\; \hat{z}\ . \tag{3.33}$$

The unitary representation of Wigners little group in this case can be found using Eq. (2.9), Eq. (2.10) as

$$D(W(\Lambda, \mathbf{p})) = \frac{(p^0 + m)\cosh\frac{\alpha}{2} + p_z \sinh\frac{\alpha}{2} - i\sinh\frac{\alpha}{2}\left(-p_x\sigma_y + p_y\sigma_x\right)}{\left[(p^0 + m)\left(p^0\cosh\alpha + p_z\sinh\alpha + m\right)\right]^{1/2}}\ . \tag{3.34}$$

Following same procedure as previous section we find the SRDM of the state in Eq. (3.32) with respect to the observer $\mathcal{O}^\Lambda$ as

$$\rho_s^\Lambda = \frac{1}{(\sqrt{\pi}\sigma)^3} \int d\mathbf{p}\; e^{-\frac{\mathbf{p}^2}{\sigma^2}} \begin{pmatrix} \frac{M}{AB} & 0 \\ 0 & \frac{N}{AB} \end{pmatrix} \tag{3.35}$$

where

$$\begin{aligned} A &= (p^0 + m) \\ B &= (p^0\cosh\alpha + p_z\sinh\alpha + m) \\ M &= A^2\cosh^2\frac{\alpha}{2} + p_z^2\sinh^2\frac{\alpha}{2} + A\; p_z\sinh\alpha \\ N &= (p_x^2 + p_y^2)\sinh^2\frac{\alpha}{2}\ . \end{aligned} \tag{3.36}$$

Using Eq. (3.35), Eq. (3.36) we calculate Frobenius norm based coherence C_F for narrow uncertainty neutron wave packet.

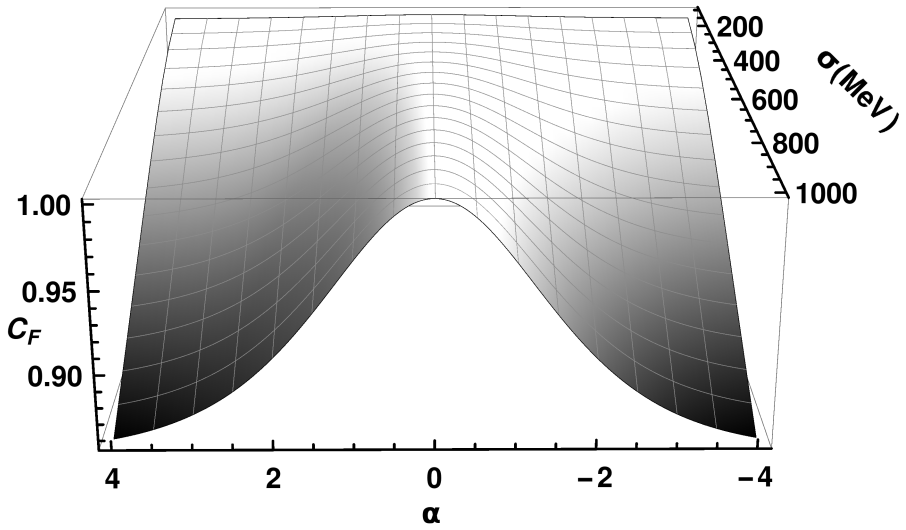

Figure 3.9: Variation of "Frobenius norm based measure of coherence" C_F with respect to the rapidity α and uncertainty σ (MeV) for narrow uncertainty UCN wave packet.

Figure (3.9) shows the variation of Frobenius norm based coherence C_F with respect to the rapidity parameter α of the observer $\mathcal{O}^\Lambda$ and the uncertainty σ for narrow uncertainty UCN wave packet. The rest mass of the neutron is 939.36 MeV. The range of values of uncertainty σ is considered as $0-1000$ MeV i.e. , the maximum value is in the order of the rest mass of the neutron. The plots show that the decoherence is very small in this range of uncertainty even for significant value of α.

In the limit $(\sigma/m) \ll 1$ the SRDM in Eq. (3.35), Eq. (3.36) can be expressed analytically as [30]

$$\rho_s^\Lambda = \frac{1}{2}\begin{pmatrix} 1+n_z & 0 \\ 0 & 1-n_z \end{pmatrix} \tag{3.37}$$

where

$$n_z = 1 - \left(\frac{\sigma}{2m}\tanh\frac{\alpha}{2}\right)^2 . \tag{3.38}$$

Frobenius norm based coherence of above state is given by

$$C_F(\rho_s^\Lambda) = 1 - \left(\frac{\sigma}{2m}\tanh\frac{\alpha}{2}\right)^2 . \tag{3.39}$$

For UCN the kinetic energy is < 300 neV [88]. Assuming $\sigma = 300$ neV and using Eq. (3.39), the loss of coherence for UCN is obtained as $\sim 10^{-30}$. Similarly for thermal neutron the upper bound of kinetic energy is 0.025 eV [89]. Assuming $\sigma = 0.025$ eV and using Eq. (3.39), the loss of coherence for thermal neutron is obtained as $\sim 10^{-20}$. In these calculations loss of coherence is obtained by quantifying the deviation of C_F from unity.

3.4 Conclusions

In this chapter we have studied the coherence of spin-1/2, Gaussian momentum wave packets in relativistic backgrounds. We have considered the wavepacket under two successive noncollinear Lorentz boost and quantified the coherence under such transformations using various coherence quantifiers from resource theoretic formulations. We have considered two notions of coherence that have been defined in resource theory of coherence in quantum information theory. First we have studied the basis dependent notion of coherence and used the quantifiers l_1-norm, relative entropy of coherence [81] and skew information [82] to quantify the coherence. Then we have considered basis independent notion of coherence and used Frobenius norm based measure as the coherence quantifier [84].

Our study show that if an observer measures quantum coherence in the spin basis of a particle, from a frame that is connected to the rest frame of the particle by two successive Lorentz transformations, then he/she will observe loss of coherence. We have plotted the coherence calculated using various quantifiers against the rapidity parameter of observers velocity (observed from lab frame) and the uncertainty in particles momentum (observed from lab frame). The reason for loss of coherence is the spin-momentum entanglement [30]. The notion of spin originates from relativistic quantum theory which shows that the spin and linear momentum are not independent degree of freedoms. Composition of two noncollinear boosts results in a pure boost and a spatial rotation known as Wigner rotation which is a function of linear momentum. Spin basis undergoes unitary transformation due to Wigner rotation and acquire momentum dependent coefficients resulting spin-momentum entanglement.

We see that the decoherence can arise in two ways. As observer measures coherence in the spin basis without the knowledge of momentum of the particle, loss of information occurs. In the calculation the lack of knowledge of momentum is introduced by tracing out the state over momentum variable resulting mixedness in the spin basis. Loss of coherence in this way is present both in case of basis dependent and independent measures of coherence. The loss increases

with increse in the uncertainty in the momentum wave packet and the rapidity of the observer's velocity. If the momentum of the particle has a sharp nonzero value, i.e. the uncertainty of the wave packet is zero, the spin state of the particle transforms under a single pure rotation. Coherence quantified by basis dependent measures, suffers loss under spatial rotation. Coherence quantified by the basis independent measure remains constant under spatial rotation because of unitary invariance. So, the basis independent coherence can be preserved by minimizing the uncertainty even at large value of rapidity. We have also verified our findings using parameters of realistic wave packets of ultracold and thermal neutrons.

Our work checks the consistency of various resource theoretic quantifiers in a basic relativistic scenario. From the calculations and plots, we see that the basis independent notion of coherence is more consistent compared to the basis dependent coherence. The relativity theory suggests that there are no universal reference frame. The resource theories we have considered in this work are defined in the framework of quantum mechanics. Quantum mechanics in general, is a basis dependent theory. So, a potential resource in the quantum information theory might not be a good resource for RQI, for example the basis dependent notion of coherence. The basis independent coherence is more effective in relativistic background because of unitary invariance. As we have seen from our calculations, using basis independent measure, a relativistic observer can identify a wave packet, with narrow momentum uncertainty, almost as a pure state.

So, the study of coherence under successive Lorentz boosts indicates that in order to build up the resource theory of quantum coherence in relativistic regime, either the correlation has to be studied form a basis independent perspective, or the observers have be well aware about the laws of transformation among their frames and the motion of the particle. As mentioned before, different resource theoretic quantifiers interpret coherence differently and each of them have different foundational aspects. Recently, the resource theory of asymmetry or reference frame has emerged which treats individual formulations of coherence measures as special cases [76–79, 84]. The Frobenius norm based measure also has a geometric interpretation and the quantifier is proportional to the Brukner-Zeilinger information [84]. The skew information and the Frobenius norm based measure have operational perspective [82, 84]. Both these geometric and operational notions have extreme importance in the context of resource theory of coherence [74, 75, 81, 84, 92]. Our calculations show that rate of degradation of coherence quantified by different measures are different. This also sheds light on the foundational and operational aspects of the different notions of coherence in relativistic background. Further investigation can be done on the application

of resource theory of coherence in relativistic scenario for example in the case of quantum state estimation, remote creation of coherence, quantum speed limit etc. [93–95].

Chapter 4

Resonance interaction of entangled atoms accelerating between two mirrors

Light-matter interaction is a significant branch of quantum electrodynamics with applications ranging from fundamental physics as well as technological developments [96, 97]. Material particles such as atoms, molecules (known as quantum emitters) absorbs and emits photons through the interaction of their internal degree of freedom with the quantized electromagnetic field. These radiative properties of quantum emitters are the building blocks of technologies such as diodes, laser, spectroscopy, elementary particle detectors etc. Later the quantum theory of photons has been generalized in case of other quasiparticles such as phonons, plasmons, excitons etc [98]. The development of material engineering has enabled us to perform controlled atom-field interaction experiments in the laboratory which provides a very wide platform for quantum information, computation and probing fundamental physics. The examples include cold atoms, superconducting circuits, micro and nano mechanical oscillators, spin ensemble etc [99–106].

The interaction between atom and quantum field gives rise to several significant phenomena such as Lamb shift, Casimir-Polder force, spontaneous excitation and emission by atoms etc. Such phenomena are triggered by the vacuum fluctuation of quantum field [107, 108] and the radiation reaction of the atom (the radiation reaction is the effect of the transition dipole moment of the atom on to itself) [109, 110]. When two atoms (one in ground state and another in excited state) interact with quantum field, The self reaction contribution leads to exchange of real photons between two atoms. This phenomenon is known as the resonance interaction [111–116]. The strength of resonance interaction depends upon interatomic distance. When the state of the two atoms are separable,

the resonance interaction between them is proportional to the 4^{th} power of the coupling constant and inversely proportional to the square of the interatomic separation in the far zone [117–120]. When the atoms are entangled i.e., they are in subradiant or superradiant state, the resonance interaction is proportional to the square of the coupling constant and inversely proportional to the interatomic separation [111,112,121–123].

The resonance interaction has been studied in the context of accelerated particle detector interacting with scalar or electromagnetic vacuum [124–126]. The works show that the resonance interaction can be observed for much lower acceleration compared to the very high value of acceleration required to observe Unruh effect. The study of acceleration in context of radiative properties of entangled atoms is significant both in the context of quantum information and foundations. The entanglement of particle under free fall and in space has become a significant area of research in order to develop space based quantum communications and tests of fundamental physics [127–129]. Acceleration is also an unavoidable phenomenon in case of experiments of particle in gravitational, magnetic and optical trap [130–132]. The trapped quantum particles are also used as a probe for acceleration [133,134].

The cutting edge technology has allowed us to simulate the relativistic motion that is difficult to achieve in case of massive system. The circuit quantum electrodynamics is the most successful platform in this context. By electrical tuning of the qubit-field coupling, acceleration as high as 10^{17} m/s^2 can be achieved in superconducting circuit. It has been shown that entanglement of superconducting qubits can be generated through acceleration [135]. Such systems are also effective for quantum information processing [136] and testing fundamental phenomena [137]. So, exploring resonance interaction under acceleration manifests how this phenomenon can be controlled in advantage of the tests cited above.

The experiments of photonics are mostly performed in the confined environment rather than free space. The progress in the field of nano-fabrication [138] has enabled us to perform quantum electrodynamical experiments in various structured environments, for example atoms trapped in optical nanofibre [139], atom-photon lattices [140]. Such systems are building blocks to device quantum communications [141]. The boundary conditions imposed by the structure of the device itself significantly affect the atom-photon dynamics of the system. So the study of radiative properties of atoms in these structured environments is necessary in order to successful implementation of quantum technology. The role of boundary conditions in relativistic atom-field interaction are very significant in simulating fundamental phenomena [137], generating quantum correlations [142]

and performing quantum tasks [143].

In this chapter, we aim to explore resonance interaction of two nonmaximally entangled atoms under the effect of both acceleration and boundary conditions. In practical experiments, a maximally entangled state is impossible to achieve due to the background noise. However no study has been performed on the effect of nonmaximal correlation in the context of resonance interaction. The studies have been performed on resonance interaction between maximally entangled neutral atoms in structured environment such as photonic lattice and cylindrical waveguide [144,145]. In realistic situation an atom can be subjected to acceleration due to the effect of different confining potentials [130–133]. Also the radiative properties of atoms under combined effect of boundary and acceleration is a significant area of research [105, 106]. The energy level shift due to resonance interaction of two maximally entangled atoms has been explored in free space and and in presence of a infinite plane mirror [124, 125]. The rate of exchange of energy between the atoms undergoing resonance interaction in the free space has been studied too [126]. Following the formalism of Dalibard, Dupont-Roc and Cohen-Tannoudji (DDC) [146,147] the above works show that the resonance interaction originates from radiation reaction (or self reaction) of the atoms interacting with the field. Vacuum fluctuation does not have any contribution in the resonance interaction and hence it is a nonthermal phenomena.

In our work we will consider two nonmaximally entangled atoms accelerating between two parallel mirrors in presence of background quantized scalar vacuum. Here the two parallel mirrors can be considered as a basic approximation of a waveguide. We assume that each mirror impose the Dirichlet boundary condition on the field modes. We consider two spatial configuration of the atoms

> **Configuration 1:** The line joining two atoms is perpendicular to the plane of the plates.
>
> **Configuration 2:** The line joining two atoms is parallel to the plane of the plates.

The acceleration of the particles is 1-dimentional and parallel to the plane of the mirrors. In our calculation the scalar field captures the basic features of electromagnetic field which is sufficient for present purpose. We have also assumed that the atoms are entangled (nonmaximally) in their superradiant or subradiant state. Using DDC formalism we calculate the resonance energy shift and relaxation rate of energy exchange due to resonance interaction between two atoms.

As the presence of boundary conditions modify the density of states of the quantum field, the response of the field also gets modified. Such boundary depen-

dent modifications affect the radiative properties of atoms interacting with the field. We see such boundary dependent terms present in the expressions, of resonance energy shift and relaxation rate of energy exchange, we have calculated. We have presented various plots to show the variation of quantities of interest against acceleration, various boundary parameters and interatomic separation. The results show that the resonance interaction can be enhanced or inhibited by proper choice of acceleration and configurational parameters. Our calculations enable us to study the limiting cases such as low acceleration free space and single mirror. All calculations in this chapter are done in natural units. The work presented in this chapter is based on our publication [57].

The chapter is organized as follows: in the Section 4.1 we discuss how resonance energy shift and relaxation rate of energy exchange can be calculated using DDC formalism [146–149]. In Section 4.2 we mathematically describe the systems under study and then calculate the resonance energy shift and relaxation rate of energy exchange for these systems. We explain the dependence of these quantities on various system parameters, with numerous plots and analysis. In Section 4.3 we present summary of our work and concluding remarks.

4.1 Interaction of accelerated atom with quantized scalar field in Heisenberg picture

In the past studies on spontaneous emission of atoms, the role of vacuum fluctuation and radiation reaction have been historically invoked either separately or together [107–110]. The contribution of vacuum fluctuation and radiation reaction in radiative processes of atoms depend upon the choice of operator ordering in the atom-field Hamiltonian. DDC considered a specific operator ordering in their formalism such that the vacuum fluctuation and radiation reaction contributes to the Hamiltonian through independent Hermitian operators [146,147]. Hence the effect of these two phenomena can be distinguished [116,150]. Following the implementation of DDC formalism in case of energy level shifts and radiative processes of atoms [124,125,151–153], we first discuss the formalism in context of our system.

We consider two identical, neutral, two level atoms (designated by the labels A and B) are interacting with quantized, massless, real, scalar vacuum. We assume that the atoms are pointlike particles with internal energy eigenstates $\{|g\rangle, |e\rangle\}$ and corresponding eigenvalues $\mp\frac{1}{2}\hbar\omega_0$. Let the atoms are accelerating within two perfectly reflecting mirrors situated at $z = 0$ and $z = L$, extending upto $\pm\infty$

along the $x-y$ direction. Let the atoms move along the parallel trajectories $X_{A/B}(\tau)$ ($\tau \rightarrow$ proper time of the atoms) such that the separation between two atoms remain constant. We assume that atoms are interacting with the field from infinite past to infinite future and neglect the transient effects due to switching on-off of the interaction in our calculation.

In the comoving frame of atoms, the system we have considered can be described by the multipolar Hamiltonian [126,148,149]

$$H(\tau) = \omega_0 \sigma_3^A(\tau) + \omega_0 \sigma_3^B(\tau) + \int d^3k\ \omega_k\ a_k^\dagger a_k\ \frac{dt}{d\tau} + \lambda[\sigma_2^A(\tau)\phi(X_A(\tau)) + \sigma_2^B(\tau)\phi(X_B(\tau))] \tag{4.1}$$

where ϕ is the scalar field given by

$$\phi(X) = \int d^3k \frac{1}{\sqrt{2(2\pi)^3\omega_k}}\ [a_k(t)e^{i\vec{k}\cdot\vec{x}} + a_k^\dagger(t)e^{-i\vec{k}\cdot\vec{x}}]. \tag{4.2}$$

$a_k(t)$, $a_k^\dagger(t)$ are the annihilation and creation operators of the k^{th} mode and the constant λ is the atom-field coupling strength. The atomic pseudo spin operators σ_2 and σ_3 are given by

$$\begin{aligned} \sigma_3 = &\quad \frac{1}{2}(|e\rangle\langle e| - |g\rangle\langle g|) \\ \sigma_2 = &\quad \frac{i}{2}(|g\rangle\langle e| - |e\rangle\langle g|). \end{aligned} \tag{4.3}$$

We assume the atom and the field as the system and reservoir respectively. Following DDC formalism [126,146,147], the Heisenberg equation for the field operator is given by

$$\begin{aligned} \frac{da_k(t(\tau))}{d\tau} &= i[H(\tau), a_k(t(\tau))] \\ &= -i\omega_k a_k(t(\tau))\frac{dt}{d\tau} + i\lambda\sigma_2^A[\phi(X_A(\tau)), a_k(t(\tau))] + i\lambda\sigma_2^B[\phi(X_B(\tau)), a_k(t(\tau))]. \end{aligned} \tag{4.4}$$

the Heisenberg equations for the atomic operators are given by

$$\begin{aligned}\frac{d\sigma_3(\tau)}{d\tau} &= i[H(\tau), \sigma_3(\tau)] \\ &= i\lambda[\sigma_2(\tau), \sigma_3(\tau)]\phi(X(\tau)) \qquad (4.5)\\ \frac{d\sigma_\pm(\tau)}{d\tau} &= i[H(\tau), \sigma_\pm(\tau)] \\ &= i\omega_0[\sigma_3(\tau), \sigma_\pm(\tau)] + i\lambda[\sigma_2(\tau), \sigma_\pm(\tau)]\phi(X(\tau)) \qquad (4.6)\end{aligned}$$

where $\sigma_+ = |e\rangle\langle g|$ and $\sigma_- = |g\rangle\langle e|$. Integrating Eq. (4.4), Eq. (4.5), Eq. (4.6) we get the solutions of these equation upto first order in λ :

$$\begin{aligned}a_k(t(\tau)) &= a_k^f(t(\tau)) + a_k^s(t(\tau)) \\ a_k^f(t(\tau)) &= a_k(t(\tau_0))e^{-i\omega_k(t(\tau)-t(\tau_0))} \\ a_k^s(t(\tau)) &= i\lambda\{\int_{\tau_0}^{\tau} d\tau' \sigma_2^A[\phi(X_A(\tau')), a_k^f(t(\tau))] + A \leftrightarrows B \text{ term}\}. \qquad (4.7)\end{aligned}$$

$$\begin{aligned}\phi(X(\tau)) &= \phi^f(X(\tau)) + \phi^s(X(\tau)) \\ \phi^f(X) &= \int d^3k \frac{1}{\sqrt{2\omega_k}}[a_k(t)e^{i\vec{k}\cdot\vec{x}} + a_k^\dagger(t)e^{-i\vec{k}\cdot\vec{x}}] \\ \phi^s(X(\tau)) &= i\lambda\{\int_{\tau_0}^{\tau} d\tau' \sigma_2^A[\phi(X_A(\tau')), \phi^f(X(\tau))] + A \leftrightarrows B \text{ term}\}. \qquad (4.8)\end{aligned}$$

$$\begin{aligned}\sigma_3(t(\tau)) &= \sigma_3^f(t(\tau)) + \sigma_3^s(t(\tau)) \\ \sigma_3^f(t(\tau)) &= \sigma_3^f(t(\tau_0)) \\ \sigma_3^s(t(\tau)) &= -i\lambda \int_{\tau_0}^{\tau} d\tau' \phi(x(\tau'))[\sigma_2^f(t(\tau')), \sigma_3^f(t(\tau))]. \qquad (4.9)\end{aligned}$$

$$\begin{aligned}\sigma_\pm(t(\tau)) &= \sigma_\pm^f(t(\tau)) + \sigma_\pm^s(t(\tau)) \\ \sigma_\pm^f(t(\tau)) &= \sigma_\pm^f(t(\tau_0))e^{-i\omega_k(t(\tau)-t(\tau_0))} \\ \sigma_\pm^s(t(\tau)) &= -i\lambda \int_{\tau_0}^{\tau} d\tau' \phi(x(\tau'))[\sigma_2^f(t(\tau')), \sigma_\pm^f(t(\tau))]. \qquad (4.10)\end{aligned}$$

In above equations, the superscript f and s implies free and source part of the solutions.

Let us consider an arbitrary system observable $G_A(\tau)$ associated to atom A

(alternatively we could have choose observable associated to B or both A and B) in the Heisenberg picture. Employing symmetric operator ordering and using the solution of Heisenberg equations obtained above, the rate of change of $G_A(\tau)$ averaged over field variables is given by (upto order λ^2)

$$\left\langle\left(\frac{dG_A}{d\tau}\right)_{vf}\right\rangle_\phi = -\lambda^2\int_{\tau_0}^{\tau} d\tau' C^F(X_A(\tau),X_A(\tau'))\left[\sigma_2^{A,f}(t(\tau')),\left[\sigma_2^{A,f}(t(\tau)),G_A^f(\tau)\right]\right]$$

$$\left\langle\left(\frac{dG_A}{d\tau}\right)_{sr}\right\rangle_\phi = -\lambda^2\int_{\tau_0}^{\tau} d\tau'\Big[\chi^F(X_A(\tau),X_A(\tau'))\left[\sigma_2^{A,f}(t(\tau')),\left[\sigma_2^{A,f}(t(\tau)),G_A^f(\tau)\right]\right]+ \chi^F(X_B(\tau),X_A(\tau'))\left[\sigma_2^{B,f}(t(\tau')),\left[\sigma_2^{A,f}(t(\tau)),G_A^f(\tau)\right]\right]\Big]. \tag{4.11}$$

where the subscripts "vf" and "sr" imply vacuum fluctuation and self reaction respectively. C^F and χ^F are symmetric and anti-symmetric field correlations respectively defined as

$$C^F(X(\tau),X(\tau')) = \frac{1}{2}\langle 0 \mid \{\phi^F(X(\tau)),\phi^F(X(\tau'))\} \mid 0\rangle \tag{4.12}$$

and

$$\chi^F(X(\tau),X(\tau')) = \frac{1}{2}\langle 0 \mid [\phi^F(X(\tau)),\phi^F(X(\tau'))] \mid 0\rangle \ , \tag{4.13}$$

where $|0\rangle$ is the Minkowski vacuum. The anti-symmetric field correlation is also known as susceptibility. The commutator part of Eq. (4.11) can be considered as the effective Hamiltonian (operating on the atom A) [124]

$$\begin{aligned}(H_{A,\ eff}) &= (H_{A,\ eff})_{vf} + (H_{A,\ eff})_{sr}\\ (H_{A,\ eff})_{vf} &= -\frac{i\lambda^2}{2}\int_{\tau_0}^{\tau} d\tau' C^F(X_A(\tau),X_A(\tau'))\left[\sigma_2^{A,f}(t(\tau)),\sigma_2^{A,f}(t(\tau'))\right]\\ (H_{A,\ eff})_{sr} &= -\frac{i\lambda^2}{2}\int_{\tau_0}^{\tau} d\tau'\Big[\chi^F(X_A(\tau),X_A(\tau'))\left[\sigma_2^{A,f}(t(\tau)),\sigma_2^{A,f}(t(\tau'))\right]\\ &\qquad + \chi^F(X_A(\tau),X_B(\tau'))\left[\sigma_2^{A,f}(t(\tau)),\sigma_2^{B,f}(t(\tau'))\right]\Big] \ .\end{aligned} \tag{4.14}$$

4.1.1 Energy level shift in the two atom system

The effective Hamiltonian operating on each atom will cause energy level shift. Sum of energy level shift in each atom gives the total energy level shift in the two particle system. The total energy level shift is evaluated using non-degenerate

perturbation theory [124]

$$\begin{aligned}
\delta E &= (\delta E)_{vf} + (\delta E)_{sr} \\
(\delta E)_{vf} &= -i\lambda^2 \int_{\tau_0}^{\tau} d\tau' \Big[C^F(X_A(\tau), X_A(\tau')) \chi_A(\tau,\tau') + A \leftrightarrows B \text{ term} \Big] \\
(\delta E)_{sr} &= -i\lambda^2 \int_{\tau_0}^{\tau} d\tau' \Big[\chi^F(X_A(\tau), X_A(\tau')) C_A(\tau,\tau') + \chi^F(X_A(\tau), X_B(\tau'))\, C_{A,B}(\tau,\tau') \\
&\qquad + A \leftrightarrows B \text{ term} \Big] .
\end{aligned} \tag{4.15}$$

The terms $C(\tau,\tau')$ and $\chi(\tau,\tau')$ are the symmetric and anti-symmetric atomic correlations, defined as

$$\chi(\tau,\tau') = \frac{1}{2} \langle \psi \mid [\sigma_2^f(t(\tau)), \sigma_2^f(t(\tau'))] \mid \psi \rangle \tag{4.16}$$

$$C(\tau,\tau') = \frac{1}{2} \langle \psi \mid \{\sigma_2^f(t(\tau)), \sigma_2^f(t(\tau'))\} \mid \psi \rangle \ , \tag{4.17}$$

where $|\psi\rangle$ is the state of the two atoms. $(\delta E)_{vf}$ and the first term of $(\delta E)_{sr}$ (along with their $A \leftrightarrows B$ counterparts) cause Lamb shift in the two particle system. The second term of $(\delta E)_{sr}$ (along with their $A \leftrightarrows B$ counterparts) is the energy level shift due to resonance interaction in the two particle system.

4.1.2 Relaxation rate of change of energy in the two atom system

We substitute $G_A(\tau)$ in Eq. (4.11) by total atomic Hamiltonian $H_s(\tau) = \omega_0 \sigma_3^A(\tau) + \omega_0 \sigma_3^B(\tau)$ and compute the expectation with respect to the two particle state $|\psi\rangle$. The resulting expression gives the relaxation rate of change of energy of the two particle system [126]

$$\begin{aligned}
R &= R_{vf} + R_{sr} \\
R_{vf} &= 2i\lambda^2 \int_{\tau_0}^{\tau} d\tau' \Big[C^F(X_A(\tau), X_A(\tau')) \frac{d}{d\tau} \chi_A(\tau,\tau') + A \leftrightarrows B \text{ term} \Big] \\
R_{sr} &= 2i\lambda^2 \int_{\tau_0}^{\tau} d\tau' \Big[\chi^F(X_A(\tau), X_A(\tau')) \frac{d}{d\tau} C_A(\tau,\tau') + \chi^F(X_A(\tau), X_B(\tau')) \frac{d}{d\tau} C_{A,B}(\tau,\tau') \\
&\qquad + A \leftrightarrows B \text{ term} \Big]
\end{aligned} \tag{4.18}$$

with $R = \left\langle \left(\frac{dH_s(\tau)}{d\tau} \right) \right\rangle_{\phi,\psi}$, $R_{vf} = \left\langle \left(\frac{dH_s(\tau)}{d\tau} \right)_{vf} \right\rangle_{\phi,\psi}$, $R_{sr} = \left\langle \left(\frac{dH_s(\tau)}{d\tau} \right)_{sr} \right\rangle_{\phi,\psi}$. R_{vf} and the first term of R_{sr} (along with their $A \leftrightarrows B$ counterparts) is the total

relaxation rate of change of energy through spontaneous emission. The second term of R_{sr} (along with their $A \leftrightarrows B$ counterparts) is the total relaxation rate of change of energy through resonance interaction.

4.2 Energy level shift and rate of change of energy due to resonance interaction two entangled atoms accelerating between parallel mirrors

We will now apply above formulation in case of the system we have considered. Let the quantum state of the two atoms is given by

$$|\psi\rangle = \sin\theta\,|g_A, e_B\rangle + \cos\theta\,|e_A, g_B\rangle \tag{4.19}$$

with $0 \leq \theta \leq \pi$. At $\theta = 0, \frac{\pi}{2}, \pi$ the state of the atoms are separable. At $\theta = \frac{\pi}{4}, \frac{3\pi}{4}$ the state is maximally entangled. $\theta = \frac{\pi}{4}$ and $\theta = \frac{3\pi}{4}$ corresponds to superradiant and subradiant states respectively. The atoms are confined in the z direction, by two mirrors placed at $z = 0$ and $z = L$ respectively.

As we have mentioned in the introduction, we consider two spatial configurations of the atoms : the line joining two atoms is perpendicular to the plane of the plates as shown in the Figure (4.1) and the line joining two atoms is parallel to the plane of the plates as shown in the Figure (4.2).

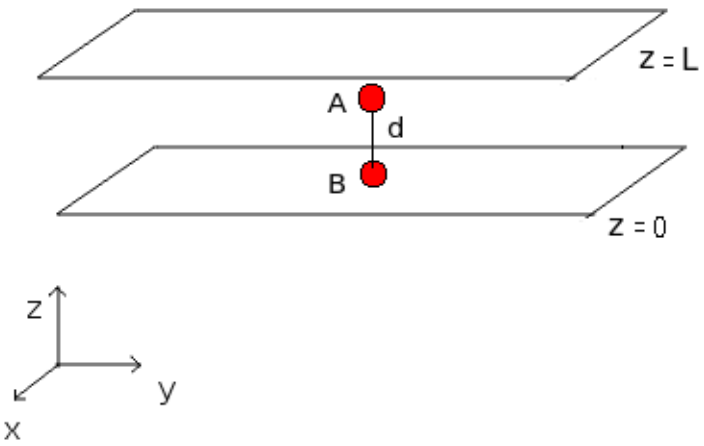

Figure 4.1: Line joining two atoms is perpendicular to the plates

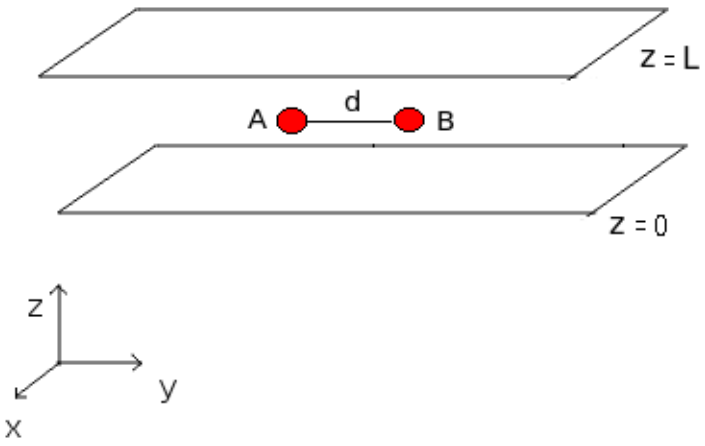

Figure 4.2: Line joining two atoms is parallel to the plates

Let, the atoms are accelerating along x-direction.

Configuration 1: The trajectories of the atoms, when line joining two atoms is perpendicular to the plane of the plates, are

$$\begin{aligned} t_{A/B}(\tau) &= \frac{1}{a}\sinh a\tau \\ x_{A/B}(\tau) &= \frac{1}{a}\cosh a\tau \\ y_A &= y_B = 0 \\ z_A &= z_0 \\ z_B &= z_0 + d \end{aligned} \tag{4.20}$$

where a is the proper acceleration of both the atoms, and d is the interatomic distance. Since atoms are confined within the mirrors, $d + z_0 \leq L$ should hold for this configuration.

Configuration 2: The trajectories of the atoms, when line joining two atoms

is parallel to the plane of the plates, are

$$\begin{aligned} t_{A/B}(\tau) &= \frac{1}{a}\sinh a\tau \\ x_{A/B}(\tau) &= \frac{1}{a}\cosh a\tau \\ y_B &= y_A + d \\ z_A &= z_B = z_0 \ . \end{aligned} \tag{4.21}$$

We will calculate energy level shift and rate of change of energy due to resonance interaction of atoms in above two configurations. For that we need to calculate susceptibility $\chi^F(X_A(\tau), X_B(\tau'))$ and symmetric atomic correlation $C_{A,B}(\tau,\tau')$. For the system considered, Eq. (4.13) takes the form

$$\chi^F(X_A(\tau), X_B(\tau')) = \frac{1}{2}\langle 0 \mid [\phi^F(X_A(\tau)), \phi^F(X_B(\tau'))] \mid 0\rangle \ . \tag{4.22}$$

In case of space-time bounded by two parallel mirrors, the Wightman function between two space-time points is obtained using the method of images [154]

$$\begin{aligned} &W(X(\tau), X(\tau')) = \langle 0 \mid \phi^F(X(\tau))\phi^F(X(\tau')) \mid 0\rangle \\ &= -\frac{1}{4\pi^2}\sum_{n=-\infty}^{\infty}\Big[\frac{1}{(\Delta t - i\eta)^2 - \Delta x^2 - \Delta y^2 - (2Ln - \Delta z)^2} - \frac{1}{(\Delta t - i\eta)^2 - \Delta x^2 - \Delta y^2 - (2Ln - z - z')^2}\Big]. \end{aligned} \tag{4.23}$$

Using above definition susceptibility can be expressed as

$$\begin{aligned} \chi^F(X(\tau), X(\tau')) = -\frac{i}{4\pi}\sum_{n=-\infty}^{\infty}\epsilon(\Delta t)\Big[&\delta(\Delta t^2 - \Delta x^2 - \Delta y^2 - (2Ln - \Delta z)^2) \\ &-\delta(\Delta t^2 - \Delta x^2 - \Delta y^2 - (2Ln - z - z')^2)\Big] \end{aligned} \tag{4.24}$$

with

$$\begin{aligned} \epsilon(\Delta t) &= 1 \quad \text{for} \ \ \Delta t > 0 \\ &= -1 \quad \text{for} \ \Delta t < 0. \end{aligned} \tag{4.25}$$

Substituting trajectories of the particles in two configurations, described by Eq. (4.20), Eq. (4.21), in the above expression and using the relation $\delta(f(r)) = \sum_j \frac{\delta(r-r_j)}{|f'(r_j)|}$ (r_j(s) are the roots of $f(r)$) we evaluate the susceptibility for the two cases:

Configuration 1:

$$\chi_{\perp}^{F}(X_A(\tau), X_B(\tau')) = -\frac{1}{8\pi^2}\int_0^{\infty} d\omega\ (e^{i\omega\Delta\tau} - e^{-i\omega\Delta\tau})\ \times \sum_{n=-\infty}^{\infty}\Big[\frac{\sin(\frac{2\omega}{a}\sinh^{-1}(\frac{z_1 a}{2}))}{z_1\sqrt{1+\frac{z_1^2a^2}{4}}} - \frac{\sin(\frac{2\omega}{a}\sinh^{-1}(\frac{z_2 a}{2}))}{z_2\sqrt{1+\frac{z_2^2a^2}{4}}}\Big] \tag{4.26}$$

where $\Delta\tau = (\tau - \tau')$, $z_1 =\mid 2nL - d \mid$ and $z_2 =\mid 2nL - 2z_0 - d \mid$.

Configuration 2:

$$\chi_{\parallel}^{F}(X_A(\tau), X_B(\tau')) = -\frac{1}{8\pi^2}\int_0^{\infty} d\omega\ (e^{i\omega\Delta\tau} - e^{-i\omega\Delta\tau})\ \times \sum_{n=-\infty}^{\infty}\Big[\frac{\sin(\frac{2\omega}{a}\sinh^{-1}(\frac{z_3 a}{2}))}{z_3\sqrt{1+\frac{z_3^2a^2}{4}}} - \frac{\sin(\frac{2\omega}{a}\sinh^{-1}(\frac{z_4 a}{2}))}{z_4\sqrt{1+\frac{z_4^2a^2}{4}}}\Big] \tag{4.27}$$

where $z_3 = \sqrt{d^2 + 4n^2L^2}$ and $z_4 = \sqrt{d^2 + 4(nL - z_0)^2}$.

Using Eq. (4.17), Eq. (4.19) we obtain the symmetric atomic correlation for the system under consideration

$$\begin{aligned} C_{A,B}(\tau,\tau') &= \frac{1}{2}\langle\psi \mid \{\sigma_2^{A,f}(t(\tau)), \sigma_2^{B,f}(t(\tau'))\} \mid \psi\rangle \\ &= \frac{\sin 2\theta}{8}(e^{i\omega_0\Delta\tau} - e^{-i\omega_0\Delta\tau}). \end{aligned} \tag{4.28}$$

4.2.1 Resonance energy level shift

From Eq. (4.15) the resonance energy level shift for two particle system can be written as

$$\delta E_r = -i\lambda^2\int_{\tau_0}^{\tau} d\tau'[\chi^F(X_A(\tau), X_B(\tau'))\ C_{A,B}(\tau,\tau') + A \leftrightarrows B \text{ term}]. \tag{4.29}$$

Using above equation along with Eq. (4.26), Eq. (4.27), Eq. (4.28) we calculate the resonance energy shift for the two configurations we have considered. In order to evaluate the integrals we set $\tau \to \infty$ and $\tau_0 \to -\infty$ following DDC formalism [147]. This implies that correlation time of the atoms are very small compared to their time of flight $(\tau - \tau_0)$. However the relaxation time of the atoms are much larger than$(\tau - \tau_0)$.

Hence the resonance energy shift for

Configuration 1:

$$(\delta E_r)_\perp = -\frac{\lambda^2 \sin 2\theta}{16\pi} \sum_{n=-\infty}^{\infty} \left[\frac{\cos(\frac{2\omega_0}{a} \sinh^{-1}(\frac{z_1 a}{2}))}{z_1 \sqrt{1+\frac{z_1^2 a^2}{4}}} - \frac{\cos(\frac{2\omega_0}{a} \sinh^{-1}(\frac{z_2 a}{2}))}{z_2 \sqrt{1+\frac{z_2^2 a^2}{4}}} \right] \quad (4.30)$$

Configuration 2:

$$(\delta E_r)_\parallel = -\frac{\lambda^2 \sin 2\theta}{16\pi} \sum_{n=-\infty}^{\infty} \left[\frac{\cos(\frac{2\omega_0}{a} \sinh^{-1}(\frac{z_3 a}{2}))}{z_3 \sqrt{1+\frac{z_3^2 a^2}{4}}} - \frac{\cos(\frac{2\omega_0}{a} \sinh^{-1}(\frac{z_4 a}{2}))}{z_4 \sqrt{1+\frac{z_4^2 a^2}{4}}} \right]. \quad (4.31)$$

In order to understand the dependence of resonance energy shift on various system parameters we plot $(\delta E_r)_\perp$ and $(\delta E_r)_\parallel$ with respect to initial acceleration of the atoms (a), interatomic separation (d), and distance of any one atom from adjacent plate (z_0). In this work we choose z_0 to be the distance between the plate at $z = 0$ and the nearest atom(s). In the plots all physical quantities have been represented in the dimensionless units. The order of magnitude of the quantities $\omega_0 L$, $\omega_0 z_0$ and $\omega_0 d$ are chosen in the similar range (here ω_0 is a constant, not a parameter) to maximize the effect of the cavity on the dynamics of the system [156].

The expression in Eq. (4.30), Eq. (4.31) suggests that the resonance energy level shift changes sinusoidally with entanglement. In realistic situations it is very difficult to preserve entanglement in the laboratory. So, the quantum states used during the experiments are usually non-maximally entangled. The plots are presented for maximum entanglement. Since magnitude of resonance energy shift is same for both $\theta = \frac{\pi}{4}, \frac{3\pi}{4}$, we have done all the plots by setting $\theta = \frac{3\pi}{4}$.

First, we study the variation of energy level shift due to varying acceleration. As mentioned earlier, atoms may be subjected to acceleration inside waveguides by the background potential. Figure (4.3) shows variation of resonance energy shift (per unit $\left(\frac{\lambda^2\omega_0}{16\pi}\right)$) with respect to acceleration for both configurations. At lower values of acceleration the resonance energy shift increases with increase in acceleration. Then it reaches a peak and decreases with increase in acceleration for higher values of acceleration. The plots also show that atomic configuration and cavity parameters affect the value of resonance energy level shift.

Let us now study how resonance energy level shift is affected by interatomic distance and their position with respect to the plates. Figure (4.4) shows variation of resonance energy shift (per unit $\left(\frac{\lambda^2\omega_0}{16\pi}\right)$) with respect to the distance $(\omega_0 z_0)$

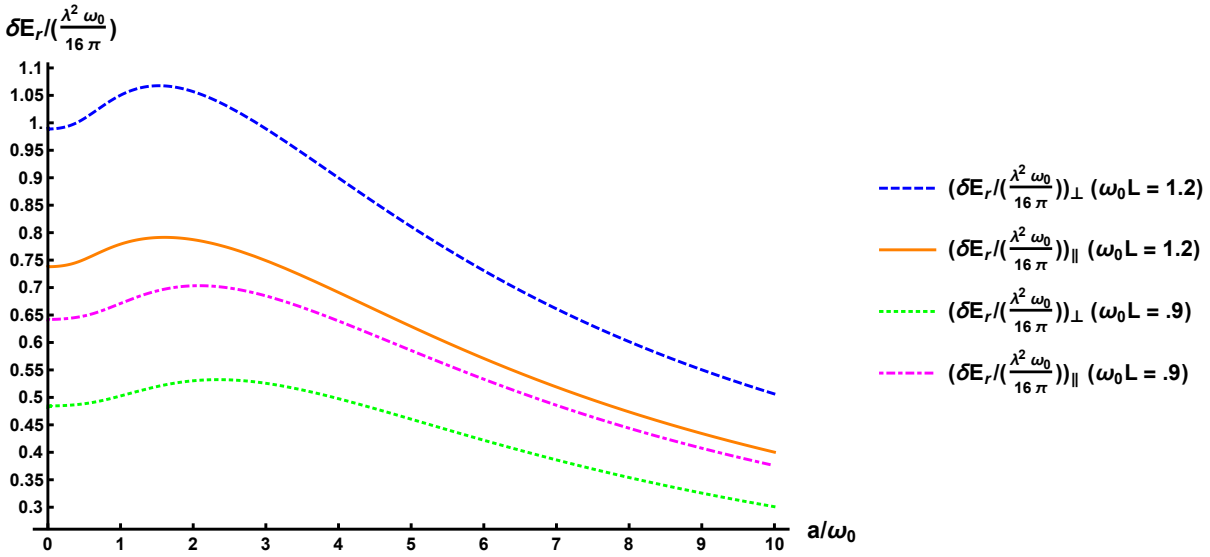

Figure 4.3: Resonance energy level shift (per unit $\left(\frac{\lambda^2\omega_0}{16\pi}\right)$) versus acceleration (the symbol $\mathbf{a}\equiv a$), $((E_r/\left(\frac{\lambda^2\omega_0}{16\pi}\right))_\perp$ stands for atoms aligned perpendicular to the plates, $(E_r/\left(\frac{\lambda^2\omega_0}{16\pi}\right))_\parallel$ stands for atoms aligned parallel to the plates), $\theta = 3\pi/4$, $\omega_0 d = 0.5$, $\omega_0 z_0 = 0.3$.

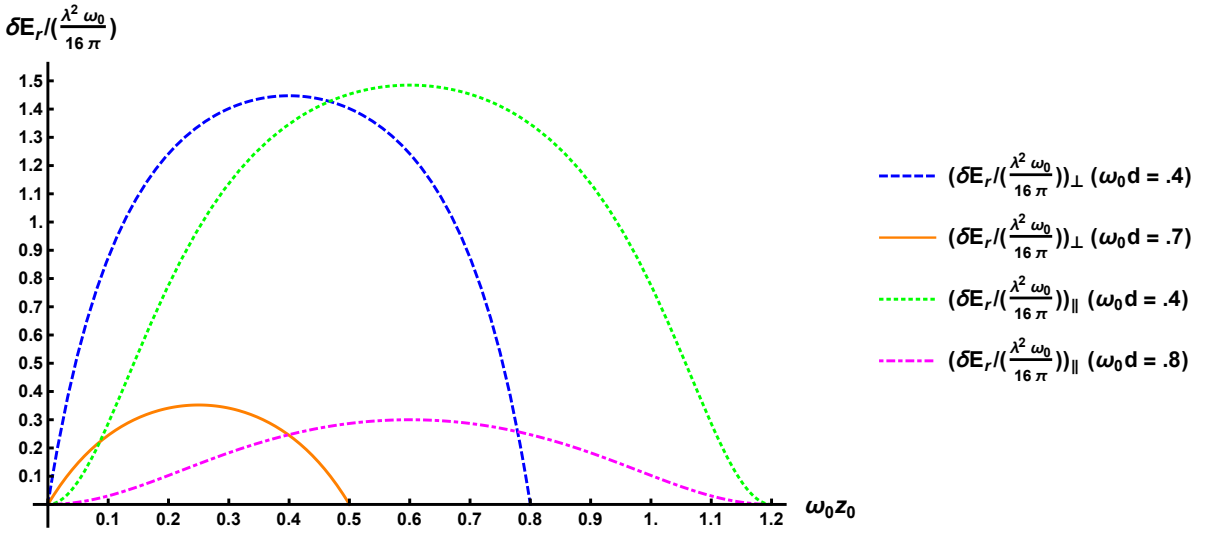

Figure 4.4: Resonance energy level shift (per unit $\left(\frac{\lambda^2\omega_0}{16\pi}\right)$) versus distance of any one atom from one plate (both configurations), $\theta = 3\pi/4$, $a/\omega_0 = 4$, $\omega_0 L = 1.2$.

of one atom from the adjacent plate. The plots have been presented for different values of interatomic separation in case of both configurations. From the plots,

we see that both the energy shifts and their difference due to different interatomic separations get enhanced when atoms are farther from the boundaries, and diminish as they get closer to the boundary. The energy shift becomes maximum when the atoms are equidistant from both plates (true for both configurations). If either of the atoms touches the plate, resonance interaction will vanish (as can be seen from the relevant mathematical expressions, as well).

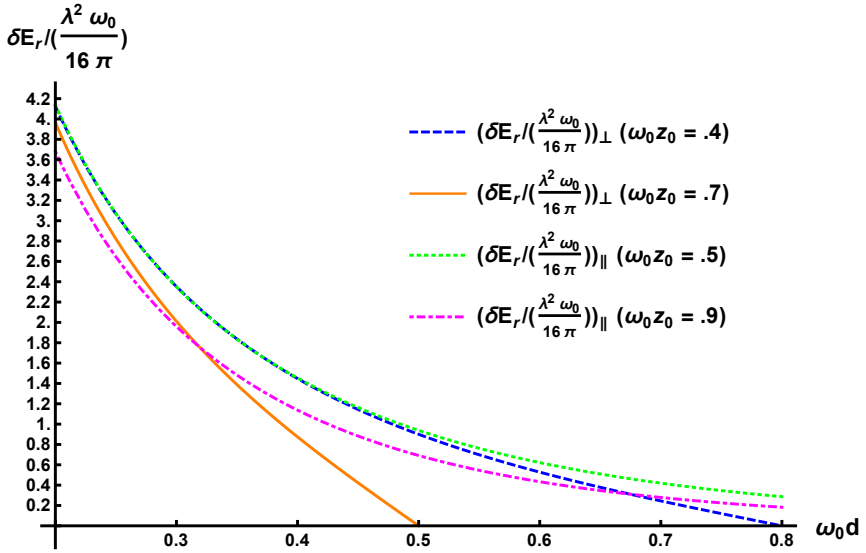

Figure 4.5: Resonance energy level shift (per unit $\left(\frac{\lambda^2\omega_0}{16\pi}\right)$) versus interatomic distance (for both configurations), $\theta = 3\pi/4$, $a/\omega_0 = 4$, $\omega_0 L = 1.2$.

Figure (4.5) shows variation of resonance energy shift (per unit $\left(\frac{\lambda^2\omega_0}{16\pi}\right)$) with respect to interatomic separation for both configurations. In all the cases the resonance energy shift decreases monotonically with increase in the interatomic separation. In case of configuration 1 the rate of decrement is sharper than that of configuration 2. This is because of the fact that with increase in the interatomic separation the atoms moves closer to the mirrors in case of configuration 1. In case of configuration 2, z_0 remains constant with increase in the interatomic separation.

So far we have studied the dependence of resonance energy shift on various system parameters. Next we will calculate the energy shift for limiting cases of various parameters.

Low acceleration limit

When the acceleration is low such that $a \ll L^{-1}, d^{-1}, z_0^{-1}$ i.e, aL, az_0, $ad \ll 1$. The 1$^{\text{st}}$ term of Eq. (4.30) can be rewritten as

$$((\delta E_r)_\perp)_{1st\ \text{term}} = \frac{\lambda^2 \sin 2\theta}{16\pi}\Bigg[\frac{\cos\left(\frac{2\omega_0}{a}\sinh^{-1}\left(\frac{da}{2}\right)\right)}{d\sqrt{1+\frac{d^2a^2}{4}}}+ \sum_{n=0}^{\lfloor\frac{1}{aL}\rceil}\left(\frac{\cos\left(\frac{2\omega_0}{a}\sinh^{-1}\left(nLa\left(1-\frac{d}{2nL}\right)\right)\right)}{(2nL-d)\sqrt{1+n^2L^2a^2\left(1-\frac{d}{2nL}\right)^2}}+\frac{\cos\left(\frac{2\omega_0}{a}\sinh^{-1}\left(nLa\left(1+\frac{d}{2nL}\right)\right)\right)}{(2nL+d)\sqrt{1+n^2L^2a^2\left(1+\frac{d}{2nL}\right)^2}}\right)+ \sum_{n\ =\lfloor\frac{1}{aL}\rceil+1}^{\infty}\left(\frac{\cos\left(\frac{2\omega_0}{a}\sinh^{-1}\left(nLa\left(1-\frac{d}{2nL}\right)\right)\right)}{(2nL-d)\sqrt{1+n^2L^2a^2\left(1-\frac{d}{2nL}\right)^2}}+\frac{\cos\left(\frac{2\omega_0}{a}\sinh^{-1}\left(nLa\left(1+\frac{d}{2nL}\right)\right)\right)}{(2nL+d)\sqrt{1+n^2L^2a^2\left(1+\frac{d}{2nL}\right)^2}}\right)\Bigg] \tag{4.32}$$

where $\lfloor\cdot\rceil$ is the nearest integer. In the limit $aL \to 0$, 3$^{\text{rd}}$ term of Eq. (4.32) vanishes. So, the Eq. (4.32) reduces to

$$((\delta E_r)_\perp)_{1st\ \text{term}} = \frac{\lambda^2 \sin 2\theta}{16\pi}\Bigg[\frac{\cos\left(\frac{2\omega_0}{a}\sinh^{-1}\left(\frac{da}{2}\right)\right)}{d\sqrt{1+\frac{d^2a^2}{4}}}+ \sum_{n=0}^{\infty}\left(\frac{\cos\left(\frac{2\omega_0}{a}\sinh^{-1}\left(nLa\left(1-\frac{d}{2nL}\right)\right)\right)}{(2nL-d)\sqrt{1+n^2L^2a^2\left(1-\frac{d}{2nL}\right)^2}}+\frac{\cos\left(\frac{2\omega_0}{a}\sinh^{-1}\left(nLa\left(1+\frac{d}{2nL}\right)\right)\right)}{(2nL+d)\sqrt{1+n^2L^2a^2\left(1+\frac{d}{2nL}\right)^2}}\right)\Bigg]. \tag{4.33}$$

Similar reduction can be done for $2nd$ term of Eq. (4.30). In the limit aL, az_0, $ad \to 0$, expanding the surviving term upto order a^2 and simplifying we get

$$((\delta E_r)_\perp)_{\text{low acc.}} = \frac{\lambda^2 \sin 2\theta}{16\pi}\sum_{i=1,2}\Bigg[\sum_{n=1}^{\infty}\Bigg[\frac{\cos(\omega_0 M_i)}{M_i}-\frac{a^2}{8}\Big(M_i\cos(\omega_0 M_i) - \frac{M_i^2\omega_0}{3}\sin(\omega_0 M_i)\Big)\Bigg]+\sum_{n=0}^{\infty}\Bigg[\frac{\cos(\omega_0 Q_i)}{Q_i}-\frac{a^2}{8}\Big(Q_i\cos(\omega_0 Q_i)-\frac{Q_i^2\omega_0}{3}\sin(\omega_0 Q_i)\Big)\Bigg]\Bigg] \tag{4.34}$$

where $M_1 = (2nL-d)$, $M_2 = (2nL-2z_0-d)$, $Q_1 = (2nL+d)$ and $Q_1 = (2nL+2z_0+d)$. Above expression contains no term in the linear order in a which resembles inertial limits obtained with other systems in similar context [155]. The low acceleration limit of parallel configuration can be calculated in similar

manner.

Single mirror and free space limit

When $L \to \infty$, the system reduces to entangled atoms and field in presence of a single mirror. Substituing this limit in Eq. (4.30), Eq. (4.31) we get

$$(\delta E_r)_\perp = -\frac{\lambda^2 \sin 2\theta}{16\pi}\left[\frac{\cos(\frac{2\omega_0}{a}\sinh^{-1}(\frac{da}{2}))}{d\sqrt{1+\frac{d^2a^2}{4}}} - \frac{\cos(\frac{2\omega_0}{a}\sinh^{-1}(\frac{D_1 a}{2}))}{D_1\sqrt{1+\frac{D_1^2a^2}{4}}}\right] \tag{4.35}$$

where $D_1 = d + 2z_0$. The expression for $(\delta E_r)_\parallel$ in this limit is given by replacing D_1 in Eq. (4.35) by $D_2 = \sqrt{d^2 + 4z_0^2}$. These results match with the expression of resonance energy shift calculated explicitly for entangled atom and field in presence of single mirror [125].

When $L \to \infty$ and $z_0 \to \infty$, the system reduces to entangled atoms and field in free space. Substituing these two limits in Eq. (4.30), Eq. (4.31) we get

$$\delta E_r = -\frac{\lambda^2 \sin 2\theta}{16\pi} \cdot \frac{\cos(\frac{2\omega_0}{a}\sinh^{-1}(\frac{da}{2}))}{d\sqrt{1+\frac{d^2a^2}{4}}} \ . \tag{4.36}$$

Above expression holds for both configurations. This result matches with the expression of resonance energy shift calculated explicitly for entangled atoms and field in free space [124].

4.2.2 Relaxation rate of change of energy due to resonance interaction

From Eq. (4.18) the relaxation rate of energy exchange for two particle system can be written as

$$R_r = -i\lambda^2 \int_{\tau_0}^{\tau} d\tau' [\chi^F(X_A(\tau), X_B(\tau'))\frac{d}{d\tau}C_{A,B}(\tau,\tau') + A \leftrightarrows B \text{ term}]. \tag{4.37}$$

Using above equation and Eq. (4.26), Eq. (4.27), Eq. (4.28) we evaluate R_r for the two configurations. With similar arguments as in the case of energy shift, we set the limits of the integrals as $\tau \to \infty$, $\tau_0 \to -\infty$.

So, relaxation rate of energy exchange for

Configuration 1:

$$(R_r)_\perp = -\frac{\lambda^2\omega_0 \sin 2\theta}{8\pi}\sum_{n=-\infty}^{\infty}\left[\frac{\sin(\frac{2\omega_0}{a}\sinh^{-1}(\frac{z_1 a}{2}))}{z_1\sqrt{1+\frac{z_1^2a^2}{4}}} - \frac{\sin(\frac{2\omega_0}{a}\sinh^{-1}(\frac{z_2 a}{2}))}{z_2\sqrt{1+\frac{z_2^2a^2}{4}}}\right] \tag{4.38}$$

Configuration 2:

$$(R_r)_\parallel = -\frac{\lambda^2\omega_0 \sin 2\theta}{8\pi}\sum_{n=-\infty}^{\infty}\left[\frac{\sin(\frac{2\omega_0}{a}\sinh^{-1}(\frac{z_3 a}{2}))}{z_3\sqrt{1+\frac{z_3^2a^2}{4}}} - \frac{\sin(\frac{2\omega_0}{a}\sinh^{-1}(\frac{z_4 a}{2}))}{z_4\sqrt{1+\frac{z_4^2a^2}{4}}}\right]. \tag{4.39}$$

Now we plot the variation of relaxation rate of energy exchange $(R_r)_\perp$ and $(R_r)_\parallel$ against parameters such as the atom-plate distance (z_0), and separation between the plates (L). All the physical quantities have been represented in the dimensionless units and the entanglement parameter has been chosen as $\theta = \frac{3\pi}{4}$. The quantitative behaviour of the plots in the two cases have lot of similarities but there are a lot of significant differences that we will discuss below.

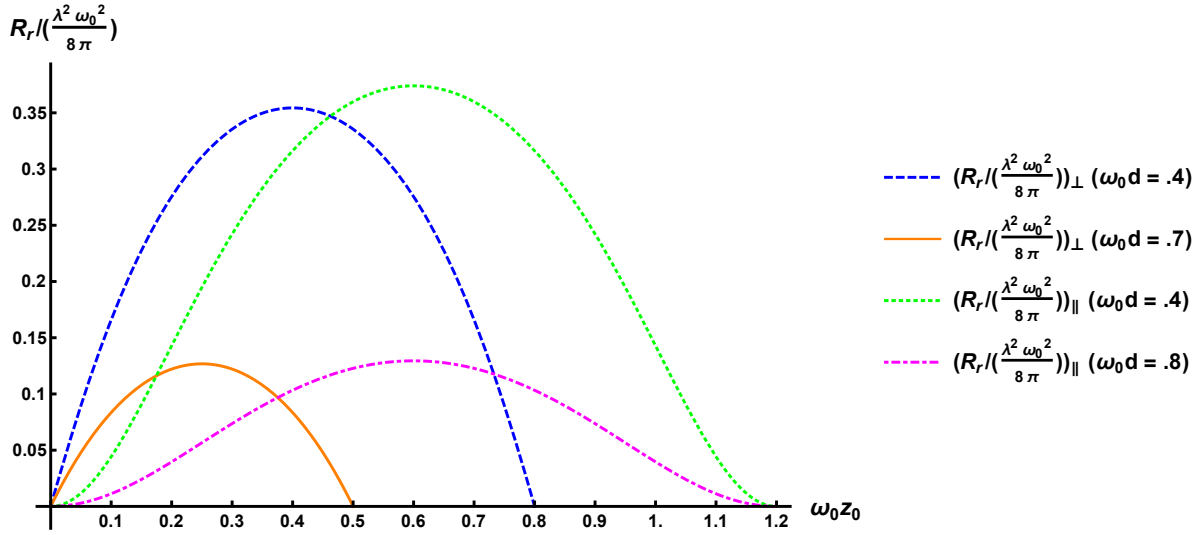

Figure 4.6: Relaxation rate due to resonance interaction (per unit $\left(\frac{\lambda^2\omega_0^2}{8\pi}\right)$) versus distance of any one atom from one plate (atoms aligned perpendicular to the plates), $\theta = 3\pi/4$, $a/\omega_0 = 4$, $\omega_0 L = 1.2$.

Figure (4.6) shows the variation of relaxation rate of energy exchange (per unit $\left(\frac{\lambda^2\omega_0^2}{8\pi}\right)$) for both configurations, with respect to the distance $(\omega_0 z_0)$ of one

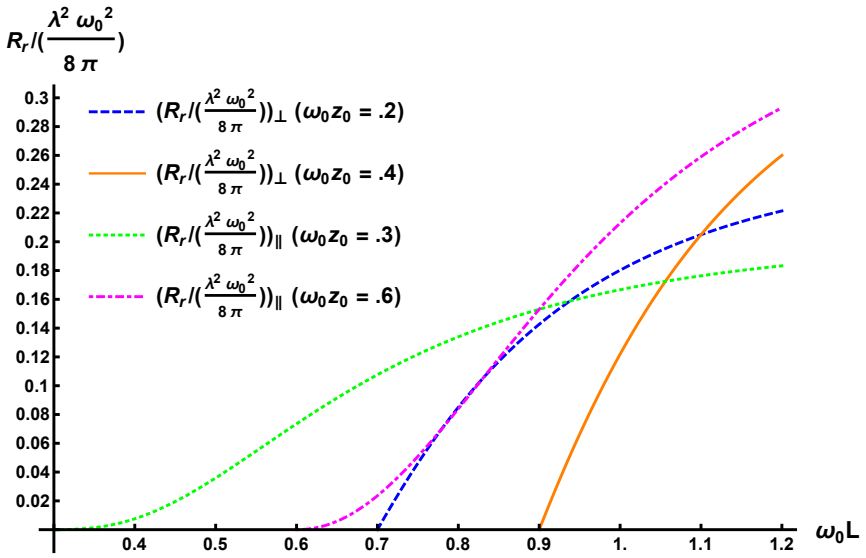

Figure 4.7: Relaxation rate due to resonance interaction (per unit $\left(\frac{\lambda^2\omega_0^2}{8\pi}\right)$) versus separation between two mirrors (for both configurations), $\theta = 3\pi/4$, $a/\omega_0 = 4$, $\omega_0 d = 0.5$.

atom from the adjacent plate. The plots have been done for various values of interatomic separation. Similar to the case of resonance energy level shift, $(R_r)_\perp$ and $(R_r)_\parallel$ get enhanced when the atoms are farther from the mirror and become maximum when the atoms are equidistant from both plates (for both configuration 1 and 2). So, the rate of energy exchange will get diminished as the atoms move nearer the mirror and vanishes as any of the atoms touches the mirror.

Figure (4.7) shows variation of relaxation rate of energy exchange (per unit $\left(\frac{\lambda^2\omega_0^2}{8\pi}\right)$), for both configurations, with respect to the separation between the two mirrors ($\omega_0 L$). For both configurations the rate of energy exchange increases with increase in the separation within two mirrors and tends toward the saturation value of the single boundary limit. This happens as increase in the plate separation makes our system access a larger number of modes. The variation is steeper for larger atom-plate distance, as seen from the plots.

Similar to the previous section, next we calculate relaxation rate of change of energy in the limiting cases of various parameters. In case of low acceleration the expression of $(R_r)_\perp$ and $(R_r)_\parallel$ can be obtained following the method described in Section 4.2.1. So let us now focus on the limiting cases of cavity parameters L and z_0.

Single mirror and free space limit

When $L \to \infty$, the system represents the entangled atoms and field in presence of a single mirror. Substituing this limit in Eq. (4.38), Eq. (4.39) we get

$$(R_r)_\perp = -\frac{\lambda^2 \omega_0 \sin 2\theta}{8\pi}\left[\frac{\sin(\frac{2\omega_0}{a}\sinh^{-1}(\frac{da}{2}))}{d\sqrt{1+\frac{d^2a^2}{4}}} - \frac{\sin(\frac{2\omega_0}{a}\sinh^{-1}(\frac{D_1 a}{2}))}{D_1\sqrt{1+\frac{D_1^2a^2}{4}}}\right] \tag{4.40}$$

with $D_1 = d + 2z_0$. The expression of $(R_r)_\parallel$ can be evaluated by replacing D_1 in Eq. (4.40) by $D_2 = \sqrt{d^2 + 4z_0^2}$.

When $L \to \infty$ and $z_0 \to \infty$, the system represents the entangled atoms and field in the free space. Substituting this limit in Eq. (4.38), Eq. (4.39) we get

$$R_r = -\frac{\lambda^2 \sin 2\theta}{8\pi} \cdot \frac{\sin(\frac{2\omega_0}{a}\sinh^{-1}(\frac{da}{2}))}{d\sqrt{1+\frac{d^2a^2}{4}}} \tag{4.41}$$

The above expression holds for both configuration 1 and 2. The expression of Eq. (4.41) matches with the result in the reference [126], where the relaxation rate of energy exchange has been explicitly calculated for entangled atoms and field in the free space.

4.3 Conclusions

In this chapter we have calculated energy level shift and relaxation rate of energy exchange of two entangled atoms, in their superradiant or subradiant state, accelerating between two mirrors. Resonance interaction is a significant phenomena which results from the interaction of two atoms, one in ground state and another in the excited state, with the quantum vacuum. The two atoms exchange real photons via the quantum field, as a result of such interaction.

The presence of mirrors invoke Dirichlet boundary conditions on the quantum field modes. We have considered two spatial configurations of the system : the line joining the two atoms are perpendicular and parallel to the plane of the plates respectively. Following the formalism proposed by DDC [146, 147], we have calculated the quantities of interest, the energy level shift and relaxation rate of energy. We have presented numerous plots showing the dependence of the above two quantities on various system parameters. We have also discussed our results for the limiting cases of the values of the parameters involved.

The aim of this work is to explore how the radiative process of entangled,

neutral atoms in noninertial frame in presence of boundary conditions can be manipulated by various parameters related to the atom and the atom-mirror spatial configuration. In order to evaluate the quantities of interest we have employed Wightman function of quantized scalar field bounder by two parallel mirrors. This function represents the correlation between the field at two space-time point resulting from the reflection of individual photons within the mirrors. Following DDC formalism we have studied resonance interaction between entangled atoms whose order of magnitude (proportional to square of atom-field coupling strength λ) is different from that of separable atom (proportional to fourth power of atom-field coupling strength). Our study show that, in the order λ^2, resonance interaction can occur even when the state of the two atoms are non-maximally entangled. Our results are also consistent with the fact that the resonance interaction in this order vanishes when the state of the atoms are separable suggested by earlier studies [111, 112, 121–123].

We have analytically evaluated the expression for energy level shift and relaxation rate of energy exchange due to resonance interaction and plotted these quantities against acceleration, distance of the atoms from the mirrors, separation between the atoms and separation within the two mirrors. The plots show that the choice of appropriate values of above parameters enables us to enhance or inhibit the resonance interaction. In the plots the value of acceleration is chosen in the order of transition energy ω_0 of the atoms. This gives a very high range of values of acceleration which is impossible to achieve with current technology. So, we analytically calculate the resonance energy shift for very small acceleration and same method can be used to calculate energy exchange rate for small acceleration. Putting appropriate limiting values of parameters in our results, we have also evaluated the resonance energy shift and energy exchange rate for single mirror and free space limit. The expressions obtained for these limiting cases matches with the results of the earlier studies which has explicitly calculated those cases.

In recent time, the development in the field of technology has enabled us to engineer cavity with dimension in the nanometer range and perform quantum electrodynamical experiment in such setup [138]. So, we can provide a quantitative estimation of the resonance energy level shift with realistic experimental parameters. We choose separation between the mirrors $L = 50$ nm, the distance of one mirror from the nearest atom $z_0 = 12$ nm, interatomic separation $d = 20$ nm and the acceleration of the atoms $\sim 10^{17}$ m/s^2 (maximum value of acceleration simulated through parametric amplification in the superconducting circuits [137]). We also set $\lambda = 0.1$ and $\omega_0 = 5$ eV. Using Eq. (4.34), we obtain the

correction in the resonance energy level shift because of the effect of acceleration as $\sim 10^{-11}$ eV. The experimentally measured value of Lamb shift of hydrogen atoms are $\sim 10^{-6}$ eV [157]. So, such correction in energy shift due to acceleration should be possible to probe with future technology.

In conclusion our analysis provides a platform to explore whether the resonance interaction of accelerated quantum emitters interacting with background electromagnetic vacuum can be manipulated in structured environment such as waveguide. In this work we have considered the effect of acceleration and Dirichlet boundary conditions. Further studies can be performed in this set-up to look for the effect of decoherence in practical situations. Similar studies can be performed for various other type of boundary conditions. Also our study can be extended in realistic situations such as quantum transport phenomena [158].

Chapter 5

Atom, mirror and GUP modified vacua : a test of weak equivalence principle

General relativity predicts that gravity is a manifestation of the geometry of space-time [159]. The geometry of space-time affects the dynamics of physical entities residing in it. In context of quantum field theory the background space-time geometry gives rise to production of particles from vacuum. The significant examples of such phenomena are cosmological particle production [6], Hawking radiation [7, 8], Unruh effect [12] etc. Since their discovery, the physics of such particle production phenomena have reached important milestones developing the foundation of quantum theory. The produced particles have a thermal spectrum which implies a deep connection between thermodynamics and gravity. This understanding has led the scientific community to formulate black hole thermodynamics [160]. The black hole information paradox in this context has indicated the requirement of consistency between quantum information theory and gravity.

The particle produced by quantum field due to background space-time geometry can excite atoms (Unruh-DeWitt detector) via atom-field interaction. Unruh effect predicts that the vacuum of an inertial observer will appear excited with respect to an observer with constant proper acceleration measured from comoving frame (Rindler observer) [12]. An atom accelerating with respect to Minkowski space-time can become excited by absorption of Rindler particle. As a consequence the inertial observer will observe the emission of Minkowski particle which is known as acceleration radiation [67]. An accelerated mirror also leads to particle production from vacuum [11] which can excite an Unruh-DeWitt detector [106].

In the theories mentioned above the gravity is treated classically. One of the

major goal of research in quantum foundation is to develop quantum theory of gravity. These efforts have developed the formulations of string theory [161] and loop quantum gravity [162]. These theories suggest that, a consistent theory of quantum gravity should correspond to a minimum observable length scale [163]. This minimum length scale is basically the Planck scale $l_P = \sqrt{G\hbar/c^3} \sim 10^{-33}$ cm. The existence of minimum length scale should modify Heisenberg's uncertainty principle. This modified uncertainty principle is known as the generalized uncertainty principle (GUP) [164, 165]. As GUP is associated to a minimum measurable length it is expected to violate Lorentz covariance [166].

Study of GUP has been performed in several directions such as black hole thermodynamics [167], Unruh effect [168] and low energy phenomenology such as quantum mechanics [169, 170], quantum optics [171] etc. These studies in the low energy quantum regime have opened up the possibilities to search for indirect evidence of quantum gravity in laboratory. Violation of equivalence principle is an interesting topic to explore in this context, after all GUP violates Lorentz covariance. However no studies has been performed in this directions. Violation of classical weak equivalence principle [172] has been explored in the context of interference experiments under gravitational acceleration [173], gravitationally bound particles [174] and freelly falling quantum mechanical particles [175] etc. The quantum state under the transformation of reference frames have profound significance in the context of equivalence principle for quantum systems [176]. Quantum formulation of equivalence principle has also been proposed [177].

The equivalence principle in the context of quantum electrodynamics has faced significant challenges [178, 179]. A very popular model to test weak equivalence principle (WEP) is the relative acceleration of detector and cavity [179, 180]. Such models compares the response of a detector accelerating through a static cavity and the response of a static detector when an accelerating cavity crossing it. In general the nonlocality of quantum field (massive/massless) can distinguish the two situations described above [180] which can be considered as a manifestation of violation of equivalence. In the work described above the cavity contains multimode vacuum. A similar problem has been studied in case of an atom-mirror system in relative acceleration in single mode vacuum [106]. Surprisingly in this specific case the transition probability of accelerated atom in presence of static mirror is equal to the transition probability of static atom in presence of accelerated mirror upto some constant phase factor. Equating the field frequency with the atomic transition frequency we see that, the position dependent Fano interference is same in both cases. This can be considered as a manifestation of symmetry between the two systems. So, this very set-up fails to register violation

of equivalence caused by quantum mechanical system.

Our aim in this work is to look for violation of equivalence introduced by GUP, in a system of particle detector and boundary in relative acceleration, with GUP modified single mode background quantum vacuum. For that purpose, we choose a GUP modified version of the system considered by Svidzinsky *et al.* [106]. So, in our calculation we consider two cases

(a) An accelerated two level atom interacting with single mode GUP modified vacuum in presence of a static mirror.

(b) A static two level atom interacting with single mode GUP modified vacuum in presence of an accelerated mirror.

We calculate excitation probability of atoms in each of the above cases and study the effect of GUP. The spatial dependence of the interference pattern exhibited by the transition probabilities are explicitly obtained in the single mode cavity set-up. We then compare the result obtained in the two cases in order to see the violation of equivalence introduced by GUP. It is important to note here that experimental implementation of the accelerating atom-mirror system has been proposed using superconducting circuits [54,137,181,182] which provides a direct experimental platform for the set-up we have considered in this work.

The work presented in this chapter is based on our publication [58]. In our calculation we have separately shown the contribution of field and atomic transition frequency in the excitation probabilities. The result shows that GUP affects the system through field frequency and has a damping effect on the system in both cases . In case (b) GUP modifies the Unruh temperature. Also in case (b) GUP introduces position dependent modulation in the Fano interference term. This breaks the symmetry observed, in absence of GUP, between the Fano interference pattern in the excitation probability in the two cases. Hence violation of equivalence due to GUP is obtained. We define a equivalence violation parameter in the context of our system and discuss how GUP can put bound on the violation. We also estimate a weak bound on GUP from the damping factor. All the calculations in this chapter has been done in SI units.

The organization of the chapter is as follows: in Section 5.1 we discuss the definition of GUP that we will use in our study. In Section 5.2 we will calculate the excitation probabilities of an accelerated two level atom interacting with single mode GUP modified vacuum in presence of a static mirror and the excitation probability of a static two level atom interacting with single mode GUP modified vacuum in presence of an accelerated mirror. In Section 5.3 we discuss the

violation of equivalence in our system. In Section 5.4 summarize our results and make concluding remarks.

5.1 The definition of generalized uncertainty principle (GUP)

The simplest definition of GUP is [169]

$$\Delta q_i \Delta p_i \geq \frac{\hbar}{2}\left[1+\beta(\Delta p^2+\langle p\rangle^2)+2\beta(\Delta p_i^2+\langle p_i\rangle^2)\right] \tag{5.1}$$

where $\beta=\beta_0/(M_{Pl}c)^2$ is the GUP parameter, β_0 is a constant, M_{Pl} is the Planck mass and $p^2=\sum_i p_i^2$, $(i=1,2,3)$. Setting $\beta=0$ in Eq. (5.1) we recover Heisenberg uncertainty principle. This modified uncertainty leads to following algebra

$$[q_i,p_j]=i\hbar(\delta_{ij}+\beta\delta_{ij}p^2+2\beta p_i p_j)\ . \tag{5.2}$$

Putting $\beta=0$ in above equation gives Heisenberg algebra. The GUP modifies relativistic dispersion relation [168].

5.1.1 GUP deformed Klein-Gordon equation

GUP modified dispersion relation leads to the deformed Klein-Gordon equation in $(1+1)$ dimensions [168] :

$$\left(c^{-2}\ \partial_t^2-\partial_z^2+2\beta\hbar^2\ \partial_z^4\right)\phi(t,z)=0\ . \tag{5.3}$$

$\beta=0$ gives standard Klein-Gordon equation in $(1+1)$ dimensions. Since β is a very small parameter the above equation can be solved perturbatively.

5.2 Excitation probability of atom by GUP modified vacua

Let us consider a two level atom with internal energy levels $\{|g\rangle\,,|e\rangle\}$ and energy eigenvalues $\{-\frac{\omega_0}{2},\frac{\omega_0}{2}\}$ respectively. The atom is interacting with single mode background quantized vacuum in presence of a mirror. The canonical operators of the quantum field satisfies GUP defined by Eq. (5.1). We will calculate the excitation probabilities of the atom in the following two situations:

5.2.1 Accelerating atom and static mirror

Let the mirror is static in the position $z = z_0$ in the Minkowski space-time. The atom is moving with uniform proper acceleration a through the Minkowski vacuum. The atom is considered as a point particle. The coordinate transformation b/w frame of the atom and Minkowski frame is

$$t = \frac{c}{a}\sinh\frac{a\eta}{c} \qquad\qquad z = \frac{c^2}{a}\cosh\frac{a\eta}{c} \tag{5.4}$$

with η is proper time of atom and $z_0 < c^2/a$.

In order to find excitation probability of atom we first solve Eq. (5.3), in Minkowski space-time with the boundary condition $\phi(t, z_0) = 0$ because of the mirror at $z = z_0$. We choose the solution ϕ of the form

$$\phi_\nu(t, z) = e^{-i\nu t}e^{nz} \tag{5.5}$$

where $\nu(> 0)$ is the frequency of the single mode field. Substituting this solution in Eq. (5.3), we get

$$n^2 - 2\beta\hbar^2 n^4 + \frac{\nu^2}{c^2} = 0\ . \tag{5.6}$$

In order to solve this equation we choose

$$n = (n_0 + \beta\ \widetilde{n}) \tag{5.7}$$

where n_0 and $\widetilde{n}$ has to be determined. Substituting this in the above equation and comparing coefficients of powers of β up to $\mathcal{O}(\beta)$ on both sides of the equation, we get

$$n_0 = \pm\frac{i\nu}{c} \tag{5.8}$$

$$\widetilde{n} = \mp\frac{i\hbar^2\nu^3}{c^3}\ . \tag{5.9}$$

So, we get

$$n = \pm\ i\frac{\nu}{c}\Big(1 - \beta\hbar^2\frac{\nu^2}{c^2}\Big)\ . \tag{5.10}$$

Hence the solution of Eq. (5.3) with the boundary condition $\phi(t, z_0) = 0$ is

$$\phi_\nu(t, z) = e^{-i\nu t}e^{-i\frac{\nu}{c}(1-\beta\hbar^2\frac{\nu^2}{c^2})(z-z_0)} -\ e^{-i\nu t}e^{i\frac{\nu}{c}(1-\beta\hbar^2\frac{\nu^2}{c^2})(z-z_0)}\ . \tag{5.11}$$

The atom-field interaction Hamiltonian can be written as

$$H_I(\eta) = \hbar g(\hat{a}_\nu^\dagger \phi_\nu^*(t,z) + \hat{a}_\nu \phi_\nu(t,z)) \cdot \frac{i}{2}(|g\rangle \langle e| e^{-i\omega_0 \eta} - |e\rangle \langle g| e^{i\omega_0 \eta}). \tag{5.12}$$

where the coupling constant g is assumed to be independent of η. $\hat{a}_\nu, \hat{a}_\nu^\dagger$ are the annihilation and creation operators of the field mode. The transition amplitude of the atom is given by

$$\mathcal{A} = \frac{1}{\hbar} \int d\tau \, \langle 1_\nu, e \mid H_I(\tau) \mid 0, g \rangle \, . \tag{5.13}$$

The excitation probability of the atom is given by

$$\begin{aligned} P_1 &= \frac{1}{\hbar^2} \left| \int d\tau \, \langle 1_\nu, e \mid H_I(\tau) \mid 0, g \rangle \right|^2 \\ &= \frac{g^2}{4} \left| \int_{-\infty}^{\infty} d\tau \; \phi_\nu^*(t,z) e^{i\omega_0 \tau} \right|^2 . \end{aligned} \tag{5.14}$$

Substituting Eq. (5.11), Eq. (5.4) in the above expression and after some calculation we get

$$\begin{aligned} P_1 = \frac{g^2}{4} \Bigg| \int_{-\infty}^{\infty} d\tau \Big[& e^{(\frac{i\nu}{c}\alpha_1 e^{\frac{a\tau}{c}} - i\alpha_2 e^{-\frac{a\tau}{c}} - \frac{i\nu}{c}\alpha_3 z_0)} \\ & - e^{-(\frac{i\nu}{c}\alpha_1 e^{-\frac{a\tau}{c}} - i\alpha_2 e^{\frac{a\tau}{c}} - \frac{i\nu}{c}\alpha_3 z_0)} \Big] e^{i\omega_0 \tau} \Bigg|^2 \end{aligned} \tag{5.15}$$

where $\alpha_1 = (1 - \frac{\beta\hbar^2\nu^2}{2c^2})$, $\alpha_2 = \frac{\beta\hbar^2\nu^3}{2ac}$, $\alpha_3 = (1 - \frac{\beta\hbar^2\nu^2}{c^2})$. Evaluating above integral we get the excitation probability of atom as

$$\begin{aligned} P_1 &= \frac{1}{\hbar^2} \left| \int d\eta \, \langle 1_\nu, e \mid H_I(\eta) \mid 0, g \rangle \right|^2 \\ &= \frac{2\pi g^2 c}{a\omega_0} \cdot \frac{e^{-\left(\frac{\beta\hbar^2\nu^4}{a^2}\Omega \cos\Delta\right)}}{e^{(\frac{2\pi\omega_0 c}{a})} - 1} \sin^2\left(\frac{\tilde{\nu} z_0}{c} - \tau - \frac{\beta\hbar^2\nu^2\omega_0}{2ac} + \frac{\beta\hbar^2\nu^4}{2a^2}\Omega \sin\Delta\right) \end{aligned} \tag{5.16}$$

where

$$\begin{aligned}
&\tilde{\nu} = \nu\big(1 - \tfrac{\beta\hbar^2\nu^2}{c^2}\big), \qquad \Omega = \frac{\big|\Gamma\big(-\frac{i\omega_0 c}{a}-1\big)\big|}{\big|\Gamma\big(-\frac{i\omega_0 c}{a}\big)\big|}, \qquad \theta = Arg\big(\Gamma\big(-\tfrac{i\omega_0 c}{a}\big)\big),\\
&\theta_1 = Arg\big(\Gamma\big(-\tfrac{i\omega_0 c}{a}-1\big)\big), \quad \Delta = (\theta_1 - \theta), \quad \tau = \delta + \theta,\\
&\delta = \tfrac{\omega_0 c}{a}\ln\tfrac{a}{\nu c}.
\end{aligned} \tag{5.17}$$

The Unruh temperature is independent of GUP. The interference term, arising due to the incident and reflected waves, is governed by field frequency and GUP parameter β. GUP has introduced a damping parameter $e^{-\left(\frac{\beta\hbar^2\nu^4}{a^2}\Omega\cos\Delta\right)}$.

5.2.2 Accelerating mirror and static atom

Let the atom is static at $z = z_0 < c^2/a$ in the Minkowski space-time and the mirror is accelerating with constant proper acceleration a. Coordinate transformation b/w frame of the mirror and Minkowski frame is

$$t = \frac{c}{a}e^{a\bar{z}/c^2}\sinh\frac{a\bar{t}}{c} \qquad\qquad z = \frac{c^2}{a}e^{a\bar{z}/c^2}\cosh\frac{a\bar{t}}{c}\ . \tag{5.18}$$

The mirror is spatially static in the Rindler frame and its trajectory is given by $\bar{z} = 0$. The presence of the accelerating mirror modulates the field mode.

Perturbative solution of deformed Klein-Gordon equation (Eq. (5.3)) in the frame of mirror

$$\phi_\nu(\bar{t},\bar{z}) = e^{-i\nu\bar{t}}\Big(e^{i\frac{\nu}{c}(1-\beta\hbar^2\frac{\nu^2}{c^2})\bar{z}} - e^{-i\frac{\nu}{c}(1-\beta\hbar^2\frac{\nu^2}{c^2})\bar{z}}\Big). \tag{5.19}$$

We now need the inverse transformations of Eq. (5.18) which are given by

$$\begin{aligned}
\bar{t}(t,z) &= \frac{c}{2a}\ln\left(\frac{z+ct}{z-ct}\right)\\
\bar{z}(t,z) &= \frac{c^2}{2a}\ln\left(\frac{a^2}{c^4}\left(z^2 - c^2t^2\right)\right).
\end{aligned} \tag{5.20}$$

The above transformations are defined for $z > c|t|$. Substituting these transformations in Eq. (5.19) and simplifying, we get the field mode observed by atom

$$\begin{aligned}
\phi(t,z) = {} & e^{i\left[\frac{\tilde{\nu}c}{a}\ln\left(\frac{a}{c^2}(z-ct)\right)\right]}\left(\frac{a}{c^2}(z+ct)\right)^{-\frac{i\beta\hbar^2\nu^3}{2ac}}\Theta(z-ct)\\
& - e^{-i\left[\frac{\tilde{\nu}c}{a}\ln\left(\frac{a}{c^2}(z+ct)\right)\right]}\left(\frac{a}{c^2}(z-ct)\right)^{\frac{i\beta\hbar^2\nu^3}{2ac}}\Theta(z+ct)
\end{aligned} \tag{5.21}$$

where $\bar{\nu} = (1-\frac{\beta\hbar^2\nu^2}{2c^2})\nu$. The atom-field interaction Hamiltonian and the transition probability amplitude are the same as Eq. (5.12), Eq. (5.13) with η replaced by t and (t, z) replaced by $(\bar{t}, \bar{z})$. The atomic transition probability evaluated at atomic position (t, z_0) is given by

$$P_2 = \frac{g^2}{4}\left|\int_{-\infty}^{\infty} dt\ \phi_\nu^*(z_0, t)e^{i\omega_0 t}\right|^2 . \tag{5.22}$$

Substituting the expression of $\phi^*(t, z)$ from Eq. (5.21) in above equation and after some calculation, we get

$$P_2 = \frac{g^2}{4}\left|\int_{-z_0/c}^{\infty} dt\ e^{-i\left[\frac{\bar{\nu}c}{a}\ln\left(\frac{a}{c^2}(z_0+ct)\right)+\omega_0 t\right]}\left(\frac{az_0}{c^2}\left(1-\frac{ct}{z_0}\right)\right)^{\frac{i\beta\hbar^2\nu^3}{2ac}} + cc.\right|^2 . \tag{5.23}$$

Evaluating the above integral, we get

$$P_2 = \frac{2\pi g^2\bar{\nu}c}{a\omega_0^2}\cdot\frac{e^{-\left(\frac{\beta\hbar^2\nu^3}{az_0\omega_0}\right)}}{e^{\left(\frac{2\pi\bar{\nu}c}{a}\right)}-1}\cdot\sin^2\left(\frac{\omega_0 z_0}{c}-\frac{\bar{\nu}c}{a}\ln\left(\frac{a}{\omega_0 c}\right)+\frac{\beta\hbar^2\nu^3}{2ac}\ln\left(\frac{az_0}{c^2}\right)\right.$$
$$\left.+\frac{\beta\hbar^2\nu^3}{2ac}+\frac{\beta\hbar^2\nu^4 c}{2a^2 z_0\omega_0}+Arg\left(\Gamma\left(\frac{i\bar{\nu}c}{a}\right)\right)\right) .$$

The Planck factor here is governed by a GUP modified photon frequency. However, different from the reference [106], the spatial oscillation in the interference pattern here is very interesting. Apart from the usual position dependent atomic frequency term, there is another position dependent term which depends on the field frequency. This term owes its origin to the GUP. It implies that the interference pattern gets modified by the field frequency in the presence of the GUP.

5.3 Violation of the equivalence principle

The weak equivalence principle proposed by Einstein states that a free falling observer or test mass in a stationary cavity in a uniform gravitational field cannot distinguish itself from a stationary observer or test mass in an accelerating cavity. As discussed earlier, weak equivalence principle (WEP) has been studied in the quantum regime from various perspective. One such direction is in the context of particle detector and cavity (or mirror) in relative acceleration in background quantum vacuum [71, 106, 179, 180]. These works compares the response of the detector in following two cases

(i) An atom (Unruh-DeWitt detector) accelerating with respect to a stationary mirror in presence of background quantum field.

(ii) A mirror accelerating with respect to a stationary atom in presence of background quantum field.

Any qualitative symmetry between these two system is considered as a manifestation of WEP [71,106,179,180]. So, in a more general language, the equivalence principle may be envisaged in terms of a symmetry between excitation of a stationary atom by an accelerating mirror (Rindler vacuum) and the excitation of an atom freely falling under gravity with respect to a stationary mirror (Boulware vacuum). A similar argument can be put forward in terms of symmetry between the excitation of an atom accelerating in Minkowski spacetime relative to a stationary mirror (Minkowski vacuum) and the excitation of a stationary atom by a mirror freely falling in a gravitational field (Hartle-Hawking vacuum). A deviation from such symmetry can be regarded as a manifestation of violation of the equivalence principle.

We apply above notions in our system in order to study the violation of WEP. In this work we have calculated the excitation probability of atom when

(a) the accelerated two level atom interacting with single mode GUP modified vacuum in presence of a static mirror

(b) the static two level atom interacting with single mode GUP modified vacuum in presence of an accelerated mirror.

Let us now set $\omega_0 = \nu$, making the frequencies of the atom and the photon same in both cases. It can be observed that, the spatial oscillations for the two probabilities are not the same, as is evident from Eq. (5.16), Eq. (5.24), in contrast to the framework based on the Heisenberg uncertainty relation [106]. This therefore breaks the symmetry between the excitation of an atom accelerating in Minkowski spacetime relative to a stationary mirror and a stationary atom excited by an uniformly accelerating mirror. This feature can hence be regarded as a manifestation of violation of the equivalence principle originating from the GUP. It can be checked that by setting $\beta = 0$ in Eq. (5.16), Eq. (5.24), the symmetry ensues, restoring the equivalence in the Heisenberg uncertainty framework.

There have been proposals to provided bounds on the value of the GUP parameter β resulting from various effects such as, correction in Lamb shift, Landau levels, simple harmonic oscillators, and gravitational wave detections [169,183]. Here we provide an estimate of the upper bound on β from the exponent of the

damping factor. It is clear from the exponential factor in Eq. (5.24) that in order to ensure that the GUP corrections do not dominate over the results obtained in the Heisenberg uncertainty principle framework, we must have $\left(\frac{\beta\hbar^2\nu^3}{az_0\omega_0}\right) \ll 1$. Taking $\nu = \omega_0 = 1\text{GHz}$ [106] and $az_0 \sim c^2$, we find $\beta \ll 10^{67}/(M_P c)^2$, with M_P being the Planck mass. Though this bound is weaker than the bound obtained on β in the context of gravitational waves [183], our result provides an example of the possibility of formulating testable bounds on the GUP parameter in the context of controllable low energy atom-photon interactions.

Interestingly, bounds on the GUP parameter also arise from the mismatch in the spatial oscillation of the two probabilities. The ratio between the spatial part of the second and first probabilities is given by

$$R = 1 + \mathcal{Q}(z_0) \tag{5.24}$$

where

$$\mathcal{Q}(z_0) = \frac{\beta\hbar^2\nu^2c^2}{2a^2z_0^2} + \frac{\beta\hbar^2\nu^2}{2az_0}\ln\left(\frac{az_0}{c^2}\right) \tag{5.25}$$

can be regarded as an equivalence violation parameter. This provides a similar bound on β as obtained above.

5.4 Conclusion

We now summarize our findings with some observations. The main focus of this paper is to look at the status of the symmetry between the excitation of a stationary atom by an accelerating mirror and a uniformly accelerating atom relative to a stationary mirror taking into account Planck scale effects. Such a symmetry has been shown to be valid in the framework of the Heisenberg uncertainty relation, and has been interpreted as a manifestation of the principle of equivalence in [106,179]. It should be noted however, that the interpretation of this symmetry as a manifestation of the equivalence principle goes beyond the well known classical version which states that by local measurements it would be impossible to distinguish between an inertial observer in Minkowski spacetime and a free-falling observer in a gravitational field (or, equivalently, a static observer in a uniform gravitational field and a uniformly accelerated observer in flat spacetime).

Our methodology is to consider a quantized scalar field vacuum that obeys the GUP modified dispersion relation. From the GUP modified Klein-Gordon equation, we obtain the solutions of the scalar field with particular boundary

conditions imposed by the mirror in the two separate cases. Using these solutions we calculate the excitation probabilities of the atom in both the cases, which are found to display significant physical differences.

In the first case, the GUP contributes as a constant phase in the interference. However, in the second case the spatial oscillation gets modified by an additional term containing the field frequency and the GUP parameter β. Hence, we find that the symmetry observed in [106] gets broken in the framework of the GUP even when $\nu = \omega_0$. This is the most striking result of our study, and may be interpreted as an explicit violation of the equivalence principle. This is because the symmetry between the excitation of an atom accelerating in Minkowski spacetime relative to a stationary mirror and a stationary atom excited by a uniformly accelerating mirror (considered to be a manifestation of the equivalence principle in [106,179]) gets broken. Further, using the condition that the GUP induced corrections do not dominate over the corresponding expressions obtained using the Heisenberg uncertainty relation, it is possible to constrain the value of the GUP parameter in the context of this low energy interacting atom-mirror set-up.

Before concluding, it may be noted that in both the cases the excitation probabilities contain a GUP induced damping factor. In the first case the probability is proportional to the Planck factor containing the atomic transition frequency and the Unruh temperature given by $T_U = \frac{\hbar a}{2\pi k_B c}$, that one gets when $\beta = 0$. In the second case, the atomic excitation probability is proportional to the Planck factor which is a function of $\bar{\nu} = (1 - \frac{\beta\hbar^2\nu^2}{2c^2})\nu$. Thus, in the presence of the GUP modification, the excitation probability is proportional to the Planck factor containing the field frequency and the modified Unruh temperature given by $T'_U = T_U/(1 - \frac{\beta\hbar^2\nu^2}{2c^2})$. Since the Planck distribution in Eq. (5.24) is analogous to the photon spectrum of an atom falling freely in the gravitational field of a Schwarzschild black hole [97], this implies that the acceleration radiation observed by a distant observer will be a thermal distribution with a GUP modified Hawking temperature.

Chapter 6

Bell nonlocality of dynamical Casimir photons in a superconducting microwave circuit

The fluctuaing vacuum of quantum field produces particles when the geometry of the background space-time is curved or changes with time. In Section 2.2.3, we have presented extensive mathematical discussion on how a moving mirror or a time dependent boundary condition leads to particle production. The phenomena is known as as Dynamical Casimir effect (DCE) or Moore-DeWitt effect [9, 10]. DCE was first theoretically proposed by G. T. Moore, in case of electromagnetic field confined within a cavity with a nonrelativistically oscillating mirrors (oscillating boundary conditions) [9]. Later the works of DeWitt, Fulling and Davies have discovered the phenomena of excitation of quantum vacuum by relativistically accelerating mirrors in flat space-time [10, 11, 184].

With choice of appropriate trajectories, a perfectly reflecting accelerating mirror mimics many features of black hole radiation [184, 185]. However experimental verification of particle production due to varying space-time geometry in nature seems to be out of reach of current technology. With the development of quantum material technology, it has been possible to create analogue DCE in the laboratory by varying bulk properties of materials such that time dependent boundary conditions are induced (quantum simulation of moving mirrors) in the medium containing the quantum field [186–189]. The time dependent boundary condition makes the vacuum state of the field evolve into a superposition of states of various numbers of particles, by a Bogolyubov transformation [11, 184, 190]. This results in the emission of Casimir photon pairs. If the background space-time

is flat apart from the boundary condition, the emission can be localized as the radiation from a moving mirror [9,11,184,190]. A relativistically moving mirror causes the rapid nonadiabatic modulation of quantum field modes. To accommodate the modulated modes, the quantum vacuum throws up particles that follow Planck's distribution.

Though for the case of the non-relativistically moving mirror, particles can be created through nonuniform acceleration, the rate of particle production is extremely small [9]. Moreover, a cavity set-up is generally introduced to obtain parametric amplification. In practice, making a mechanical mirror move near the speed of light has been technologically challenging for a long time. DCE was first observed experimentally [188,189] in superconducting microwave circuits, by simulating the relativistic motion of mirrors [186,187]. Here the superconducting transmission line is interrupted by superconducting quantum interference devices (SQUIDs). Inductance of the SQUID is ultra-rapidly tuned by making high frequency modulation of external magnetic flux threading the SQUID. Change in the inductance causes change in the electrical length of the transmission line. Hence, a time dependent boundary condition similar to that induced by a relativistically moving mirror is imposed to the quantized microwave field in the transmission line through the screening current flowing through the SQUID. In the above circuit quantum electrodynamical (cQED) set-up, the simulated velocity of the mirror can reach $\sim 10^6$ ms^{-1}, and the number of photons generated per second is 10^5 [187]. DCE can also be observed in optomechanical set-up [53].

The DCE creates entanglement within the field modes resulting two mode squeezed state. The nature of DCE radiation is nonclassical [191]. The Entanglement in the DCE is a consequence of the energy and momentum conservation, just like in the parametric down conversion process. Quantum correlations generated through DCE can be used as a resource for quantum information processing. Even in a realistic cQED set-up where the background noise is present, the microwave radiation can be nonclassical [191]. Apart from its significance as a resource for quantum tasks, the above experimental set-up provides a platform for simulation of fundamental phenomena [58,106,192]. Quantum features such as entanglement, coherence and discord of noisy Casimir photons have been studied with respect to various circuit parameters [193,194]. Gaussian interferometric power, and steering have also been studied in presence of noise [195–197].

In Chapter 1 we have discussed on the proposal of Bell nonlocality as a quantitative formulation of the ideas of EPR that suggested quantum mechanics as an incomplete theory [15]. Bell nonlocality is the strongest of all quantum correlations, manifesting the violation of local realism [17,18]. EPR based their

argument on states having continuous spectrum in the phase space. However, the formalisms of Bohm [198] and Bell [17,18] were based on discrete dimensional systems, as was the work of CHSH [19]. Subsequently, Bell's inequality violation has been extensively investigated both in discrete and continuous variable systems [199–206]. The significance of Bell nonlocality in the security of quantum cryptography [207] has come under sharper focus with the development of device independent quantum key distribution protocols [208]. Bell's inequality violation has been studied in diverse domains ranging from fundamental phenomena such as Unruh effect [209] and cosmic photons [210,211] to the case of laboratory experiments using quantum materials [212].

In this chapter we investigate Bell's inequality violation by dynamical Casimir radiation using non-Gaussian pseudospin measurements. Our primary motivation arises from the fact that the study of Bell's inequality in context of particle production through time dependent boundary conditions was hitherto unexplored in the literature, even though the moving mirror can be simulated in the laboratory [53,188,189]. In presence of noise the accelerated mirror in a basic experimental set-up will produce two mode squeezed thermal state [188,189] though advance material engineering has enabled us to create NOON state using DCE array [213]. Quantum correlation in the DCE has been studied using Gaussian measurements [193–197] but no work has been done on the non-Gaussian measurement in this set-up. Non-Gaussian measurement is a significant tool in quantum information such as quantum teleportation [214], steering and cryptography [215–217], non-Gaussian state preparation from Gaussian state [218] etc. As it is possible to implement DCE in the laboratory, our analysis should be relevant to understand the efficiency of DCE as a resource for quantum information.

Our approach is based on employing pseudospin mesurements represented in configuration space [204,205]. Such measurements have been used to study the Bell nonlocality of a two mode squeezed vacuum [204,205], cosmic photons [211] and quantum steering of two mode squeezed thermal state [216]. The pseudospin operators represented in configuration space are easier to handle compared to their representation in the number basis [216]. It may be noted that optimization of the expectation value of the Bell operator in configuration space involves additional parameters compared to that in the number state representation [204]. Pseudospin measurement in configuration space has also been used to study nonlocality of different classes of multimode Gaussian states [219], enhancement of nonlocality [220], and quantum teleportation [214]. Our aim is to use this measurement to explore the Bell-CHSH inequality violation by Casimir photon pairs in the cQED set-up. We investigate how the optimal value of the Bell violation

depends on various circuit parameters. Specifically, we consider the effect of local noise, nonzero detuning and signal loss. All calculations in this chapter are done in SI units. This chapter is based on the our publication [59].

Our work is organized as follows: In Section 6.1 we describe DCE in the cQED set-up. In Section 6.2 we study violation of the Bell-CHSH inequality by Casimir photon pairs generated via the cQED set-up described in Section 6.1. We explore the dependence of optimal Bell violations on different system parameters. In Section 6.3 we study the robustness of the Bell violation under signal loss. In Section 6.4 we present a summary of our main results along with some concluding remarks.

6.1 DCE in superconducting circuit

6.1.1 System specification

We consider the cQED setup described in [186–188, 191]. A superconducting coplanar waveguide (CPW) with characteristic capacitance C_0 and inductance L_0 per unit length is terminated to ground (say at $x = 0$) by a SQUID loop threaded by external magnetic flux $\phi_{ext}(t)$. The quantized microwave field inside the waveguide is described by its flux field $\phi^i(x,t)$ that obeys the one-dimentional massless Klein-Gordon equation

$$\left(\partial_{xx} - v^{-2}\partial_{tt}\right)\phi^i(x,t) = 0, \tag{6.1}$$

with Dirichlet boundary condition at $x = 0$. In the framework of input-output theory, the total flux field in the CPW transmission line is

$$\phi(x,t) = \phi^{in}(x,t) + \phi^{out}(x,t) \tag{6.2}$$

where $\phi^{in}(x,t)$ and $\phi^{out}(x,t)$ are the incoming (right moving) and outgoing (left moving) components of the total flux field.

In terms of the second quantized solution of Klein-Gordon equations, the expression in Eq. (6.2) can be written as [186, 187, 191, 221]

$$\phi(x,t) = \sqrt{\frac{\hbar Z_0}{4\pi}}\int_{-\infty}^{\infty}\frac{d\omega}{\sqrt{|\omega|}}\left[\hat{a}_\omega^{in}\ e^{-i(\omega t - k_\omega x)} + \hat{a}_\omega^{out}\ e^{-i(\omega t + k_\omega x)}\right],\ (x<0). \tag{6.3}$$

$\hat{a}_\omega^{in}$ and $\hat{a}_\omega^{out}$ are annihilation operators for modes of frequency ω, propagating with velocity v to the right (incoming) and left (outgoing) respectively.

$\left[\hat{a}_{\omega}^{in(out)}, (\hat{a}_{\omega'}^{in(out)})^{\dagger}\right] = \delta(\omega - \omega')$ and we use the convention $\hat{a}_{-\omega} = \hat{a}_{\omega}^{\dagger}$. The velocity $v = \omega/k_{\omega} = 1/\sqrt{C_0 L_0}$ and $Z_0 = \sqrt{L_0/C_0}$ is the characteristic impedance of CPW.

At large plasma frequency, when the charging energy is much smaller than the external flux dependent effective Josephson energy $E_J(t) = E_J(\phi_{ext}(t))$, the SQUID is a passive element that provides the following boundary condition at $x = 0$, to the flux field inside CPW line [186,187]

$$\phi(0,t) + L_{eff}(t)\ \partial_x \phi(x,t)\Big|_{x=0} = 0, \tag{6.4}$$

where $L_{eff}(t) = L_J(t)/L_0$ and $L_J = \left(\frac{\phi_0}{2\pi}\right)^2 \frac{1}{E_J(t)}$ is the tunable Josephson inductance of the SQUID. $\phi_0 = (h/2e)$ is the magnetic flux quantum. The boundary condition at $x = 0$ depends only upon the tunable Josephson inductance of the SQUID [186–188], which creates a mirror at an effective length $L_{eff}(t)$ from the physical end of the CPW line. For sinusoidal modulation $E_J(t) = E_J^0(1+\epsilon \sin \omega_d t)$ with driving amplitude ϵ and driving frequency ω_d [186,187], the effective length modulation amplitude is $\delta L_{eff} = \epsilon L_{eff}^0$, where $L_{eff}^0 = L_{eff}(0)$. So, the effective velocity of the mirror is $v_{eff} = \omega_d L_{eff}^0$. When v_{eff} is a significant fraction of the velocity v of light in the CPW line, nonadiabatic modulation occurs in the field modes resulting in a significant amount of photon pair production.

In case of weak harmonic drive (perturbative regime) [186,187], $\epsilon E_J^0 \ll E_J^0$ and the output photon-flux density has a parabolic spectrum with a maximum at $\omega_d/2$. Output photon pairs are correlated with frequency $\omega_{\pm}$, where $\omega_+ + \omega_- = \omega_d$. The simplest choice is $\omega_{\pm} = \omega_d/2 \pm \delta\omega$, where $\delta\omega$ is the detuning parameter. Using Eq. (6.3) and Eq. (6.4) and applying scattering theory, the Bogolyubov transformation between incoming and outgoing modes can be obtained analytically in the perturbative regime [187,191,222]

$$\hat{a}_{\omega_{\pm}}^{out} = -\hat{a}_{\omega_{\pm}}^{in} - if(\hat{a}_{\omega_{\mp}}^{in})^{\dagger} \tag{6.5}$$

where

$$f = \frac{\epsilon L_{eff}^0 \sqrt{\omega_+ \omega_-}}{v}. \tag{6.6}$$

Pair production results in two mode squeezing of the output field [187,191]. So, if the input state ϕ^{in} in Eq. (6.2) is a vacuum state, the output DCE state ϕ^{out} is ideally a two mode squeezed vacuum.

6.1.2 Covariance matrix of input/output modes

Let us consider the DCE input/output states in the framework of Gaussian covariance matrix formalism [191]. In our work we follow the convention of [223]. Input/output state can be written in terms of the covariance matrix (CM)

$$V_{\alpha\beta} = \langle \hat{R}_\alpha \hat{R}_\beta + \hat{R}_\beta \hat{R}_\alpha \rangle - 2\langle \hat{R}_\alpha \rangle \langle \hat{R}_\beta \rangle, \tag{6.7}$$

where $\hat{R} = (\hat{q}_-, \hat{p}_-, \hat{q}_+, \hat{p}_+)^T$ is a vector containing field quadrature elements with $[\hat{q}_\alpha, \hat{p}_\beta] = i\delta_{\alpha\beta}$ and

$$\begin{aligned} \hat{q}_\pm^{in(out)} &= \frac{\hat{a}_{\omega_\pm}^{in(out)} + (\hat{a}_{\omega_\pm}^{in(out)})^\dagger}{\sqrt{2}} \\ \hat{p}_\pm^{in(out)} &= -i\,\frac{\hat{a}_{\omega_\pm}^{in(out)} - (\hat{a}_{\omega_\pm}^{in(out)})^\dagger}{\sqrt{2}}. \end{aligned} \tag{6.8}$$

where we have restricted ourself to a pair of entangled modes $\{\pm\}$ with frequencies adding up to the driving frequency. The nonclassicality of DCE radiation originates from the entanglement of Casimir photon pairs [191]. Ideal input state will be a vacuum state which is impossible to create in practical situation. So, we will use a quasi-vacuum state, containing small number of thermal photons $\left\{n_\pm^{th} = \left(e^{\frac{\hbar\omega_\pm}{kT}} - 1\right)^{-1}\right\}$ [191, 194], as the input state.

Note that the choice of the initial thermal state modifies the Green's function and the power spectrum, and the frequencies of the incoming and outgoing signals are doppler shifted [224]. However, the effect on the correlation of the outgoing modes is negligible for our chosen temperature range [189]. Hence, correlation of the output modes are observed in experiments despite the fact that the effects of temperature are not explicitly monitored during the experiments [189, 224]. The quadrature elements have zero 1^{st}-moment. The CM of the input field is given by

$$V_{in} = \begin{pmatrix} n_0 & 0 & 0 & 0 \\ 0 & n_0 & 0 & 0 \\ 0 & 0 & m_0 & 0 \\ 0 & 0 & 0 & m_0 \end{pmatrix} \tag{6.9}$$

where

$$\begin{aligned} n_0 &= (2n_-^{th} + 1) \\ m_0 &= (2n_+^{th} + 1). \end{aligned} \tag{6.10}$$

Using Eq. (6.5), Eq. (6.6), Eq. (6.8), Eq. (6.9), Eq. (6.10), the CM of the output

field is obtained (in standard form) as

$$V_{out} = \begin{pmatrix} n & 0 & r & 0 \\ 0 & n & 0 & -r \\ r & 0 & m & 0 \\ 0 & -r & 0 & m \end{pmatrix} \tag{6.11}$$

where

$$\begin{aligned} n &= (2n_-^{th} + 1) + f^2(2n_+^{th} + 1) \\ m &= (2n_+^{th} + 1) + f^2(2n_-^{th} + 1) \\ r &= 2f(n_+^{th} + n_-^{th} + 1). \end{aligned} \tag{6.12}$$

V_{out} corresponds to a two mode squeezed thermal state with squeezing parameter $2f$.

6.2 Bell violation by DCE radiation

We will study Bell's inequality violation by the output DCE radiation described by the CM in Eq. (6.11),Eq. (6.12), using the definition of pseudospin measurement represented in configuration space [204, 205]

$$\begin{aligned} \hat{\Pi}_x &= \int_0^\infty dq \left[|\mathcal{Q}^+\rangle \langle \mathcal{Q}^-| + |\mathcal{Q}^-\rangle \langle \mathcal{Q}^+| \right] \\ \hat{\Pi}_y &= i \int_0^\infty dq \left[|\mathcal{Q}^+\rangle \langle \mathcal{Q}^-| - |\mathcal{Q}^-\rangle \langle \mathcal{Q}^+| \right] \\ \hat{\Pi}_z &= -\int_0^\infty dq \left[|\mathcal{Q}^+\rangle \langle \mathcal{Q}^+| - |\mathcal{Q}^-\rangle \langle \mathcal{Q}^-| \right] \end{aligned} \tag{6.13}$$

where the channels $|\mathcal{Q}^+\rangle$ and $|\mathcal{Q}^-\rangle$ are given by

$$\begin{aligned} |\mathcal{Q}^+\rangle &= \frac{1}{2} \left[|q\rangle + |-q\rangle \right] \\ |\mathcal{Q}^-\rangle &= \frac{1}{2} \left[|q\rangle - |-q\rangle \right]. \end{aligned} \tag{6.14}$$

$\{\hat{\Pi}_x, \hat{\Pi}_y, \hat{\Pi}_z\}$ satisfy $SU(2)$ algebra. Following [204], the Bell operator is defined as

$$\begin{aligned} \mathcal{B} = \vec{a} \cdot \hat{\Pi}^{(-)} \otimes \vec{b} \cdot \hat{\Pi}^{(+)} + \vec{a} \cdot \hat{\Pi}^{(-)} \otimes \vec{b'} \cdot \hat{\Pi}^{(+)} + \vec{a'} \cdot \hat{\Pi}^{(-)} \otimes \vec{b} \cdot \hat{\Pi}^{(+)} \\ - \vec{a'} \cdot \hat{\Pi}^{(-)} \otimes \vec{b'} \cdot \hat{\Pi}^{(+)} \end{aligned} \tag{6.15}$$

where $\vec{a}, \vec{a'}, \vec{b}, \vec{b'}$ are the unit vectors that specify the orientation of the first and second channels respectively. $\hat{\Pi}^{(\pm)}$ designates channel $\hat{\Pi}$ applied on the mode $\{\pm\}$.

In order to calculate the optimal Bell violation, first we perform orientational optimization of the measurement directions following [203, 204, 206]. We choose $\vec{a}, \vec{a'}, \vec{b}, \vec{b'}$ in spherical polar coordinate as

$$\begin{aligned} \phi_a = \phi_{a'} = \phi_b = \phi_{b'} = 0, \\ \theta_a = 0, \quad \theta_{a'} = \pi/2, \quad \theta_b = -\theta_{b'}. \end{aligned} \tag{6.16}$$

So, the Bell operator reduces to

$$\mathcal{B} = 2\left(cos\theta_b\ \hat{\Pi}_x^{(-)} \otimes \hat{\Pi}_x^{(+)} + sin\theta_b\ \hat{\Pi}_z^{(-)} \otimes \hat{\Pi}_z^{(+)}\right). \tag{6.17}$$

Maximizing over θ_b we get the maximal expectation value of $\mathcal{B}$,

$$B_{max} = 2\sqrt{\left\langle \hat{\Pi}_x^{(-)} \otimes \hat{\Pi}_x^{(+)} \right\rangle^2 + \left\langle \hat{\Pi}_z^{(-)} \otimes \hat{\Pi}_z^{(+)} \right\rangle^2} \tag{6.18}$$

where $\langle \cdot \rangle$ is the expectation value of an operator for a given state. Bell violation occurs when

$$B_{max} > 2. \tag{6.19}$$

We now calculate B_{max} for our output state described by the covariance matrix V_{out} in Eq. (6.11), Eq. (6.12) and study how the value of B_{max} depends upon various system parameters. In order to calculate the expectation value of two mode pseudospin operators we use the definitions [205, 216]

$$\begin{aligned} \left\langle \hat{\Pi}_i^{(-)} \otimes \hat{\Pi}_j^{(+)} \right\rangle = \frac{1}{(2\pi)^2} \int d^4X\ W_{out}(X) \\ \times W_{\hat{\Pi}_i^{(-)}}(q_-, p_-)\ W_{\hat{\Pi}_j^{(+)}}(q_+, p_+) \end{aligned} \tag{6.20}$$

where $X = (q_-, p_-, q_+, p_+)^T$,

$$\begin{aligned} W_{\hat{\Pi}_x}(q,p) = sgn(q) \\ W_{\hat{\Pi}_z}(q,p) = -\pi\delta(q)\delta(p) \end{aligned} \tag{6.21}$$

and the Wigner function of the output state is

$$W_{out}(X) = \frac{1}{\pi^2}\frac{1}{det(V_{out})} e^{-\left(X^T\ V_{out}^{-1}\ X\right)}. \tag{6.22}$$

Plugging everything in Eq. (6.18) we evaluate B_{max} for output DCE radiation in terms of circuit parameters

$$B_{max} = 2\left(\frac{1}{(f^2-1)^4\,(2n_-+1)^2\,(2n_++1)^2} + \frac{4\tan^{-1}\left(\frac{4f^2(n_-+n_++1)^2}{(f^2-1)^2(2n_-+1)(2n_++1)}\right)^2}{\pi^2}\right)^{\frac{1}{2}} \tag{6.23}$$

with $\{n_\pm\}$ defined above Eq. (6.9) and f is given by Eq. (6.6), as a function of driving amplitude ϵ. Now we plot the variation of B_{max} with respect to different experimental parameters to observe the Bell's inequality violation.

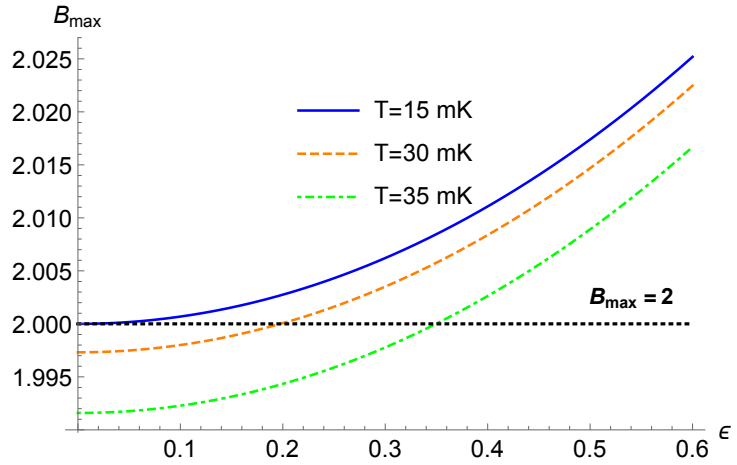

Figure 6.1: Variation of B_{max} with the driving amplitude ϵ in different temperatures of the system. Driving frequency $\omega_d = 20\pi$ GHz. $v = 1.2 \times 10^8$ ms^{-1}. $L^0_{eff} = 0.5$ mm. Detuning $\delta\omega = 0$.

Figure (6.1) shows the variation of B_{max} with increasing driving amplitude ϵ in different temperatures of the system. Here detuning is zero, which means $n_- = n_+$ and hence both modes are symmetric and have equal local noises. The driving amplitude is considered upto $\epsilon = 0.6$, that corresponds to $f = 0.0786$ which is well inside the perturbative regime. The plot shows that the value of B_{max} has dropped significantly at $T = 35$ mK compared to its values at $T = 15$ mK and 30 mK. Also at 35 mK, it requires significantly larger driving amplitude ($\epsilon > 0.35$), in order to observe Bell's inequality violation compared to the other two temperatures. The highest value of the Bell violation obtained here, at 15 mK and with $\epsilon = 0.6$, is 2.025.

Figure (6.2) shows the variation of B_{max} with increase in the driving amplitude ϵ and $\frac{\delta\omega}{\omega_d}$ which is the detuning expressed as a fraction of driving frequency ω_d. The dash-dotted curve represents the points $B_{max} = 2$. So, the region on the right

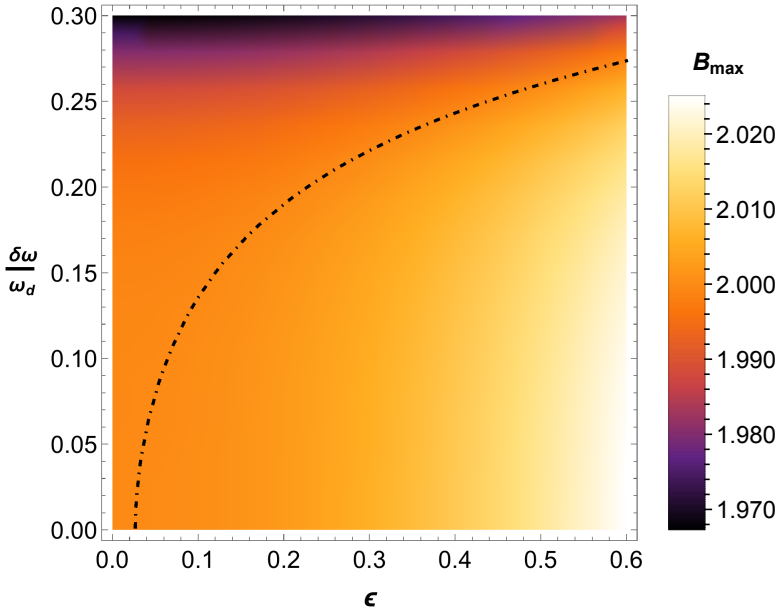

Figure 6.2: Variation of B_{max} with respect to the driving amplitude ϵ and detuning $\delta\omega$ as the fraction of Driving frequency $\omega_d = 20\pi$ GHz. $v = 1.2 \times 10^8$ ms^{-1}. $L^0_{eff} = 0.5$ mm. $T = 20$ mK.

side of this curve violates Bell's inequality. The increase in detuning increases the asymmetry between the two modes, decreasing the value of B_{max}. The plot also shows that in order to observe Bell's inequality violation in the chosen parameter range, detuning needs to satisfy $\frac{\delta\omega}{\omega_d} < 0.27$.

Figure (6.3) shows the variation of B_{max} with increase in temperature T and $\frac{\delta\omega}{\omega_d}$ which is the detuning expressed as a fraction of driving frequency ω_d. The dash-dotted curve represents the points $B_{max} = 2$. The region on the left side of this curve violates Bell's inequality. The plot indicates that at very low temperature, the effect of detuning on the value of B_{max} is not significant and Bell violation is always achieved. This is because at low temperature, local noise is very small and hence the asymmetry between the modes is very small even with a significant value of detuning and driving amplitude ϵ (driving parameter f is a function of detuning and driving amplitude, see Eq. (6.6)). For temperature $20 - 30$ mK, the value of B_{max} falls below 2 for significant detuning. Around temperature 34 mK, Bell violation is absent when $\frac{\delta\omega}{\omega_d}$ is approximately greater than 0.15. For temperature $T \geqslant 42$ mK, Bell's inequality violation is completely absent for our chosen parameter range.

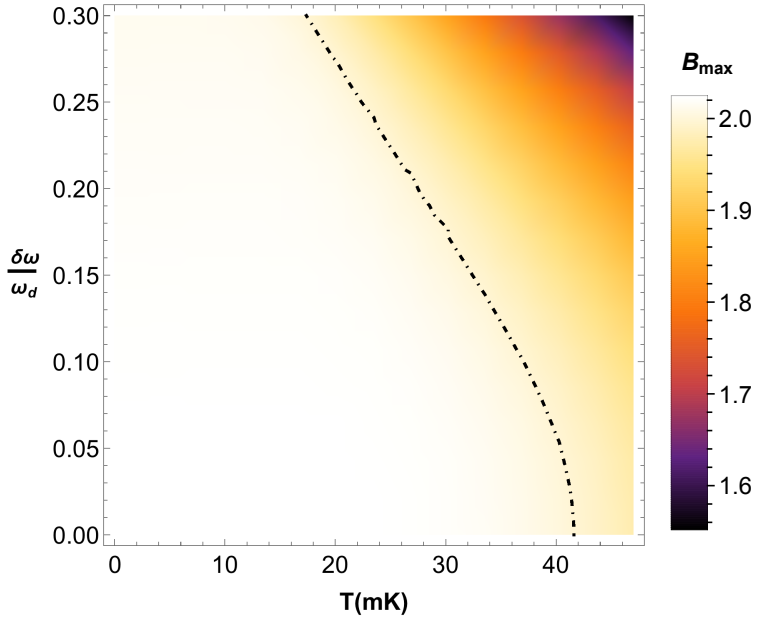

Figure 6.3: Variation of B_{max} with respect to the temperature T (mK) and detuning $\delta\omega$ as the fraction of driving frequency $\omega_d = 20\pi$ GHz, with $v = 1.2 \times 10^8$ ms^{-1}, $L^0_{eff} = 0.5$ mm, and $\epsilon = 0.6$.

6.3 Robustness under signal loss

In realistic scenarios, an experiment may suffer from imperfections. The two most relevant types of noise in the present set-up are noise due to the presence of thermal photons in the signal and signal loss in the transmission line. In our analysis we consider both the above types of noise. The thermal noise that is observed to be present in DCE experiments implemented so far [188, 189, 225], is taken into account in our analysis. We further study the tolerance of nonlocality of DCE radiation under another source of experimental defect, *viz.*, photon loss which is, in general, one of the most studied defects in the context of Bell violation [226]. Signal loss can occur due to various reasons such as the presence of impurities, measurement inefficiency and so on [227], and has been discussed in the context of generation and measurement of DCE radiation [188, 189, 225]. In our study we mimic the signal loss by beam splitter operation and study the tolerance of Bell nonlocality of DCE radiation against such noise.

Our goal here is to study if we can observe Bell's inequality violation in the experimental set-up under consideration, in the presence of signal loss in one of the modes (say the first mode). We apply a pure loss channel on mode $\{-\}$ and obtain the output covariance matrix following the method of [216]. We couple

the state described by V_{out}, with a single mode vacuum (ancilla). Thus, the resultant covariance matrix is given by $V' = V_{anc} \oplus V_{out}$, where $V_{anc} = \mathbb{1}_{2\times2}$ is the covariance matrix of the ancilla, with $\mathbb{1}_{2\times2}$ being the 2×2 identity matix. We next transform the ancillary mode and $\{-\}$ mode though the beam splitter channel B_s. We apply $B_s \oplus \mathbb{1}_{2\times2}$ on V' where

$$B_s = \begin{pmatrix} \sqrt{\eta}\ \mathbb{1}_{2\times2} & -\sqrt{1-\eta}\ \mathbb{1}_{2\times2} \\ \sqrt{1-\eta}\ \mathbb{1}_{2\times2} & \sqrt{\eta}\ \mathbb{1}_{2\times2} \end{pmatrix} \tag{6.24}$$

with $\eta \in (0, 1)$ being the transmission efficiency. Tracing out the ancillary modes leads us to obtain the covariance matrix of the output DCE radiation with signal loss on mode $\{-\}$, given by

$$V_{out}^{L} = \begin{pmatrix} n' & 0 & r' & 0 \\ 0 & n' & 0 & -r' \\ r' & 0 & m' & 0 \\ 0 & -r' & 0 & m' \end{pmatrix} \tag{6.25}$$

where

$$\begin{aligned} n' &= \eta\left(f^2\left(2n_+ + 1\right) + 2n_- + 1\right) - \eta + 1 \\ m' &= (2n_+^{th} + 1) + f^2(2n_-^{th} + 1) \\ r' &= 2f\sqrt{\eta}\left(n_- + n_+ + 1\right) \end{aligned} \tag{6.26}$$

and $\{n_\pm\}$, f have the same definitions as in Eq. (6.12). Following a similar procedure as in Section 6.2, we find the expectation value of the Bell operator, optimized with respect to the measurement orientations for the state described by the covariance matrix V_{out}^{L} in terms of the system parameters in the presence of signal loss, given by

$$B_{max}^{L} = 2\sqrt{\frac{4}{\pi^2}\tan^{-1}\left(\frac{A_1}{A_2}\right)^2 + \frac{1}{A_2^2}} \tag{6.27}$$

where

$$\begin{aligned} A_1 &= 4f^2\eta\left(n_- + n_+ + 1\right)^2 \\ A_2 &= -4f^2\eta\left(n_- + n_+ + 1\right)^2 + \Big(\left(2f^2n_- + f^2 + 2n_+ + 1\right) \\ &\qquad \times \left(f^2\eta + 2f^2\eta\ n_+ + 2\eta\ n_- + 1\right)\Big) . \end{aligned} \tag{6.28}$$

We plot the variation of B^L_{max} with respect to various system parameters, in order to observe the violation of Bell's inequality under signal loss.

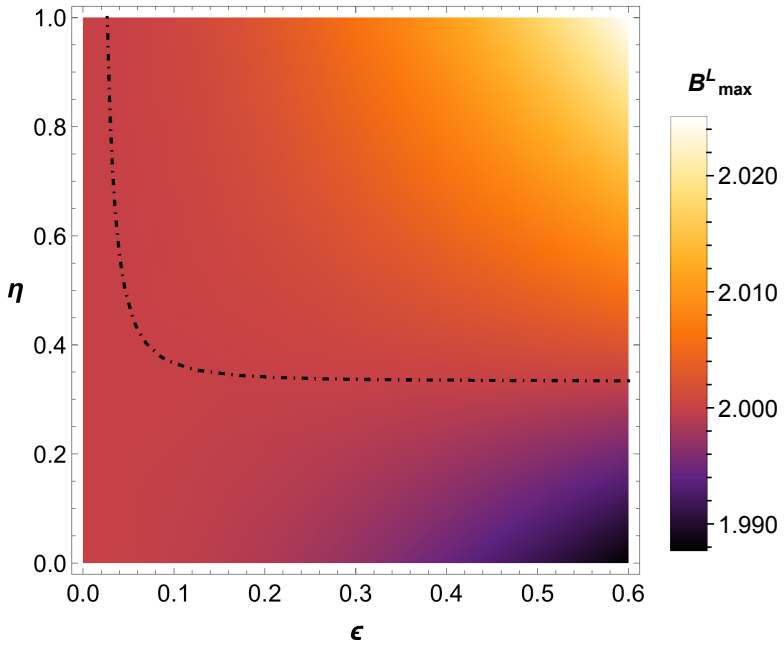

Figure 6.4: Variation of B^L_{max} with respect to the driving amplitude ϵ and transmission efficiency η. Driving frequency $\omega_d = 20\pi$ GHz. Detuning $\delta\omega = 0$. $v = 1.2 \times 10^8$ ms^{-1}. $L^0_{eff} = 0.5$ mm. $T = 20$ mK.

Figure (6.4) shows the variation B^L_{max} with respect to the driving amplitude ϵ and transmission efficiency η in the absence of detuning. The dash-dotted curve represents the points $B_{max} = 2$. The region above this curve violates Bell's inequality. Below $\eta = 0.4$, the threshold of Bell violation becomes less sensitive to the increase of the driving amplitude. Bell violation is completely absent when $\eta < 0.35$, i.e., when the signal loss is greater than 65%. The plot indicates that to observe noticeable Bell violation for our chosen range of parameters, the transmission efficiency should be greater than 0.4.

Figure (6.5) shows the variation B^L_{max} with respect to the temperature T and transmission efficiency η in absence of detuning. The dash-dotted curve represents the points $B_{max} = 2$. The region above this curve violates Bell's inequality. For temperature above 24 mK, Bell violation is absent when the transmission efficiency $\eta < 0.35$ (signal loss $> 65\%$). For higher temperatures, a greater amount of transmission efficiency is needed in order to observe Bell violation. At temperatures near 40 mK, the transmission efficiency has to be greater than 0.8 (signal loss is required to be less than 20%) for our chosen range of parameters.

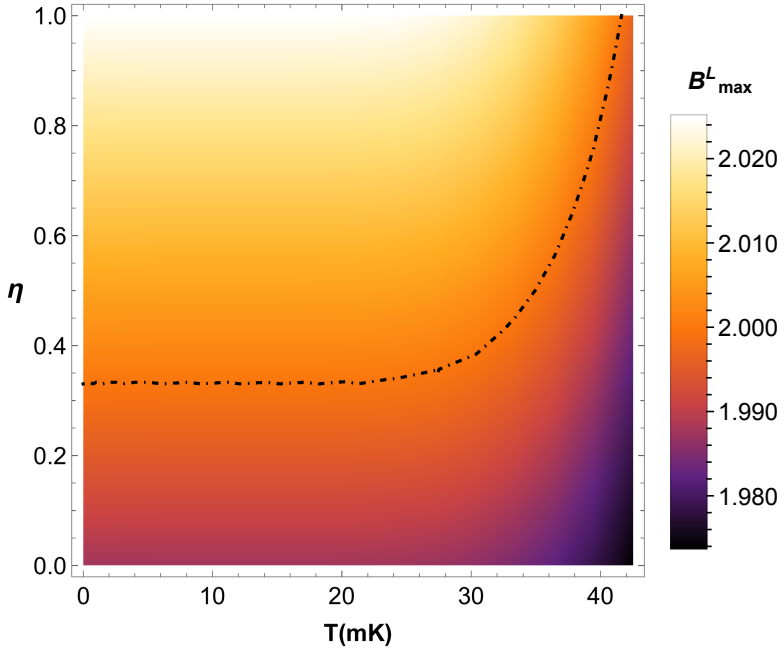

Figure 6.5: Variation of B^L_{max} with respect to the temperature T and transmission efficiency η. Driving frequency $\omega_d = 20\pi$ GHz. Detuning $\delta\omega = 0$. $v = 1.2 \times 10^8$ ms^{-1}. $L^0_{eff} = 0.5$ mm. $\epsilon = 0.6$.

Figure (6.6) shows the variation of B^L_{max} with respect to the transmission efficiency η and the detuning as a fraction of the driving frequency ω_d. The dash-dotted curve represents the points $B_{max} = 2$. The region above this curve violates Bell's inequality. The plot indicates that Bell violation occurs for $\eta \geq 0.35$ (signal loss $\leq 65\%$) up to the detuning $\frac{\delta\omega}{\omega_d} = 0.2$. However, for value of the detuning $0.2 < \frac{\delta\omega}{\omega_d} < 0.27$, a higher transmission efficiency is required. For detuning $\frac{\delta\omega}{\omega_d} > 0.27$ Bell violation is completely absent irrespective of the value of the transmission efficiency. This is consistent with the result of Figure (6.2).

Figure (6.7) shows the variation of B^L_{max} with respect to the temperature T and the transmission efficiency η in the presence of detuning $\frac{\delta\omega}{\omega_d} = 0.2$. The dash-dotted curve represents the points $B_{max} = 2$. The region above this curve violates Bell's inequality. From the plot we see that for temperature up to 19 mK Bell violation is absent when the transmission efficiency $\eta < 0.35$ ($> 65\%$ signal loss). For temperature higher than 19 mK, a greater value of transmission efficiency is required to observe Bell violation. B^L_{max} falls sharply with increasing signal loss for temperature $T > 21$ mK. For our chosen range of parameters Bell violation is absent when $T \geq 28$ mK.

Though the main purpose of the present work is to show that Bell viola-

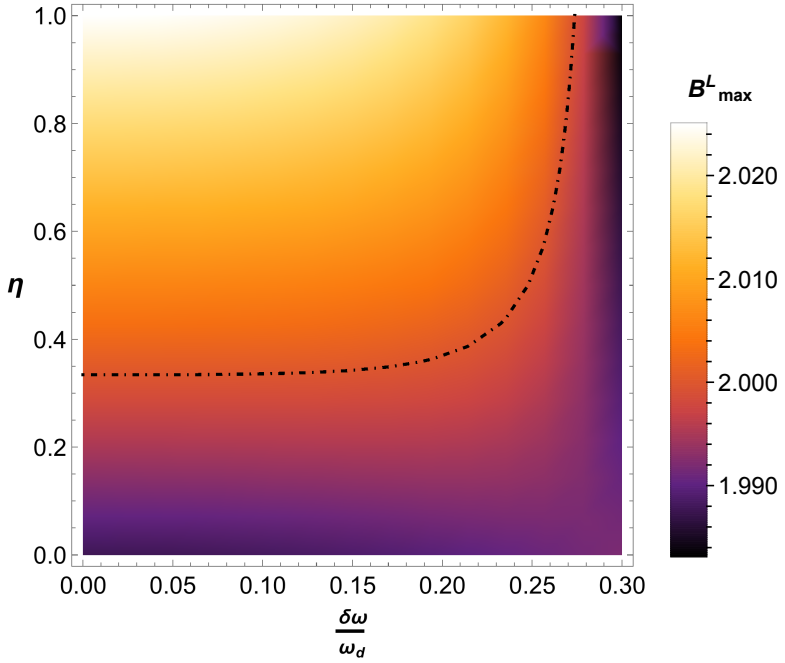

Figure 6.6: Variation of B^L_{max} with respect to the transmission efficiency η and the detuning as a fraction of the driving frequency $\omega_d = 20\pi$ GHz. $v = 1.2 \times 10^8$ ms^{-1}. $L^0_{eff} = 0.5$ mm. $\epsilon = 0.6$, $T = 20$ mK.

tion is indeed possible in the DCE set-up, it is also indeed feasible to conceive schemes to experimentally measure such Bell violation. Entanglement in DCE radiation has been quantitatively measured in a recent experiment in a superconducting circuit [225]. Experimental studies on DCE radiation show that, in our chosen temperature range, the thermal photons are quite challenging to resolve. Nonetheless, quantum correlation is observed for some chosen range of parameters in the presence of noise due to thermal photons. Note that Bell-violating states form a subset of all entangled states [228]. Hence, a study of entanglement is not equivalent to a study of Bell violation. In the context of the present set-up, the range of system parameters for which Bell violation is obtained is much smaller than that of entanglement.

In the present analysis the Bell operator consists of two measurements $\hat{\Pi}_x \otimes \hat{\Pi}_x$ and $\hat{\Pi}_z \otimes \hat{\Pi}_z$. The measurement $\hat{\Pi}_x$ can be written as $sgn(\hat{q})$ ($\hat{q} \rightarrow$ canonical position operator) [205]. It is basically the sign of the quadrature and can be measured by the homodyne measurement that has been implemented in experiments [188, 189]. The operator $\hat{\Pi}_z$ is the parity operator in the spatial basis and it has the same expectation value with the parity operator in the number basis [204]. So, it is possible to measure $\langle \hat{\Pi}_z \otimes \hat{\Pi}_z \rangle$ using a number resolving detector. Alter-

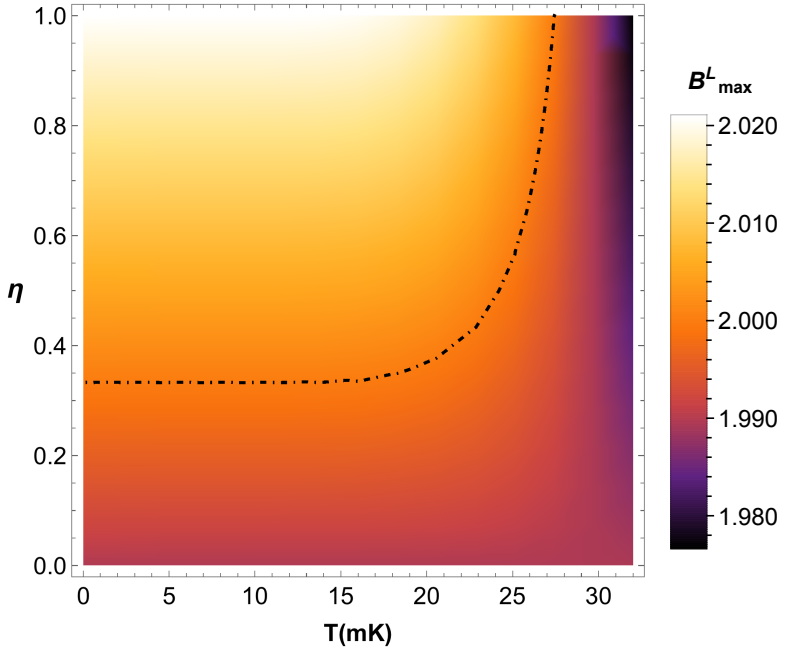

Figure 6.7: Variation of B^L_{max} with respect to the temperature T and transmission efficiency η. $(\delta\omega/\omega_d) = 0.2$ where $\delta\omega$ is the detuning and $\omega_d = 20\pi$ GHz is the driving frequency. $v = 1.2 \times 10^8$ ms^{-1}. $L^0_{eff} = 0.5$ mm. $\epsilon = 0.6$.

natively, parity can also be measured in the spatial basis using a parity analyser which is the parity sensitive Mach-Zehnder interferometer [229, 230]. Schemes for implementing the Mach-Zehnder interferometer in superconducting CPW have been proposed [227]. Detailed discussions on implementing various components such as mirrors, phase shifts, and photon detectors for coincidence circuits in CPW have been provided (see, for instance, [231]).

Before concluding, it may be pertinent to note the following issue. There are several important loopholes in the experimental violation of a Bell inequality [232]. Two of the most widely discussed loopholes are the locality loophole and the detection loophole. While the locality loophole cannot be closed in the present set-up, further analysis is required in respect of the detection loophole here. In general, sufficiently high detector efficiencies enable the closure of the detection loophole in Bell tests involving parametric down conversion [233]. Note that, though in case of the set-up involving DCE photons that we have considered here, a small magnitude of Bell violation is obtained in the perturbative regime of the driving amplitude; such violation still persists under considerable signal loss. Moreover, our study indicates that Bell violation increases with the driving amplitude, and hence, a detailed study will be required involving a non-perturbative

analysis in conjunction with tolerance to signal loss in order to estimate the threshold of detector efficiency needed for the closure of the detection loophole.

6.4 Conclusions

Quantum nonlocality as manifested by the violation of Bell's inequality represents a basic paradigm of quantum theory, which is of importance for the test of foundational principles, as well as for potential technological applications, such as in quantum cryptography. In this work we have studied Bell violation by dynamical Casimir photon pairs generated from quantized vacuum by the relativistic motion of a mirror. We have considered the circuit quantum electrodynamical set-up that has been experimentally implemented [188]. Though Bell's inequality has been studied earlier theoretically in the noninertial relativistic domain [209–211], experimental verification of such proposals remain beyond the reach of current technology. On the other hand, the framework of Bell violation proposed in the present work can be probed efficiently in the laboratory [186–189].

The analysis performed in this work is based on the measurement induced spin-like quantum correlations within Casimir photon pairs. Previously, several theoretical and experimental studies have been performed on Gaussian quantum correlation of DCE photons using homodyne measurement. Our present study focuses on nonlocal quantum correlations between Casimir photon pairs generated through non-Gaussian measurements [204, 205]. Such correlations have been shown to be of significance in several domains of quantum information and communication [214–218]. The Bell violation obtained here through the above framework is thus of direct relevance to several information theoretic protocols.

Let us now briefly summarize the main results of our study. We have analytically derived the expectation value of the Bell operator for DCE radiation, optimized with respect to channel orientations in the context of pseudospin measurements. We have studied the behaviour of Bell violation in terms of experimental parameters such as the driving frequency. We have further considered the effect of local thermal noise in each mode and asymmetry between the entangled modes introduced through the detuning in the frequency of photon pairs. We show that for our chosen parameter range, the violation of Bell's inequality can be observed up to the temperature about 40 mK. Our results further show that the asymmetry between the entangled modes degrades the Bell nonlocality at relatively higher temperature. However, at low temperatures detuning has a negligible effect on Bell's inequality violation. Finally, we have also derived the expectation value of the Bell operator in the presence of signal loss and explored

the robustness of Bell nonlocality in this scenario. We show that in the system under consideration, Bell nonlocality is robust up to 65% signal loss.

To conclude, in our analysis we have presented multiple plots showing the variation of Bell's nonlocality with different circuit parameters in the presence of local noise, asymmetry between the entangled modes because of nonzero detuning, and signal loss. Our results clearly demarcate the parameter regions where Bell nonlocality of Casimir photons can be observed. The choice of parameters considered in the present study is well within the perturbative regime. Since Bell violation is seen to rise rapidly with the increase of the driving frequency, it is expected that higher values of the driving parameter would yield significantly larger magnitudes of Bell violation. Our results thus motivate further analysis in the nonperturbative framework. It might be also interesting to consider in future works the Bell violation in the cQED set-up using other measurement schemes. A comparative analysis of such studies may lead to an optimal framework for quantum state preparation of Casimir photons, as a vital step towards information processing through the cQED set-up.

Chapter 7

Summary and outlook

A recent trend of research in relativistic quantum theory is to look for the observable signatures of relativity in low energy and quantum mechanical systems which will be useful for the progress in foundations of physics and/or development of technology. Quantum information theory becomes relevant in this context because of its operational framework. However the quantum information theory developed so far are based on non-relativistic quantum mechanics and hence are not covariant. In order to develop a quantum information theory in the relativistic regime, first we have to formulate an information theory that is consistent with relativistic quantum mechanics and QFTCS. We also need to understand how relativistic background affects the various notions of quantum information theory. The works presented in this thesis have made some effort in that direction.

Quantum correlations are used as resources to perform various quantum tasks. So, we need to understand whether these resources are useful too in relativistic background. In the Chapter 3 we consider the effect of relativistic boosts on the coherence of the single-particle Gaussian wave packets [56]. The coherence is measured by the boosted observer as a function of the boost parameter of the observer and the uncertainty in momentum of the wave packet. In quantum information theory the term 'quantum coherence' has been used to describe quantum features in different physical contexts. Each of these have their own resource theoretic importance. Using quantifiers defined in different formulations of coherence, it is shown that in general the coherence decreases with the increase of the uncertainty in momentum of the state, as well as the boosts applied to it. However our analysis show that the basis independent notion of coherence are more consistent in the relativistic background compared to the basis dependent formulations. Using basis-independent quantifier, coherence may be preserved even for large boosts applied on wave packets with narrow uncertainty. Our result has been exempli-

fied quantitatively for realistic neutron wave packet. Our work can be extended in case of spin-1/2 particle moving in curved space-time [33,34]. Similar analysis can also be done for photons [32].

With the development of material technology nano and micro structured environment provides a very efficient platform for quantum optics experiments [138–140,234]. Such structured environments impose various boundary conditions on the atom-field systems. The atom in such structured environment does not necessarily remain static. The atom can be subjected to acceleration because of various potentials [130–132] or external tuning of atom-field coupling [142,143]. So, the study radiative process of accelerating atoms subjected to boundary conditions is significant in context of quantum foundations as well as for performing quantum tasks. In the Chapter 4, we have studied the resonance interaction of two entangled, identical, neutral atoms interacting with quantized real, massless, scalar vacuum and accelerating between two mirrors [57]. We assume that the entangled atoms are either in superradiant or subradiant state. Using formalism of Dalibard *et al.* [146,147] and Zhou *et al.* [124,126], we calculate the energy level shift and the relaxation rate of energy exchange between the atoms, accelerating within the two mirrors, due to resonance interaction. Our analysis accompanied by various plots showing that resonance interaction can be manipulated by the various system parameters such as atomic configuration, cavity parameters etc. We have also discussed dependence of resonance interaction on atomic acceleration and evaluated the energy level shift and rate of change of energy in the low acceleration limit. We have numerically calculated the correction in the resonance energy shift due to atomic acceleration using realistic experimental parameters. This work can be extended in case of accelerated detectors with various other boundary conditions such as Neumann boundary conditions, accelerated mirror cylindrical waveguide etc [3,235].

The universe is both relativistic and quantum at the fundamental length scale. However the quantum theory of gravity still remains a mystery. A very important trend in research is to look for signatures of Planck scale effect, as an emergent term in the quantum theory in classical space-time background. The modification in Heisenberg's uncertainty principle, due to existence of minimum observable length, results in generalized uncertainty principle (GUP). In Chapter 5, we have considered an atom-mirror system in relative acceleration, in presence of single mode quantized scalar field [58] whose canonical momentum operator satisfies GUP. The GUP modifies the energy-momentum dispersion relation resulting the GUP deformed Klein-Gordon equation. We solve the deformed Klein-Gordon equation with suitable Dirichlet boundary conditions and calculate the excitation

probabilities of the atom when, (a) atom is accelerating uniformly and the mirror is static in the Minkowski space-time and (b) mirror is accelerating uniformly and the atom is static in the Minkowski space-time. Svidzinsky *et al.* [106] have studied the same problem in absence of GUP (i.e. their system obey Heisenberg uncertainty) and their work show that the two probabilities are equal (upto some constant phase factor) manifesting a symmetry between system (a) and (b). Our calculations show that GUP introduces a position (of atom) dependent modulation in the Fano interference pattern in case (b) and such modulation is absent in case (a). GUP also modifies the Unruh temperature in case (b). Thus GUP breaks the symmetry, manifested when the field obeys Heisenberg uncertainty, between cases (a) and (b). According to the works in ref. [179,180], any qualitative symmetry between the cases (a) and (b) are a manifestation of weak equivalence principle (WEP). So, in our work GUP results in violation WEP between the cases (a) and (b). Apart from WEP violation, GUP introduces damping effect in both cases. We define a WEP violation parameter which is a function of GUP parameter. Any experimental bound on GUP parameter will also put a bound on the WEP violation by GUP in our system. Our system represents a very basic 1-dimensional waveguide structure. Our work can be extended in case of more realistic set-up(s) such as cavities and cylindrical waveguides etc. [3, 180]. Our work can also be studied in case of different boundary conditions [3, 235] and also for different kind of quantum fields such as Dirac and electromagnetic fields [3].

The particle production by quantum fields subjected to curved space-time geometry, for example Hawking radiation, is impossible to probe with current technology. However analogue models such as dynamical Casimir effect (DCE) can be simulated in laboratory [53, 188, 189]. This open up the platform to study quantum properties of the particles produced by quantum vacuum subjected to time dependent boundary conditions. Such platforms also enables us to simulate fundamental phenomena, for example cosmological particle creation [192]. When quantum field is subjected to curved space-time geometry or time dependent boundary conditions, quantum entanglement is generated within the field modes [3, 35, 36]. While the quantum correlation generated in case of Unruh effect and Hawking radiation is impossible to utilise, the entanglement generated during DCE simulated in laboratory can be used as a resource [143, 191]. In Chapter 6 we study the Bell's inequality violation by dynamical Casimir radiation in cQED set-up [186–188, 191]. Bell nonlocality is the strongest form of quantum correlation with significant application in the field of quantum information and computation [207, 208]. So the study of Bell nonlocality of DCE radiation is important for foundational perspective as well as its efficiency as a quantum

resource. In our work we study Bell's inequality violation by DCE photons using pseudospin measurements represented in configuration space. We analytically obtain expectation values of the Bell operator optimized with respect to channel orientations, in terms of the system parameters. We consider the effects of local noise in the microwave field modes, asymmetry between the field modes resulting from nonzero detuning, and signal loss. Our analysis provides ranges of the above experimental parameters for which Bell violation can be observed. We show that Bell violation can be observed in this set-up up to $40mK$ temperature as well as up to 65% signal loss. The accelerated mirror is simulated, in cQED set-up, by inducing a current driven by ultra-rapid tuning of magnetic flux in a SQUID. In our work we have studied the DCE radiation generated by relatively smaller values of driving amplitude so that mathematically the dynamics of the system can be handled perturbatively. At perturbative regime the magnitude of Bell violation is quite low. Hence in order to obtain greater value of Bell violation we need to go beyond perturbative regime of value of driving amplitude. This is a serious numerical task and can be addressed in future. Further studies can be done on efficiency of DCE radiation as a resource in the field of continuous variable quantum information [223, 236].

Bibliography

[1] W. Greiner, Relativistic Quantum Mechanics: Wave equation, Springer-Verlag, Berlin, (1990).

[2] E. Wigner, Ann. Math. **40**, 149-204 (1939).

[3] N. Birrell, & P. Davies, Quantum Fields in Curved Space, Cambridge University Press, (1982).

[4] M. Nielsen, & I. Chuang, Quantum Computation and Quantum Information, Cambridge University Press, (2010).

[5] S. Weinberg, The Quantum Theory of Fields: Vol-I, Cambridge University Press, (1995).

[6] L. Parker, Phys. Rev. **183**, 1057 (1969); Phys. Rev. D **3**, 346 (1971).

[7] S. W. Hawking, Nature **248**, 30-31 (1974).

[8] S. W. Hawking, Commun.Math. Phys. **43**, 199-220 (1975).

[9] G. T. Moore, J. Math. Phys. **11**, 2679 (1970).

[10] B. S. DeWitt., Phys. Rept., **19**:295-357, (1975).

[11] S. A. Fulling and P. C.W. Davies, Proc. R. Soc. Lond. A **348**, 393 (1976).

[12] W. G. Unruh, Phys. Rev. D **14**, 870 (1976).

[13] J. J. Sakurai, & J. Napolitano, Modern Quantum Mechanics, Cambridge University Press, (2017).

[14] `https://en.wikipedia.org/wiki/Quantum_entanglement`.

[15] A. Einstein, B. Podolsky and N. Rosen, Phys. Rev. **47**, 777 (1935).

[16] L. E. Ballentine, Rev. Mod. Phys. **42**, 358 (1970), and references therein.

[17] J. S. Bell, Physics Physique Fizika **1**, 195 (1964).

[18] J. S. Bell, Speakable and Unspeakable in Quantum Mechanics, Cambridge University Press, (2004).

[19] J. F. Clauser, M. A. Horne, A. Shimony, and R. A. Holt, Phys. Rev. Lett. **23**, 880 (1969).

[20] M. Hayashi, Quantum Information Theory: Mathematical Foundation, Springer (2017) and references therein.

[21] C. H. Bennett, G. Brassard, Proceedings of the IEEE International Conference on Computers, Systems and Signal Processing, (Bangalore, India, 1984), pp. 175-179; Theoretical Computer Science, Vol. **560** (Part 1), 2014, pp. 7-11.

[22] M. Ozawa, J. Math. Phys. **25**, 79 (1984).

[23] H. Nagaoka, Differential Geometrical Aspects of Quantum State Estimation and Relative Entropy. In: Belavkin, V.P., Hirota, O., Hudson, R.L. (eds) Quantum Communications and Measurement. Springer, Boston, MA, (1995).

[24] R. P. Feynman, Int J Theor Phys **21**, 467-488 (1982); Found Phys **16**, 507-531 (1986).

[25] Y. Manin, Computable and Uncomputable (in Russian), Sovetskoye Radio, Moscow (1980).

[26] H. Ollivier and W. H. Zurek, Phys. Rev. Lett. **88**, 017901 (2001).

[27] H. M. Wiseman, S. J. Jones, A. C. Doherty, Phys. Rev. Lett. **98**, 140402 (2007).

[28] E. Chitambar, G. Gour, Rev. Mod. Phys. **91**, 025001 (2019).

[29] H. Terashima, M. Ueda, Int. J. Quantum Inform. **1**, 93-114 (2003).

[30] A. Peres, P. F. Scudo, D. R. Terno, Phys. Rev. Lett. **88**, 230402 (2002).

[31] R. M. Gingrich, C. Adami, Phys. Rev. Lett. **89**, 270402 (2002).

[32] A. Peres, D. R. Terno, Rev. Mod. Phys. **76**, 93 (2004).

[33] H. Terashima, M. Ueda, Phys. Rev. A **69**, 032113 (2004).

[34] J. Said, K. Z. Adami, Phys. Rev. D **81**, 124012 (2010).

[35] I. Fuentes, LECTURE SERIES ON RELATIVISTIC QUANTUM INFORMATION : Diversities in Quantum Computation and Quantum Information, pp 107-147 (2012).

[36] P. M. Alsing and I. Fuentes, Class. Quantum Grav. **29**, 224001 (2012).

[37] I. Fuentes-Schuller, R. B. Mann, Phys. Rev. Lett. **95**, 120404 (2005).

[38] P. M. Alsing, I. Fuentes-Schuller, R. B. Mann, T. E. Tessier, Phys. Rev. A **74**, 032326 (2006).

[39] A. Datta, Phys. Rev. A **80**, 052304 (2009).

[40] J. L. Ball, I. Fuentes-Schuller, F. P. Schuller, Phys. Lett. A **359**, 550-554 (2006).

[41] N. Liu, J. Goold, I. Fuentes, V. Vedral, K. Modi, D. E. Bruschi, Class. Quantum Grav. **33**, 035003 (2016).

[42] J. Wang, H. Cao, J. Jing, H. Fan, Phys. Rev. D **93**, 125011 (2016).

[43] L. C. Céleri, F. Pascoal, M. H. Y. Moussa, Class. Quantum Grav. **26**, 105014 (2009).

[44] P. M. Alsing and G. J. Milburn, Phys. Rev. Lett. **91**, 180404 (2003).

[45] J. D. Franson, Phys. Rev. A **84**, 033809 (2011).

[46] A. G. S. Landulfo and A. C. Torres, Phys. Rev. A **87**, 042339 (2013).

[47] G. Adesso, I. Fuentes-Schuller, M. Ericsson, Phys. Rev. A **76**, 062112 (2007).

[48] J. Wang, J. Deng, J. Jing, Phys. Rev. A **81**, 052120 (2010).

[49] L. C. B. Crispino, A. Higuchi, G. E. A. Matsas, Rev. Mod. Phys. **80**, 787 (2008).

[50] M. P. G. Robbins, N. Afshordi, Robert B. Mann, JCAP **07**, 032 (2019).

[51] M. P. G. Robbins, N. Afshordi, A. O. Jamison, R. B. Mann, arXiv:2101.03691.

[52] M. A. Page, M. Goryachev, H. Miao et al., Commun Phys **4**, 27 (2021).

[53] V. Macrì *et al.*, Phys. Rev. X **8**, (2018).

[54] P. D. Nation, J. R. Johansson, M. P. Blencowe, F. Nori, Rev. Mod. Phys. **84**, 1 (2012).

[55] D. Rideout et al., Class. Quantum Grav. **29**, 224011 (2012).

[56] R. Chatterjee, A. S. Majumdar, Phys. Rev. A **96**, 052301 (2017).

[57] R. Chatterjee, S. Gangopadhyay, A. S. Majumdar, Eur. Phys. J. D **75**, 179 (2021).

[58] R. Chatterjee, S. Gangopadhyay, A. S. Majumdar, Phys. Rev. D **104**, 124001 (2021).

[59] R. Chatterjee, A. S. Majumdar, Phys. Rev. A **106**, 042224 (2022).

[60] W. K Tung, Group Theory in Physics, World Scientific, (1985).

[61] V. Palge, Relativistic entanglement of single and two particle systems. PhD thesis, University of Leeds, (2013).

[62] T. F. Jordan, A. Shaji, E. C. G. Sudarshan, Phys. Rev. A **73**, 032104 (2006).

[63] F. R. Halpern, Special Relativity and Quantum Mechanics, Prentice-Hall (1968).

[64] S. Weinberg, (1972) Gravitation and Cosmology, Principles and Applications of the General Theory of Relativity. John Wiley and Sons, New York.

[65] R. Lopp (2021), Light-Matter Interaction Models in Relativistic Quantum Information. UWSpace.

[66] Wenting Zhou and Hongwei Yu, Phys. Rev. D **101**, 085009 (2020).

[67] W. G. Unruh, R. M. Wald, Phys. Rev. D **29**, 1047 (1984).

[68] E. Martín-Martínez, M. Montero, and M. del Rey, Phys. Rev. D **87**, 064038 (2013).

[69] Á. M. Alhambra, A. Kempf, E. Martín-Martínez, Phys. Rev. A **89**, 033835 (2014).

[70] A. Pozas-Kerstjens, E. Martín-Martínez, Phys. Rev. D **94**, 064074 (2016).

[71] E. Tjoa (2019). Aspects of Quantum Field Theory with Boundary Conditions. UWSpace.

[72] R. J. Glauber, Phys. Rev. **130**, 2529 (1963).

[73] A. Streltsov, G. Adesso, M. B. Plenio, Rev. Mod. Phys. **89**, 041003 (2017).

[74] M. Horodecki, J. Oppenheim, Int. J. Mod. Phys. B **27**, 1345019 (2013).

[75] F. G. S. L. Brandão and G. Gour, Phys. Rev. Lett. **115**, 070503 (2015).

[76] G. Gour, R. W. Spekkens, New J. Phys. **10**, 033023 (2008).

[77] G. Gour, I. Marvian, R. W. Spekkens, Phys. Rev. A **80**, 012307 (2009).

[78] I. Marvian, R.W. Spekkens, New J. Phys. **15**, 033001 (2013); Phys. Rev. A **90**, 062110 (2014); Nat. Commun. **5**, 3821 (2014); Phys. Rev. A **94**, 052324 (2016).

[79] I. Marvian, R. W. Spekkens, P. Zanardi, Phys. Rev. A **93**, 052331 (2016).

[80] E. Chitambar, G. Gour, Rev. Mod. Phys. **91**, 025001 (2019).

[81] T. Baumgratz, M. Cramer, and M. B. Plenio, Phys. Rev. Lett. **113**, 140401 (2014).

[82] Davide Girolami, Phys. Rev. Lett. **113**, 170401 (2014).

[83] C. Napoli, T. R. Bromley, M. Cianciaruso, M. Piani, N. Johnston, G. Adesso, Phys. Rev. Lett. **116**, 150502 (2016).

[84] Y. Yao, G. H. Dong, X. Xiao, C. P. Sun, Sci. Rep. **6**, 32010 (2016).

[85] S. D. Bartlett, T. Rudolph, R. W. Spekkens, Phys. Rev. Lett. **91**, 027901 (2003); S. D. Bartlett, D. R. Terno, Phys. Rev. A **71**, 012302 (2005).

[86] R. Takagi, Sci. Rep. **9**, 14562 (2019).

[87] M. Banik, P. Deb, S. Bhattacharya, Quantum Inf. Process. **16**, 97 (2017).

[88] `http://lansce.lanl.gov/facilities/ultracold-neutrons/about.php`

[89] N. J. Carron, An Introduction to the Passage of Energetic Particles Through Matter, Taylor and Francis, (2007), p 308.

[90] G. V. Kulin, A. I. Frank, S. V. Goryunov, D. V. Kustov, P. Geltenbort, M. Jentschel, A. N. Strepetov, V. A. Bushuev, Nucl. Instrum. Methods Phys. Res. A **792**, 38 (2015).

[91] T. Jenke, G. Cronenberg, M. Thalhammer, T. Rechberger, P. Geltenbort, H. Abele, arXiv: 1510.03078.

[92] V. Vedral, M. B. Plenio, M. A. Rippin, and P. L. Knight, Phys. Rev. Lett. **78**, 2275 (1997).

[93] J. Rehacek and Z. Hradil, Phys. Rev. Lett. **88**, 130401 (2002).

[94] T. Ma, M. J. Zhao, S. M. Fei, and G. L. Long, Phys. Rev. A **94**, 042312 (2016).

[95] D. Mondal, C. Datta, and Sk Sazim, Phys. Lett. A **380**, 689 (2016).

[96] F Schmidt-Kaler *et al.*, New J. Phys. **12**, 065014 (2010).

[97] M. O. Scully *et al.*, PNAS **115**, 8131 (2018).

[98] N. Rivera, I. Kaminer, Nat Rev Phys **2**, 538-561 (2020).

[99] S. Ritter, C. Nölleke, C. Hahn *et al.*, Nature **484**, 195 (2012).

[100] M. H. Devoret, A. Wallraff, J. M. Martinis, arXiv:cond-mat/0411174.

[101] M. Baur, A. Fedorov, L. Steffen, S. Filipp, M. P. da Silva, A. Wallraff, Phys. Rev. Lett. **108**, 040502 (2012).

[102] A. Abdelrahman, T. Mukai, H. Häffner, T. Byrnes, Opt. Express **22**, 3501-3513 (2014).

[103] L. Liu *et al.*, Nat Commun **9**, 2760 (2018).

[104] U. L. Andersen, J. S. Neergaard-Nielsen, P. van Loock, A. Furusawa, Nat Phys **11**, 713-719 (2015).

[105] S. Kolkowitz, I. Pikovski, N. Langellier, M. D. Lukin, R. L. Walsworth, J. Ye, Phys. Rev. D **94**, 124043 (2016).

[106] A. A. Svidzinsky, J. S. Ben-Benjamin, S. A. Fulling, and D. N. Page, Phys. Rev. Lett. **121**, 071301 (2018).

[107] T. A. Welton, Phys. Rev. **74**, 1157 (1948).

[108] G. Compagno, R. Passante, and F. Persico, Phys. Lett. A **98**, 253 (1983).

[109] J. R. Ackerhalt, P. L. Knight, and J. H. Eberly, Phys. Rev. Lett. **30**, 456 (1973).

[110] P. W. Milonni, W. A. Smith, Phys. Rev. A **11**, 814 (1975); P. W. Milonni, Phys. Scr. **T21**, 102 (1988).

[111] D. P. Craig and T. Thirunamachandran, Molecular Quantum Electrodynamics, Dover, Mineola, (1998).

[112] A. Salam, Molecular Quantum Electrodynamics (John Wiley and Sons, Hoboken, New Jersey, 2010).

[113] Th. Förster, in: *Modern Quantum Chemistry*, edited by O. Sinanoğlu and O. Doğu (Academic Press, New York, 1965).

[114] G. Juzeliuas and D. L. Andrews, Adv. Chem. Phys. **112**, 357 (2000).

[115] G. S. Agarwal, S. Dutta Gupta, Phys. Rev. A **57**, 667 (1998).

[116] W. Zhou, L. Rizzuto, R. Passante; Phys. Rev. A 97, 042503 (2018).

[117] P. R. Berman, Phys. Rev. A **91**, 042127 (2015).

[118] M. Donaire, R. Guérout, and A. Lambrecht, Phys. Rev. Lett. **115**, 033201 (2015).

[119] P. Barcellona, R. Passante, L. Rizzuto, and S. Y. Buhmann, Phys. Rev. A **94**, 012705 (2016).

[120] P. W. Milonni and S. M. H. Rafsanjani, Phys. Rev. A **92**, 062711 (2015).

[121] H. Haakh, F. Intravaia, C. Henkel, S. Spagnolo, R. Passante, B. Power, and F. Sols, Phys. Rev. A **80**, 062905 (2009).

[122] H. R. Haakh and S. Scheel, Phys. Rev. A **91**, 052707 (2015).

[123] L. Rizzuto, R. Passante, and F. Persico, Phys. Rev. Lett. **98**, 240404 (2007).

[124] L. Rizzuto, M. Lattuca, J. Marino, A. Noto, S. Spagnolo, W. Zhou, R. Passante, Phys. Rev. A **94**, 012121 (2016).

[125] W. Zhou, R. Passante, L. Rizzuto, Symmetry **10**, 185 (2018).

[126] W. Zhou, H. Yu, Phys. Rev. D **101**, 025009 (2020).

[127] M. Fink *et al.*, Nat Commun **8**, 15304 (2017).

[128] A. Villar *et al.*, Optica **7**, 734-737 (2020).

[129] S. K. Joshi *et al.*, New J. Phys. **20**, 063016 (2018).

[130] A. P. Burgers, L. S. Peng, J. A. Muniz, A. C. McClung, M. J. Martin, H. J. Kimble, PNAS **116** (2), 456 (2019).

[131] S. Vorrath, S. A. Möller, P. Windpassinger, K. Bongs, K. Sengstock, New J. Phys. **12**, 123015 (2010).

[132] T. Yoon, M. Bajcsy, J. Phys. B **53**, 135002 (2020).

[133] S. Beattie, B. Barrett, M. Weel, I. Chan, C. Mok, S.B. Cahn, A. Kumarakrishnan, Phys. Rev. A **77**, 013610 (2008).

[134] K. Kożdoń, I. T. Durham, A. Dragan, Quantum **2**, 83 (2018).

[135] L. García-Álvarez, S. Felicetti, E. Rico *et al.*, Sci Rep **7**, 657 (2017).

[136] N. Friis, A. R. Lee, K. Truong, C. Sabín, E. Solano, G. Johansson, I. Fuentes, Phys. Rev. Lett. **110**, 113602 (2013).

[137] S. Felicetti, C. Sabín, I. Fuentes, L. Lamata, G. Romero, E. Solano, Phys. Rev. B **92**, 064501 (2015).

[138] E. Vetsch *et al.*, Phys. Rev. Lett. **104**, 203603 (2010); A. Goban et al., Phys. Rev. Lett. **109**, 033603 (2012).

[139] N.V. Corzo *et al.*, Nature **566**, 359 (2019).

[140] D. E. Chang *et al.*, Rev. Mod. Phys. **90**, 031002 (2018).

[141] L. M. Duan *et al.*, Nature **414**, 413-418 (2001); N. Sangouard, Rev. Mod. Phys. **83**, 33 (2011).

[142] S. Felicetti *et al.*, Phys. Rev. Lett. **113**, 093602 (2014).

[143] G. Benenti *et al.*, Phys. Rev. A **90**, 052313 (2014).

[144] V Notararigo, R Passante, L Rizzuto, Sci Rep **8**, 5193 (2018).

[145] G. Fiscelli, L. Rizzuto, R. Passante, Phys. Rev. A **98**, 013849 (2018).

[146] J. Dalibard, J. Dupont-Roc, C. Cohen-Tannoudji, J. Phys. (Paris) **43**, 1617 (1982).

[147] J. Dalibard, J. Dupont-Roc, C. Cohen-Tannoudji, J. Phys. (Paris) **45**, 637 (1984).

[148] J. Audretsch, R. Muller, Phys. Rev. A **50**, 1755 (1994).

[149] J. Audretsch, R. Muller, Phys. Rev. A **52**, 629 (1995).

[150] W. Jhe, Phys. Rev. A **43**, 5795 (1991); Phys. Rev. A **44**, 5932 (1991).

[151] R. Passante, Phys. Rev, A **57**, 1590 (1998).

[152] Z. Zhu, H. Yu, S. Lu, Phys. Rev. D **73**, 107501 (2006).

[153] W. Zhou, H. Yu, Phys. Rev. A **86**, 033841 (2012).

[154] L. Rizzuto, S. Spagnolo, Phys. Scr. T **143**, 014021 (2011); L. S. Brown, G. J. Maclay, Phys. Rev. **184**, 1272 (1969).

[155] H. Cai, Z. Li, Z. Ren, Eur. Phys. J. Plus **133**, 458 (2018).

[156] M. Donaire, J. M. Muñoz-Castañeda, L. M. Nieto, Phys. Rev. A **96**, (2017).

[157] E.W. Hagley, F.M. Pipkin, Phys. Rev. Lett. **72**, 1172 (1994).

[158] S. Datta, Quantum Transport: Atom to Transistor, Cambridge University Press (2005).

[159] A. Einstein, Ann. Phys. (Berlin) **354**, 769 (1916).

[160] S. Carlip, Int. J. Mod. Phys. D **23**, 1430023 (2014).

[161] K. Becker, M. Becker, and J. Schwarz, String Theory and M-Theory: A Modern Introduction, Cambridge University Press (2006).

[162] Dah-Wei Chiou, Int. J. Mod. Phys. D **24**, 1530005 (2015).

[163] C. A. Mead, Phys. Rev. **135**, B849 (1964).

[164] D. Amati, M. Ciafaloni, and G. Veneziano, Phys. Lett. B **216**, 41 (1989).

[165] M. Maggiore, Phys. Lett. B **304**, 65 (1993); Phys. Rev. D **49**, 5182 (1994); Phys. Lett. B **319**, 83 (1993).

[166] T. Jacobson and D. Mattingly, Phys. Rev. D **63**, 041502 (2001); Phys. Rev. D **64**, 024028 (2001).

[167] R. J. Adler, P. Chen, D. I. Santiago, Gen. Rel. Grav. **33**, 2101 (2001); S. Gangopadhyay, A. Dutta, and A. Saha, Gen. Relativ. Gravit. **46**, 1661 (2014); J. Giné, Commun. Theor. Phys. **73**, 015201 (2021).

[168] A. Mukherjee, S. Gangopadhyay, M. Dutta, Europhys. Lett. **129**, 30002 (2020).

[169] A. Kempf, G. Mangano, R. B. Mann, Phys. Rev. D **52**, 1108 (1995); A. F. Ali, S. Das, E. C. Vagenas, Phys. Lett. B **678**, 497 (2009).

[170] A. Farag Ali, S. Das, E. C. Vagenas Phys. Rev. D **84**, 044013 (2011).

[171] I. Pikovski et. al., Nature Physics **8**, 393-397 (2012).

[172] P. Holland, The Quantum Theory of Motion, Cambridge University Press, London (1993), pp. 259-266.

[173] R. Colella, A.W. Overhauser, and S. A. Werner, Phys. Rev. Lett. **34**, 1472 (1975); A. Peters, K. Y. Chung, and S. Chu, Nature (London) **400**, 849 (1999).

[174] D. M. Greenberger and A. W. Overhauser, Rev. Mod. Phys. **51**, 43 (1979); D. M. Greenberger, Ann. Phys. (N.Y.) **47**, 116 (1968); Rev. Mod. Phys. **55**, 875 (1983).

[175] L. Viola and R. Onofrio, Phys. Rev. D **55**, 455 (1997); M.A. Ali, A. S. Majumdar, D. Home, A. K. Pan, Class. Quantum Grav. **23**, 6493 (2006); P. Chowdhury, D. Home, A. S. Majumdar, S. V. Mousavi, M. R. Mozaffari, S. Sinha, Class. Quantum Grav. **29**, 025010 (2012); S. V. Mousavi, A. S. Majumdar, D. Home, Class. Quantum Grav. **32**, 215014 (2015).

[176] J. S. Ben-Benjamin, M. O. Scully, S. A. Fulling *et al.*, Int. J. Mod. Phys. A **34**, 1941005 (2019); J. S. Ben-Benjamin, M. O. Scully, W. G. Unruh, Phys. Scr. **95**, 074015 (2020).

[177] M. Zych and C. Brukner, Nat. Phys. **14**, 1027 (2018).

[178] D. Singleton, S. Wilburn, Phys. Rev. Lett. **107**, 081102 (2011); L. C. B. Crispino, A. Higuchi, G. E. A. Matsas, Phys. Rev. Lett. **108**, 049001 (2012); D. Singleton, S. Wilburn, Phys. Rev. Lett. **108**, 049002 (2012).

[179] S. A. Fulling, J. H. Wilson, Phys. Scr. **94**, 014004 (2019).

[180] E. Tjoa, R. B. Mann, E. Martín-Martínez, Phys. Rev. D **98**, 085004 (2018).

[181] D. Su, C. T. M. Ho, R. B. Mann, and T. C. Ralph, New J. Phys. **19**, 063017 (2017).

[182] M. Wallquist, K. Hammerer, P. Rabl, M. Lukin, and P. Zoller, Phys. Scr. **T137**, 014001 (2009).

[183] S. Bhattacharyya, S. Gangopadhyay, A. Saha, Class. Quantum Grav. **37**, 195006 (2020).

[184] P. C.W. Davies and S. A. Fulling, Proc. R. Soc. Lond. A **356**, 237 (1977).

[185] M. R. R. Good, P. R. Anderson, C. R. Evans, Phys. Rev. D **94**, 065010 (2016); M. R. Good, J. Foo, and E. V. Linder, Class. Quantum Grav. **38**, 085011 (2021); M. R. R. Good, Y. C. Ong, Eur. Phys. J. C **80**, 1169 (2020).

[186] J. R. Johansson, G. Johansson, C. M. Wilson, F. Nori, Phys. Rev. Lett. **103**, 147003 (2009).

[187] J. R. Johansson, G. Johansson, C. M. Wilson, F. Nori, Phys. Rev. A **82**, 052509 (2010).

[188] C. M. Wilson, G. Johansson, A. Pourkabirian, M. Simoen, J. R. Johansson, T. Duty, F. Nori, P. Delsing, Nature (London) **479**, 376 (2011).

[189] P. Lähteenmäki, G. S. Paraoanu, J. Hassel, P. J. Hakonen, Proc. Natl. Acad. Sci. U.S.A. **110**, 4234 (2013).

[190] Stephen A. Fulling and George E. A. Matsas (2014) Unruh effect. Scholarpedia, 9(10):31789.

[191] J. R. Johansson, G. Johansson, C. M. Wilson, P. Delsing, F. Nori, Phys. Rev. A **87**, 043804 (2013).

[192] Z. Tian, J. Jing, A. Dragan, Phys. Rev. D **95**, 125003 (2017).

[193] D. N. Samos-Sáenz de Buruaga, C. Sabín, Phys. Rev. A **95**, 022307 (2017).

[194] C. Sabín, I. Fuentes, G. Johansson, Phys. Rev. A **92**, 012314 (2015).

[195] C. Sabín, G. Adesso, Phys. Rev. A **92**, 042107 (2015).

[196] X. Zhang, H. Liu, Z. Wang, T. Zheng, Sci Rep **9**, 9552 (2019).

[197] Y. Long, X. Zhang, & T. Zheng, Quantum Inf Process **19**, 322 (2020).

[198] D. Bohm, Quantum Theory, Prentice Hall, Englewood Cliffs, NJ, (1951).

[199] A. Aspect, P. Grangier, G, Roger, Phys. Rev. Lett. **49**, 91 (1982).

[200] M. D. Reid and P. D. Drummond, Phys. Rev. Lett. **60**, 2731 (1988); M. D. Reid, Phys. Rev. A **40**, 913 (1989).

[201] Z.Y. Ou, S. F. Pereira, H. J. Kimble, and K. C. Peng, Phys. Rev. Lett. **68**, 3663 (1992); Z.Y. Ou, S. F. Pereira, and H. J. Kimble, Appl. Phys. B **55**, 265 (1992).

[202] S. L. Braunstein, A. Mann, and M. Revzen, Phys. Rev. Lett. **68**, 3259 (1992).

[203] Z. B. Chen, J. W. Pan, G. Hou, and Y. D. Zhang, Phys. Rev. Lett. **88**, 040406 (2002).

[204] G. Gour, F. C. Khanna, A. Mann, and M. Revzen, Phys. Lett. A **324**, 415 (2004).

[205] M. Revzen, P. A. Mello, A. Mann, and L. M. Johansen, Phys. Rev. A **71**, 022103 (2005).

[206] M M Dorantes and J L Lucio M, J. Phys. A: Math. Theor. **42**, 285309 (2009).

[207] A. K. Ekert, Phys. Rev. Lett. **67**, 661 (1991); T. Jennewein *et al.*, Phys. Rev. Lett. **84**, 4729 (2000); D. S. Naik *et al.*, Phys. Rev. Lett. **84**, 4733 (2000); W. Tittel *et al.*, Phys. Rev. Lett. **84**, 4737 (2000).

[208] U. Vazirani, T. Vidick, Phys. Rev. Lett. **113**, 140501 (2014); C. Miller, Y. Shi, J. ACM **63**, 33 (2016); R. Schwonnek, *et al.*, Nat. Comm. **12**, 2880 (2021).

[209] S. Omkar, R. Srikanth, S. Banerjee, A. K. Alok, Quantum Inf. and Comp. **16** 0757 (2016).

[210] D. Campo, R. Parentani, Phys.Rev. D **74**, 025001 (2006); J. Gallicchio, A. S. Friedman, D. I. Kaiser, Phys. Rev. Lett. **112**, 110405 (2014).

[211] J. Martin, V. Vennin, Phys. Rev. D **96**, 063501 (2017).

[212] J. R. Johansson, N. Lambert, I. Mahboob, H. Yamaguchi, F. Nori, Phys. Rev. B **90**, 174307 (2014); B. G. de Moraes, A. W. Cummings, and S. Roche, Phys. Rev. B 102, 041403(R) (2020).

[213] R. Stassi, S. De Liberato, L. Garziano, B. Spagnolo, S. Savasta, Phys. Rev. A **92**, 013830 (2015).

[214] A. Kalev, A. Mann, M. Revzen, Found Phys **37**, 125-143 (2007).

[215] S. W. Ji, J. Lee, J. Park, H. Nha, Sci Rep **6**, 29729 (2016).

[216] Y. Xiang, B. Xu, L. Mišta, Jr., T. Tufarelli, Q. He, G. Adesso, Phys. Rev. A **96**, 042326 (2017).

[217] J. Singh and S. Bose, Phys. Rev. A **104**, 052605 (2021).

[218] M. Walschaers, V. Parigi, and N. Treps, PRX Quantum **1**, 020305 (2020).

[219] A. Ferraro, M. G. A. Paris, J. Opt. B: Quantum and Semiclass. Opt. **7**, 174 (2005).

[220] S. Olivares, M. G. A. Paris, J. Opt. B: Quantum and Semiclass. Opt. **7**, S392 (2005).

[221] P. C. Ugalde (2017). Experimental prospects for detecting the quantum nature of spacetime. UWSpace.

[222] A. Lambrecht, M. T. Jaekel, and S. Reynaud, Phys. Rev. Lett. **77**, 615 (1996).

[223] G. Adesso, S. Ragy, A. R. Lee, Open Syst. Inf. Dyn. **21**, 1440001 (2014).

[224] D. T. Alves, C. Farina, P. A. Maia Neto, J. Phys. A **36**, 11333 (2003).

[225] B. H. Schneider, A. Bengtsson, I. M. Svensson, T. Aref, G. Johansson, J. Bylander, P. Delsing Phys. Rev. Lett. **124**, 140503 (2020).

[226] M. Paternostro, H. Jeong, T. C. Ralph, Phys. Rev. A **79**, 012101 (2009); C. Y. Park, H. Jeong, Phys. Rev. A **91**, 042328 (2015).

[227] S. Schuermans, M. Simoen, M. Sandberg, P. Krantz, C. M. Wilson and P. Delsing, IEEE Trans. Appl. Supercond. **21**, 448 (2011).

[228] H. M. Wiseman, S. J. Jones, and A. C. Doherty, Phys. Rev. Lett. **98**, 140402 (2007); S. J. Jones, H. M. Wiseman, and A. C. Doherty, Phys. Rev. A **76**, 052116 (2007).

[229] A. F. Abouraddy, T. Yarnall, B. E. A. Saleh, M. C. Teich, Phys. Rev. A **75**, 052114 (2007).

[230] T. Yarnall, A. F. Abouraddy, B. E. A. Saleh, M. C. Teich, Phys. Rev. Lett. **99**, 170408 (2007).

[231] G. Littich, Superconducting Mach-Zehnder Interferometers for Circuit Quantum Electrodynamics (Master's thesis), Laboratory for Solid State Physics, ETH Zürich, Switzerland (2009).

[232] J.-A. Larsson, J. Phys. A **47**, 424003 (2014).

[233] M. Giustina et al., Phys. Rev. Lett. **115**, 250401 (2015).

[234] J. You, F. Nori, Nature **474**, 589-597 (2011).

[235] D. T. Alves *et al.*, Phys. Rev. D **81**, 065002 (2010).

[236] A. Ferraro, S. Olivares, M. G. A. Paris, (Bibliopolis, Napoli, 2005) ISBN 88-7088-483-X.